QUANTAL AND STRUCTURAL ANALYSIS OF TRANSMISSION AND PLASTICITY AT INDIVIDUAL SYNAPSES IN THE HIPPOCAMPUS

By

Matthew J. MacDougall

Submitted in partial fulfillment of the requirements for the
degree of Doctor of Philosophy

at

Dalhousie University
Halifax, Nova Scotia
November 2022

My success, if I am to measure success, will always be less than my failures

- Alberto Giacometti

TABLE OF CONTENTS

LIST OF TABLES

LIST OF FIGURES

ABSTRACT

Synapses are the primary sites of information processing in the brain and effective communication between neurons relies on the efficacy of their transmission. The excitatory glutamatergic connections between CA3-CA1 neurons in the hippocampus have become a standard model system to investigate electrophysiological properties and morphological aspects of synaptic behaviour implicated in learning and memory. Detailed structure-function relationships of synapses, however, remain difficult due to the paucity of techniques capable of examining both functional and morphological aspects of synaptic behavior simultaneously in intact tissue preparations. Overall, my thesis aimed *i.* to examine, using optical quantal analyses, the quantal components of transmission in relation to key morphological aspects of mature synapses during basal states, *ii.* to assess these relationships during forms of activity-dependent plasticity, such as long-term potentiation (LTP), and *iii*. to compare functional and morphological modifications of single synapses using remote extracellular stimulation and two-photon glutamate uncaging approaches to plasticity. In this thesis, and within the confines of these experiments, I provide evidence that: *i*. transmitter release probability, p_r, but not potency (the postsynaptic response amplitude when release occurs), scales with spine size; *ii*. that p_r and potency are uncorrelated and independent quantal components of transmission; and *iii.* that potency is inversely correlated with spine neck length. I further demonstrate that *iv*. long-term potentiation (LTP), when induced via remote synaptic stimulation, is associated with persistent enhancements in p_r, but not potency, and *v*. that persistent morphological changes are not necessary for the expression of LTP at CA3-CA1 synapses. By contrast, two-photon glutamate uncaging-induced LTP (uLTP), at synapses that are functionally and structurally similar, is associated with increases in responsiveness to photo-released glutamate, persistent enlargement of spine head volume and reductions in spine neck length. Lastly, I demonstrate *vi*. that uLTP induction produces an elevation of spine Ca^{2+} that is not present when a more physiological mode of stimulation (i.e., remote stimulation) is used. Taken together, my thesis clarifies several divergent results among laboratories with respect to the loci of expression of LTP and the necessity of morphological modifications to synapses as they undergo activity-dependent changes in synaptic strength.

LIST OF ABBREVIATIONS

AA	Arachidonic acid
AMPA	α-amino-3-hydroxy-5-methyl-4-isoxazolepropionic acid
AP	Action potential
AZ	Active zone
Ca^{2+}	Divalent calcium ion
CA1	Cornu Ammonis 1
CA3	Cornu Ammonis 3
CaMKII	Calcium/calmodulin-dependent protein kinase II
CICR	Calcium-induced calcium release
CV	Coefficient of variation
DG	Dentate Gyrus
D_{Glu}	Effective glutamate diffusion coefficient
EPSP	Excitatory postsynaptic potentials
EPSCaT	Evoked postsynaptic calcium transient
HFS	High frequency stimulation
LFS	Low frequency stimulation
LTD	Long-term depression
LTP	Long-term potentiation
MAPK	Mitogen activated protein kinase
mEPSC	Miniature excitatory postsynaptic currents
MF	Mossy Fiber
Mg^{2+}	Divalent magnesium ion
NMDAR	N-Methyl-D-Aspartate receptor
NMJ	Neuromuscular junction
NO	Nitric Oxide
OGB-1	Oregon Green Bapta-1
p_r	Release probability
PDZ	Postsynaptic density protein (PSD95), Drosophila disc large tumor suppressor (DlgA), zonula occludens-1 protein (Zo-1)
PLC	Phospholipase C
PSD	Postsynaptic density
PSD-95	Postsynaptic density protein 95
SAM	Surface adhesion molecule
SNARE	Soluble NSF attachment protein
uPSCaT	Uncaging-evoked postsynaptic calcium transient
uLTP	Uncaging induced long-term potentiation
TARP	Transmembrane AMPA regulatory protein
VGCC	Voltage-gated calcium channels

ACKNOWLEDGMENTS

I would like to thank my supervisor, Alan Fine, for his continued support and encouragement, for the challenges he put before me, and for providing an aspiring young scientist with a truly stimulating learning environment.

Members of the Fine lab for their friendship and their insightful contributions.
In particular, I would like to highlight the important contributions made by my friends and colleagues, Alexey Faustov and Alexander Goroshkov, for their help identifying and resolving many technical issues related to the optical systems used in this thesis.

Dmitri Rusakov and members of his lab at UCL for hosting me during a foreign study component of my training.

Thomas Bartol and members of the MMBIOS team for insightful comments on my Monte Carlo modelling of synaptic transmission.

My committee members, Roger Croll and Bill Baldridge, for contributing to thoughtful discussions, providing encouragement, and always bringing a degree of levity to our meetings.

Most of all, I would like to thank my friends and family for their uncompromising patience and unconditional support - with a special thanks to my wife and our darling children.

CHAPTER I: INTRODUCTION

This chapter largely recapitulates concepts previously published as: *MacDougall & Fine (2014): The expression of long-term potentiation: reconciling the preists and postivists. Philosophical Transactions of the Royal Society B. 369(1633)*.

Permission to reprint the content including Fig.1.1 with slight modification has been obtained from the publisher and is found in appendix A.

1. General Introduction

Effective communication between neurons of the central nervous system depends crucially on the synaptic connections between cells. Structural and functional modifications to synapses, the sites of information processing within cells, have long been thought to underlie mnemonic function in the brain (Ramón y Cajal 1893, Tanzi 1893). Theories linking synaptic modifications to memory have been perhaps best emphasized by the oft cited and celebrated postulate of Donald Hebb: "*When an axon of cell A is near enough to excite a cell B and repeatedly or persistently takes part in firing it, some growth process or metabolic change takes place in one or both cells such that A's efficiency, as one of the cells firing B, is increased" (*Hebb 1949*).* The hippocampal formation has become a region of interest in the study of synaptic form and function due to mounting evidence of its involvement in forms of learning and memory (Scoville and Milner 1957, O'Keefe 1976, Morris et al. 1982, Whitlock et al. 2006). Specifically, the excitatory glutamatergic synapses between CA3 and CA1 pyramidal cells have become a standard model system to investigate electrophysiological properties and morphological aspects of synaptic behaviour (Andersen, Morris et al. 2006). Indeed, how synaptic strength, the presynaptic release of neurotransmitter and/or the postsynaptic responsiveness to its release relate to morphological aspects of these synapses have long held the attention of researchers and considerable efforts have accordingly been put forth to elucidate key relationships.

Despite considerable advances there remain substantial gaps in our understanding of synaptic behaviour during both basal states and under forms of activity-dependent plasticity, closely linked to learning and memory (Bliss and Lømo 1973, Bliss and Gardner-Medwin 1973). Chief among the reasons for this gap is the paucity of experimental techniques that allow for the dynamic concomitant monitoring of both pre- and postsynaptic components of transmission along with synaptic morphology in intact tissue preparations (Lisman 2017). Thus, the main objectives of this thesis were *i.* to examine the structural and functional characteristics of synaptic behaviour during basal states and *ii.* to assess these relationships during patterns of activity-dependent

plasticity. This chapter briefly outlines seminal works in the field and offers a working model of synaptic modifications thought to underlie learning and memory.

Long-term potentiation (LTP) of excitatory synaptic transmission is a dominant cellular model of learning and memory mechanisms in the vertebrate brain (Bliss and Collingridge 2013, Nicoll and Roche 2013, Nicoll 2017, Kruijssen and Wierenga 2019) and has been explored in great detail from the time of its original observation in the hippocampus (Bliss and Lømo 1973). It is now generally accepted that the induction of LTP at CA3-CA1 synapses in the rodent hippocampus ordinarily requires transient substantial elevation of postsynaptic Ca^{2+} concentration via activation of Ca^{2+}-permeable NMDA-type glutamate receptors (NMDARs) and release of Ca^{2+} from internal stores, and the subsequent activation of calcium/calmodulin-dependent protein kinase II (CaMKII; Harvey and Collingridge 1992, Bliss and Collingridge 2013, Sanhueza and Lisman 2013). There is less consensus regarding the locus of LTP expression, however, with various observations adduced in support of presynaptic mechanisms such as changes in the mode or probability of vesicular release (reviewed by Lisman and Raghavachari 2006) or of postsynaptic mechanisms such as the insertion or modulation of AMPA-type glutamate receptors (AMPARs; reviewed by Malinow and Malenka 2002, Collingridge et al. 2004). Just as Alzheimer research has been riven by arguments between Tauists and βaptists (Lee 2001, Trojanowski 2002), so has LTP research witnessed zealous disputes between Preists and Postivists. In recent years, postsynaptic models of LTP expression have become widely accepted (Nicoll 2003, Nicoll and Roche 2013, Nicoll 2017), with the authors of one prominent review concluding that there was now “conclusive evidence that LTP is mainly expressed postsynaptically” (Kerchner and Nicoll 2008). Reports of the death of presynaptic expression have been exaggerated, however. In this chapter I attempt to offer a brief and selective overview of some important findings in the history of the expression, or locus, debate and highlight results from our laboratory and others that in our view provide compelling evidence of the prime importance of

presynaptic mechanisms in LTP expression, at least during protein synthesis-independent “early” forms of LTP for which most data are available. I also offer a model of LTP expression that may help reconcile the different views across the synapse.

1.1 A history of progress and controversy

Bliss and Lømo (Bliss and Lømo 1973) were the first to demonstrate long-lasting activity-dependent alterations in synaptic efficacy that had been previously proposed as the neural substrate of learning and memory (Hebb 1949). Their initial observations did not, however, establish the relative importance of pre- and postsynaptic mechanisms in the expression of these long-lasting changes (Kullmann 2012). This seemingly innocuous issue has remained at the centre of a scientific controversy that has persisted for almost half a century. The following paragraphs offer a brief review of several key findings relevant to this debate.

Increases in presynaptic neurotransmitter release

Skrede and Malthe-Sørenssen (1981) provided early evidence of presynaptic mechanisms in the expression of LTP. They demonstrated that after bursts of electrical stimuli to the Schaffer collaterals *in vitro*, stimulus-evoked release of D-aspartate (a proxy for endogenous L-glutamate) in area CA1 was significantly and persistently increased. Shortly thereafter, Dolphin et al. (Dolphin et al. 1982) used an *in vivo* push-pull perfusion technique to demonstrate that LTP at perforant path (PP) to dentate gyrus (DG) neurons at is also associated with a prolonged increase in neurotransmitter release. Increases in extracellular glutamate after LTP have since been corroborated using an assortment of techniques including the induction of LTP *in vivo* with subsequent monitoring of glutamate levels in slices days later (Bliss et al. 1987), following learning of hippocampus-dependent behavioural tasks (Laroche et al. 1987), as well as through the use of glutamate sensitive electrodes (Errington et al. 2003). It should be noted that contrary results have also been reported: neither stimulus-evoked

glial glutamate transporter currents (Diamond et al. 1998, Luscher et al. 1998) nor rates of use-dependent pharmacological blockade of glutamate receptor-mediated currents (Manabe and Nicoll 1994, Mainen et al. 1998), both presumed to reflect levels of glutamate in the synaptic cleft, have been seen to change during LTP, but such changes may have been obscured in these experiments by confounding factors such as experimental duration and simultaneous changes in glial physiology or glutamate receptor kinetics.

More recent evidence for increases in neurotransmitter release during LTP comes from experiments using FM1-43, a fluorescent marker that binds to plasma membranes and is internalized during endocytosis. After such endocytosis and subsequent washout of remaining extracellular dye, residual fluorescence in boutons, as well as its stimulus-evoked disappearance or destaining, reflects the extent of transmitter release (Betz and Bewick 1992). Using this fluorescent maker of presynaptic activity Siegelbaum and colleagues demonstrated that both chemical- and high frequency stimulation (HFS)-induced LTP at CA1 synapses involve enhanced neurotransmitter release from presynaptic terminals, as indicated by the activity dependent rate of FM1-43 destaining (Zakharenko et al. 2001, Ahmed and Siegelbaum 2009). Such enhanced destaining was seen following LTP induction via 200 Hz stimulation as well as following a (presumably more physiological) theta-burst induction protocol, and was associated with recruitment of additional voltage gated Ca^{2+} channels (VGCCs) to terminal boutons (Ahmed and Siegelbaum 2009).

Changes in postsynaptic responsiveness

Although increases in neurotransmitter release provided a potential mechanism for LTP expression at central glutaminergic synapses, increases in the responsiveness of postsynaptic cells to released glutamate offered an alternative explanation. Indeed, evidence for such postsynaptic mechanisms was soon forthcoming. For example, LTP has been found to be associated with selective enhancement in AMPAR-mediated responses with no change in

NMDAR-mediated responses (Kauer et al. 1988, Muller and Lynch 1988), whereas LTP expression via increased glutamate release might be expected to effect evoked responses mediated by both types of glutamate receptors (Nicoll 2003). Such observations led to the hypothesis that functional glutamate receptors newly inserted into the postsynaptic membrane would be sufficient to account for the enhanced synaptic efficacy of LTP (Lynch and Baudry 1984). Several independent groups have challenged these findings, however, observing that LTP is associated with changes in both AMPAR- and NMDAR-mediated responses (Bashir et al. 1991, Clark and Collingridge 1995, Kullmann et al. 1996) or even in some cases with changes only in NMDAR-mediated responses (Grosshans, Clayton et al. 2002). These discrepancies have not as yet been resolved.

Among the evidence most persuasively supporting postsynaptic expression of LTP came from studies by Malinow and colleagues using green fluorescent protein (GFP)-tagged and electrophysiologically-distinctive GluA1-containing AMPARs (GluA1-AMPARs) to monitor AMPAR insertion into dendritic spines during LTP (Shi et al. 1999, Hayashi et al. 2000). GluA1-AMPARs display pronounced inward rectification in comparison to GluA2-containing AMPARs, and this rectification signature can be used as a measure of GluA1-AMPAR surface expression (Hayashi et al. 2000). LTP was seen to be associated with an increase in GFP localization in spines, and with a change in the rectification profile of synaptically evoked currents (Shi et al. 1999, Hayashi et al. 2000). These and related studies provided evidence that AMPARs are inserted into the membrane during NMDAR-dependent LTP, and established that such insertion is CaMKII dependent. Recent work from Malinow's group has further demonstrated that GluA1 AMPAR subunits are inserted extrasynaptically and that lateral movement of membrane-bound GluA1-AMPARs into synapses occurs prior to the extrasynaptic insertion events (Makino and Malinow 2009). Neither phosphorylation of GluA1-AMPARs (S845, S831, S818, S831), GluA1-stargazin interaction, nor the combination of the two is sufficient to drive surface expression at extrasynaptic sites, suggesting that other mechanisms are necessary (Kessels

et al. 2009). While the signaling events by which GluA1-AMPARs are driven to the membrane have not yet been fully elucidated, CAMKII is thought to be a major facilitator. Understanding the exact signaling pathways of AMPAR trafficking during plasticity remains a major focus of LTP research (Kessels and Malinow 2009). Notwithstanding recent evidence against necessary participation of GluA1 *or* GluA2 in LTP (Granger et al. 2013), in aggregate these data demonstrate the occurrence of postsynaptic receptor-related processes in association with LTP. However, as we outline below, while such processes may indeed be crucial for LTP expression, they do not function by increasing synaptic potency.

Classical quantal analysis

Evidence from early work employing quantal analysis as a means to investigate the locus of LTP expression in the hippocampus (Bekkers and Stevens 1990, Malinow and Tsien 1990, Malinow 1991) provided strong evidence that LTP was associated with increases in transmitter release probability p_r (based on changes in coefficient of variation (CV) and on decreases in synaptic failure rates) without any corresponding change in quantal size (Bekkers and Stevens 1990, Malinow and Tsien 1990, Bolshakov and Siegelbaum 1995).

Notwithstanding the elegance of these studies, the underlying assumptions of quantal analysis at hippocampal synapses have been called into question: though useful at unitary synapses such as neuromuscular junctions (Del Castillo and Katz 1954), classical quantal analysis may not be an appropriate method of analysis when, as is the case in most studies in hippocampus, evoked responses result from transmission at an unknown number of synapses (Faber and Korn 1991, Korn and Faber 1991, Larkman et al. 1991). Furthermore, as tellingly noted by Edwards (Edwards 1991), reduced failure rates can be due to postsynaptic rather than presynaptic changes. Synapses with NMDARs but not functional AMPARs in the postsynaptic membrane are “silent”, i.e., unresponsive to glutamate release at resting membrane potential; insertion

of functional AMPARs, for example following an LTP-inducing stimulus, would 'unsilence' the synapse making it responsive to presynaptic neurotransmitter release. Such unsilencing provided a plausible alternative explanation for reductions in failure rates following LTP, an explanation supported by the initial results of Kullmann (Kullmann 1994), demonstrating a reduction in the CV for AMPAR-mediated responses but no change in either the amplitude of NMDAR-mediated current or the CV for NMDAR responses. Previous observations of selective enhancement of AMPAR-mediated responses associated with LTP without corresponding increase in NMDAR-mediated respones (e.g., Kauer et al. 1988, Muller and Lynch 1988) were also compatible with this unsilencing explanation, but have not been consistently reproduced (e.g., Bashir, Alford et al. 1991, Clark and Collingridge 1995, Kullmann et al. 1996).

Compelling support for the involvement of unsilencing of silent synapses in LTP expression came from studies utilizing a minimal stimulation technique to isolate synapses with NMDAR-mediated responses (at positive holding potentials) but no AMPAR-mediated responses (at negative holding potentials). Using this method, Liao et al. (Liao et al. 1995) demonstrated that AMPAR-mediated responses could be detected after LTP at synapses previously lacking such responses (i.e., NMDAR-only synapses) in parallel with reductions in synaptic failure rates. Similar results were independently obtained by Isaac et al. (Isaac et al. 1995) around the same time. Both groups, however, worked with hippocampal slices from juvenile rats at ages (≤20 postnatal days) when postsynaptically-silent synapses are particularly abundant (Durand et al. 1996) and alternative, presynaptic silence mechanisms should not be ruled out (Voronin 2003, Voronin et al. 2004). This raises the question whether LTP expression via synapse unsilencing is a developmentally restricted phenomenon. I will return to this question shortly, but the disagreement surrounding the interpretations of classical quantal analysis indicated that a less ambiguous form of quantal analysis could help to resolve the roles of pre and postsynaptic mechanisms in LTP expression (Edwards 1991).

Optical quantal analysis

Criticisms of classical quantal analysis at hippocampal synapses have focused largely on the inability to resolve single unitary synaptic responses (Faber and Korn 1991). Optical detection of synaptically-evoked postsynaptic Ca^{2+} transients (EPSCaTs) within single dendritic spines (Malinow et al. 1994, Yuste and Denk 1995, Emptage et al. 1999) has given us a means to overcome this difficulty. EPSCaTs are mediated by Ca^{2+} entry through NMDARs and further amplified by Ca^{2+} release from internal stores (Emptage et al. 1999). To monitor EPSCaTs, a cell is impaled, loaded with fluorescent Ca^{2+} indicator, EPSPs are evoked via an extracellular stimulating electrode, and the dendritic tree is scanned for spines that display a fluorescence change in response to stimulation. Simultaneous monitoring of somatically-recorded EPSPs and EPSCaTs in the spine permits optical quantal analysis (Emptage et al. 2003, Reid et al. 2004) whereby quantal parameters of transmission can be determined at individual synapses without the interpretation difficulties of classical methods. In particular, as EPSCaTs are reliable indicators of transmission at the imaged synapse (Malinow et al. 1994, Yuste and Denk 1995, Emptage et al. 1999, Enoki et al. 2009), the probability of a presynaptic action potential generating EPSCaTs in a postsynaptic spine provides an accurate estimate of p_r at the corresponding presynaptic terminal. Using this approach, optical quantal analyses at the same synapses before and after LTP induction revealed presynaptic contributions to LTP expression both at mossy fiber (MF) synapses (Reid et al. 2004) as well as at associational and Schaffer collateral synapses on CA3 and CA1 neurons (Emptage et al. 2003). Whereas it is widely accepted that LTP at MF synapses is associated with an increase in neurotransmitter release (Nicoll and Schmitz 2005), this indication that p_r increases with LTP at Schaffer-associational synapses, though consistent with earlier classical quantal analysis (Bekkers and Stevens 1990, Malinow and Tsien 1990, Stevens and Wang 1994), was at odds with the evidence for postsynaptic expression described above, raising questions about the relative importance of these pre- and postsynaptic expression mechanisms, and about how they might relate.

Subsequently, Enoki et al. (2009) employed a subtractive procedure that allowed these questions to be addressed by establishing the contribution of the EPSCaT-generating synapse to the simultaneous somatically-recorded polysynaptic, or compound EPSP, and thus to determine the unitary EPSP due to the imaged synapse. The results (Enoki et al. 2009) were clear: LTP at Schaffer-associational synapses, whether induced by HFS or by pairing synaptic activation with postsynaptic depolarization, is associated with an increase in synaptic reliability (fewer failures, i.e., increased p_r) with no change in synaptic potency (unitary EPSP amplitude or quantal size). The same results were obtained without subtraction in the rare cases where "minimal stimulation" actually activated only one synapse; in those cases, EPSCaTs occurred in constant conjunction with EPSPs, and EPSCaT failures were in constant conjunction with EPSP failures, confirming that EPSCaTs are a reliable measure of neurotransmitter release. These experiments were carried out on hippocampal slices of young adult (≥P21) rats to reduce the prevalence of silent synapses (Durand et al. 1996, Busetto et al. 2008, Kerchner and Nicoll 2008), for reasons that will be made clear in the next section. These optical quantal analyses refined and reinforced the conclusions of the earlier classical quantal analyses cited above, and indicated not only that LTP at active hippocampal associational synapses is associated with increased probability of neurotransmitter release, but that, at least under the particular conditions by which LTP is induced in those experiments, such enhanced reliability is the principal means by which LTP is expressed.

State-dependent long-term potentiation

As noted above, observations of synaptic unsilencing in LTP raised the question of whether this phenomenon is of general importance or is developmentally restricted. Ward et al. addressed this question via optical quantal analysis, and found differential state-dependent expression mechanisms for LTP at silent versus active synapses (Ward et al. 2006): LTP at silent synapses proceeds via unsilencing, in keeping with previous reports. Postsynaptic dialysis with an inhibitor of vesicular fusion prevented unsilencing at these synapses, consistent with the notion that insertion of receptors in the postsynaptic membrane is essential for LTP expression via such unsilencing. Importantly, no changes in p_r, as inferred from EPSCaTs failure rates, were detected when LTP was expressed at silent synapses detected during Mg^{2+}-free superfusion or postsynaptic depolarization. After unsilencing, however, those same synapses displayed significant increases in p_r following a second round of LTP induction (Ward et al. 2006). Overall, these studies indicate that unsilencing by postsynaptic molecular insertion via vesicular fusion is the main mechanism for LTP expression at silent synapses, whereas an increase in p_r is the primary mechanism for LTP expression at synapses once they have been unsilenced.

Synaptic scaffolding proteins

The scaffolding protein PSD-95 has been implicated in AMPAR insertion during LTP, principally through its interactions with the transmembrane AMPAR regulatory protein (TARP) stargazin (Schnell, Sizemore et al. 2002, Ehrlich and Malinow 2004). PSD-95 contains three consecutive PDZ domains in its N-terminal region that act as ‘slots’ capable of binding various transmembrane proteins including certain ion channels and surface adhesion molecules (SAMs) and anchoring them at synaptic sites (Kim and Sheng 2004). Such binding of stargazin via its C-terminal domain to a PDZ domain of PSD-95 or related proteins appears to be crucial for AMPAR targeting to the synapse (Chen et al. 2000, Tomita et al. 2005). PSD-95 is capable of dimerization and multimerization

at postsynaptic sites through N-terminal interactions (Xu et al. 2008) and has been implicated in synapse maturation through clustering (El-Husseini et al. 2000, Dean et al. 2003). This scaffolding protein could thus plausibly mediate changes in synaptic efficacy by recruiting assemblies of proteins required for synaptic transmission. Indeed, overexpression of PSD-95 has been shown to mimic aspects of LTP, increasing both the amplitude and frequency of AMPA-mediated miniature excitatory postsynaptic currents (mEPSCs; El-Husseini et al. 2000, Beique and Andrade 2002, Stein et al. 2003); an increase in the frequency of mEPSCs is commonly correlated with increases in p_r. Both GluA1-containing AMPARs and synaptophysin levels increase following overexpression of PSD-95, as indicated by immunostaining (El-Husseini et al. 2000). Conversely, knockdown of PSD-95 decreases synaptic strength and prevents the developmental accumulation of functional w at synaptic sites (Ehrlich et al. 2007). Of particular interest, stability of PSD-95 at the PSD appears to be modulated by an interaction involving its TARP-binding PDZ domains (Sturgill et al. 2009), which may account for certain requirements for GluA1 in LTP expression (e.g., Kopec et al. 2007).

1.2 Reconciliation: one model for both sides

The following simple unifying model of LTP expression emerges from consideration of results such as those summarized above.

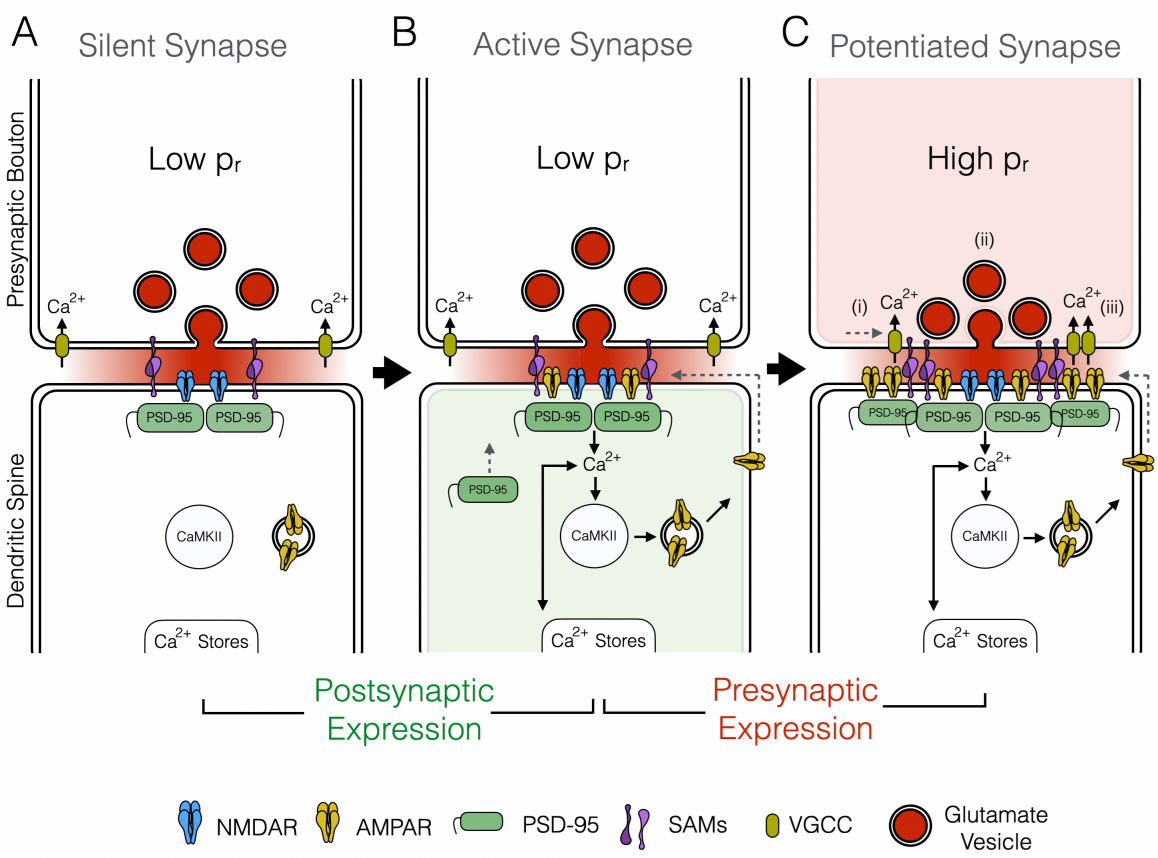

Figure 1.1: *A simplified model of the expression of NMDAR-dependent long-term potentiation at CA1 associational/commissural synapses*. (**A-B**) Postsynaptic expression mechanisms are responsible for LTP at silent synapses. (**A**) Transmission fails at silent synapses prevalent in immature CA1, as any postsynaptic AMPARs are too far from the active zone to encounter activating concentrations of released glutamate (red shading in synaptic cleft), while NMDARs, though suitably localized, are blocked by Mg^{2+} at normal resting potentials. (**B**) Following an LTP-inducing stimulus, Ca^{2+} enters the postsynaptic cell and activates CaMKII, mediating extrasynaptic insertion of GluA1-AMPAR/stargazin which then diffuses into the synaptic membrane. Stargazin (not depicted) mediates synaptic trapping of the AMPAR by binding to vacant PSD-95 PDZ1/2 domains (slots) close to the active zone. Additional GluA1-AMPARs inserted at extrasynaptic sites cannot detect glutamate released in the cleft. Synaptic GluA1-AMPARs may be subsequently exchanged for GluA2-containing AMPARs. (**C**) Presynaptic expression mechanisms are responsible for LTP at active synapses. Following an LTP-inducing stimulus, new PSD-95 is added to the edges of the postsynaptic density, making available new slots for GluA1 recruitment. GluA1-AMPARs inserted extrasynaptically diffuse laterally to these slots, but are too far from the vesicular fusion site at the presynaptic active zone to be activated by released glutamate. These GluA1-AMPARs can also exchange with GluA2-AMPARs in the PSD closer to the active zone; such exchange can alter rectification properties of synaptic currents but will have little effect on EPSP

amplitude. New GluA1-AMPARs are also recruited to replenish extrasynaptic sites. Synaptic adhesion molecules (SAMs) recruited to slots in the new synaptic PSD-95 recruit binding partners in the presynaptic membrane, in turn triggering an increase in the probability of neurotransmitter release by mechanisms that may include (i) increased spatial coupling of VGCCs to release machinery, (ii) increased number of docked/primed vesicles, and (iii) recruitment of new VGCCs to the presynaptic membrane, as well as increased Ca^{2+} sensitivity of the vesicular release machinery, change from partial to full vesicular fusion, and various other mechanisms not shown.

Silent Synapses: Postsynaptic Expression

Silent glutamatergic synapses, abundant early in development, have PSDs that contain NMDARs without functional AMPARs (**Fig.1.1A**), and are thus unresponsive to evoked glutamate release at normal resting membrane potentials. LTP-inducing stimuli, possibly by activating CaMKII, trigger the extrasynaptic insertion of GluA1-containing AMPARs into the postsynaptic membrane (**Fig.1.1B**). Complexed with stargazin, they can diffuse laterally to synaptic sites where they are anchored when stargazin binds to vacant PDZ domains in subsynaptic PSD-95 (Ehrlich and Malinow 2004, Ehlers, Heine et al. 2007). Such GluA1-AMPARs at synaptic sites can now respond to evoked vesicular release of glutamate, yielding observed increases in AMPAR currents and rectification changes as well as decreases in synaptic failures rates. Synaptic GluA1-containing AMPARs may thereafter be exchanged for GluA2-heteromeric AMPARs (Plant et al. 2006). The unsilencing of a silent synapse is also expected to reduce the threshold for subsequent LTP at that synapse by enabling AMPAR-induced partial depolarization and thus relaxing the requirements of coincident nearby synapse activation or dendritic regenerative depolarization for removal of Mg^{2+} block from NMDARs. It should be noted that transiently expressed homomeric GluA1-AMPARs (unlike GluA2-containing AMPARs) are Ca^{2+} permeable and that the additional Ca^{2+} influx is thought to contribute to the stability of LTP (Plant et al. 2006). In any case, LTP at silent synapses appears to rely largely on postsynaptic expression mechanisms.

Active Synapses: Presynaptic Expression

In contrast to silent synapses, postsynaptic elements at active, non-silent synapses already contain functional AMPARs and are thus responsive to evoked glutamate release at normal resting membrane potentials. I suggest that unsilencing of synapses permits subsequent LTP-induced aggregation of PSD-95 molecules at the postsynaptic density (PSD). This clustering of PSD-95 adds new empty slots for receptors, ion channels and SAMs to be inserted into the plasma

membrane. These new slots are central to the different way in which LTP is expressed at active, non-silent synapses. Thus, LTP induction at active synapses leads not only to extrasynaptic insertion of GluA1-containing AMPARs into the postsynaptic membrane as was the case at silent synapses, but also to the addition of new PSD-95 family proteins to the PSD (**Fig. 1.1C**). The newly inserted GluA1-containing AMPARs diffuse laterally until they are captured by vacant PDZ domains (slots) of the newly added PSD-95.

Enoki and colleagues have shown that individual synapses can sustain multiple episodes of potentiation (Enoki et al. 2009), and it is suggested here that most mature synapses, which carry the majority of synaptic weight, will have been multiply potentiated. PSD-95 forms a highly structured lattice at the PSD (Chen et al. 2011), and it is likely that net addition of new PSD-95 can only occur at the edges of the PSD. Most mature Schaffer collateral-commissural synapses have PSDs with diameter >250 nm (Harris et al. 1992), and AMPARs are preferentially distributed at the periphery of the PSD (Takumi et al. 1999, Chen et al. 2008). We propose that AMPAR-binding PDZ domains of PSD-95 present at PSDs in mature synapses under baseline conditions tend already to be filled as a consequence of earlier potentiation events. In response to new potentiating stimuli, net addition of newly inserted AMPARs therefore can only occur where new PSD-95 is added to the edges of the PSD. AMPARs, however, bind glutamate with relatively low, millimolar, affinity. Peak glutamate concentrations in the synaptic cleft may reach millimolar levels, but such levels are achieved only very close in space and time to the point of vesicular opening; from there, glutamate concentration decays rapidly within milliseconds and hundreds of nanometers. Considerations of glutamate release, kinetics of binding to AMPARs, diffusion in the cleft and uptake (Rusakov and Kullmann 1998) indicate that the AMPARs activated by evoked glutamate release are mainly those within a small “hotspot” of diameter 250 nm or less, centred opposite the release site (Raghavachari and Lisman 2004). Thus, potentiation at mature synapses would involve addition of AMPARs that will, in the main, be too far from the release site to be significantly activated, at least at low stimulus frequencies under normal

physiological conditions: *addition of new AMPARs would make little contribution to the functional potentiation of mature synapses*. Such AMPARs newly inserted in the extrasynaptic membrane can, however, *exchange* with AMPARs already in the central "hotspot" region of the PSD, or diffuse into slots vacated by GluA2-containing AMPARs undergoing constitutive recycling (Heine, Groc et al. 2008; **Fig.1.1C**). Such exchange would lead to observed changes in biophysical characteristics including rectification properties of excitatory postsynaptic currents (EPSCs). However, as the total number of AMPARs contributing to those evoked currents remains constant, such exchange would have only minor effects on EPSC or excitatory postsynaptic potential (EPSP) amplitude. There are, of course, many synapses with smaller PSDs, where AMPARs added to the margin could be within the "hotspot" of sensible glutamate release. Such small synapses, however, appear to contribute little to the aggregate EPSP at the soma and initial segment (Enoki et al. 2009); the model proposed here is concerned with the larger, stronger synapses that are the main contributors to intracellularly-recorded EPSPs and observed LTP.

Whereas LTP at active synapses thus has little effect on synaptic potency, increases in synaptic reliability are proportional to the increases in synaptic strength, and sufficient to account for them (Enoki et al. 2009). How do these presynaptic changes arise? As noted above, LTP that is induced by postsynaptic Ca^{2+} elevation but expressed by changes in the reliability of evoked transmitter release requires retrograde signaling across the synapse. Identifying the molecular basis of such retrograde signaling is now a key challenge. Although this working model is consistent with various diffusible molecules that have been suggested as signals (Regehr et al. 2009), it is particularly compatible with such a signaling role for synaptic adhesion molecules (SAMs): recruited to the PSD by newly added PSD-95, postsynaptic SAMs could in turn recruit their presynaptic binding partners. SAM recruitment could contribute to maintaining the proportionate size of active zones and postsynaptic densities at presumptive glutamatergic synapses (Schikorski and Stevens 1997, Shepherd and Harris 1998). Transsynaptic binding, with consequent dimerization or higher aggregation

of presynaptic SAMs, could then trigger an increase in p_r by a variety of mechanisms including, but not limited to, increased spatial coupling of VGCCs to the synaptic release machinery, increasing the number of docked/primed vesicles, recruitment of new VGCCs (**i, ii and iii, respectively, in Fig.1.1C**), increased Ca^{2+} sensitivity of the vesicular release machinery, and change from partial to full vesicular fusion.

I close by noting that this working model deals specifically with expression of potentiation during its early, protein synthesis-independent phase. Whether it is also relevant to expression of late, protein synthesis-dependent potentiation remains to be determined. It would be surprising if presynaptic mechanisms responsible for the majority of early LTP expression turn out to be entirely replaced by alternative postsynaptic mechanisms yielding similar levels of potentiation during late LTP expression. A requirement for postsynaptic protein synthesis would not be inconsistent with this position if, for example, synthesis of new postsynaptic scaffold proteins is essential to consolidate the transsynaptic signaling essential for maintained presynaptic expression. It will be important to determine precisely how, and how much, these or other mechanisms contribute to the modulation of synaptic reliability in LTP and other forms of long-lasting plasticity that underlie memory and its disorders.

CHAPTER II: MATERIALS AND METHODS

Some of the contents of this chapter have been previously published in *MacDougall & Fine (2019): Optical Quantal Analysis. Frontiers in Synaptic neuroscience 26; 11-18*.

Reprint permission from the publisher is not required as the manuscript is open access. Correspondence with the publisher is found in appendix A.

2.1 Hippocampal slices

Transverse 350 μm slices of hippocampus, which retain much of the functional and structural integrity of the original tissue, were cut from 2-3 week old male Wistar rats, according to standard protocols (e.g., Skrede and Westgaard 1971, Geiger et al. 2002, Bischofberger et al. 2006; see Aitken et al. 1995 for discussion). We dissected hippocampal tissue in ice cold sucrose-based cutting solution containing (in mM): 105 Sucrose, 50 NaCl, 1.25 NaH_2PO_4, 2.5 KCl, 26 $NaHCO_3$, 13 Glucose, 0.5 $CaCl_2$, 7 $MgCl_2$. Dissected hippocampi were then positioned into an agar block perpendicular to the cutting blade and slices made perpendicular to the longitudinal axis of the hippocampus using a vibrating tissue slicer (Leica VT1200, Leica Biosystems, Nussloch). Slices were then transferred to a custom interface chamber and allowed to recover for 30 minutes to 1 hour at 32-33°C while being oxygenated with 95% O_2 /5% CO_2. Under these conditions, slices remain viable for up 8 hours. For recording, acute slices were transferred to a specially designed chamber where they were continually superfused (~2 ml/min) with oxygenated (95% O_2 / 5% CO_2) artificial cerebral spinal fluid (ACSF) containing (in mM): 120 NaCl, 3 KCl, 1 $MgCl_2$, 2-3 $CaCl_2$, 1.2 NaH_2PO_4, 23 $NaHCO_3$, 11 glucose, 0.03 picrotoxin. ACSF was maintained at near physiological temperatures (32-33°C) using a temperature control unit throughout the duration of all experiments.

2.2 Two-photon microscopy:

Slices were viewed through an upright microscope (e.g., Olympus BX51W1) equipped with a high numerical aperture water immersion objective (e.g., Olympus 60x, N.A. 0.9) via a laser scan head (MRC1024MP, Bio-Rad Microsciences). Two-photon excitation was achieved using an ultrafast (100 fs pulses) Ti:Sapphire laser (Mai Tai, Spectra Physics: 3 W; 80 MHz). Emitted fluorescence was detected with photomultiplier tubes (PMTs; H7422P-40 Hamamatsu) connected to a signal amplifier. Detection at an additional wavelength was required for simultaneous Ca^{2+} and Alexa 594 imaging, so a

dichroic mirror was used to direct the two wavebands to appropriate PMTs. Care was taken when selecting fluorophores, to ensure that the emission spectra were non-overlapping. Two-photon excitation fluorescence images ('xy' and 'xt' images) were acquired at 810 nm excitation and 15-20 mW average laser power in the focal plane using LaserSharp software with 6x digital zoom. The microscope was also equipped with ordinary transmitted light and widefield fluorescence illuminators, digital camera, remotely controlled stage and micromanipulators, and temperature control units (**Fig.2.1**).

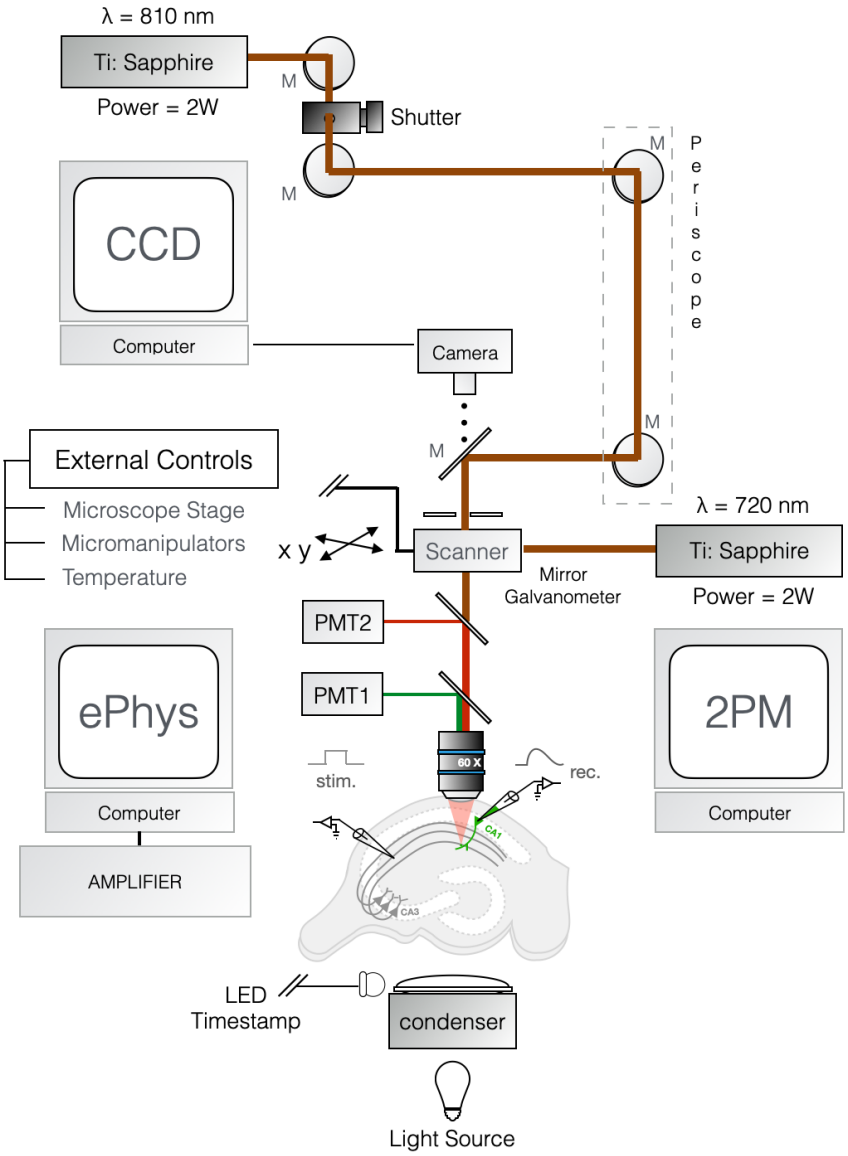

Figure 2.1: *Schematic of two-photon excitation microscopy imaging and recording configuration*. Excitation beam (red) tuned to a wavelength of 810 nm is focused by a 60X, NA 0.9 objective to a diffraction limited spot that excites the fluorescent intracellular calcium indicator (e.g., Oregon Green 488 BAPTA-1). The target neuron's membrane potential is constantly monitored through a somatic microelectrode. Excitation of inputs to the cell is achieved via a remote extracellular stimulating electrode. Fluorescence is detected by a photomultiplier tube (PMT). A second fluorophore and secondary detector (PMT2 and dichroic) were used. External control units for the micromanipulators, stage, and temperature are necessary components. Experiments involving two-photon glutamate uncaging made use of a second Ti:Sapphire laser tuned to a wavelength of 720 nm.

2.3 Electrophysiological and optical recording:

For electrophysiological recording sharp microelectrodes prevent unwanted and prolonged diffusion of cytoplasmic constituents out of, and micropipette solution into, the target neuron (Malinow and Tsien 1990). Selected pyramidal cells in the CA1 region of the hippocampus were impaled with sharp glass microelectrodes (80-120 MΩ) under full-field illumination and visual control via a digital camera. The microelectrode tips were filled with a fluorescent Ca^{2+} probe (0.5-1 mM Oregon Green 488 BAPTA-1 in H_20), and also with a spectrally distinct Ca^{2+}-insensitive fluorophore (0.25 mM Alexa 594) to serve as a morphological marker, and backfilled with 3M KCl. Ionophoretic loading of cells was achieved by delivering low frequency (2 Hz) hyperpolarizing current pulses (~100-200 pA) via the intracellular amplifier (e.g., Multiclpamp 700B, Molecular Devices, California). After 5-20 minutes of loading, fluorescence in the soma and processes could be easily visualized. Dye loading of the target cell was followed by two-photon excitation using the lowest possible power. Once sufficient loading was achieved, hyperpolarizing pulses were discontinued; note that leakage from the pipette tip may contribute to additional loading over time. To assess adequacy of loading, an action potential (AP) was evoked by a depolarizing current injection, and corresponding fluorescent Ca^{2+} responses were examined in the soma and proximal dendrites. For adequate detection of EPSCaTs in dendritic spines, back propagating APs should cause a fractional change ($\%\Delta F/F$) >80% in Ca^{2+} probe fluorescence in the spines. The extracellular stimulating electrode, a sharpened, insulated, tungsten electrode was placed in the stratum radiatum at distances no less than 50 μm (but < 500 μm) from the soma, at a depth similar to the target dendrite and typically 50-200 μm from the border of the stratum pyramidale. The extracellular stimulating pulses were increased to an intensity sufficient to elicit an AP-evoked Ca^{2+} transient in the soma and dendrites, and then decreased to 30-50% to a level at which subthreshold excitatory postsynaptic potentials (EPSPs) were reliably evoked. All electrophysiological data were collected and analyzed using Axograph software

(Axograph Scientific, Sydney). Throughout this thesis, the following false colour look-up tables (LUTs) have been used: red heat LUT for the Ca^{2+} indicator OGB-1 for compatibility with previous publications and green LUT for Alexa-594 morphological imaging. The green/red (G/R, i.e., OGB-1/Alexa-594) ratios for individual spines were determined by taking the ratio of the total corrected spine fluorescence (TCSF) of collapsed stacks from each channel,

$$TCSF = Integrated\ Density - (A_{spine} \times F_{background})$$

where, A_{spine} is the area of the spine head and $F_{background}$ is the background fluorescence of the collapsed image.

2.4 Optically searching for EPSCaTs:

Pairs or triplets of extracellular stimuli (each 100-300 μsec square pulses of intensity described above) separated by 70 msec were delivered to the tissue preparation and maintained at a constant level throughout the searching procedure. Multiple stimuli were used to increase the likelihood of finding low p_r synapses. The proximal region of the secondary and tertiary apical dendrites of the dye-filled CA1 pyramidal neuron was then systematically searched using fast raster scanning (e.g., 128x128 pixels), while simultaneously stimulating at a low frequency (~0.05-0.1 Hz), until a spine exhibiting an EPSCaT was located. Low stimulation frequencies were maintained during the searching procedure to prevent unintended plasticity induction (Collingridge et a. 2010). When optically searching the dendritic branches, it is important to follow a consistent strategy to avoid unintentionally neglecting or re-searching branches; a useful and common strategy is the wall follower, whereby a consistent direction (e.g., go right) is taken at branch points along the dendritic arbour. Given the remote positioning of the stimulating electrode relative to the apical branches, the location of responsive spines was highly variable and the time taken to identify active spines varied accordingly – spines positioned proximally tend to be found, on average, faster than those at more distal locations. Once a responsive spine was

identified, line scanning ('xt' images) can be used to image with better temporal resolution in order to record EPSCaTs with greater fidelity. Line scans ranging from 100 to 200 successive sweeps at 2 msec intervals were obtained along a line passing through the center of the activated spine and when possible, the subjacent parent dendrite. The duration and intensity of target irradiation was reduced to prevent phototoxicity and indicator bleaching. An LED positioned near the photodetector was used as a precise marker of onset for electrical stimulation. The stimulating intensity was then continually decreased until the threshold for EPSCaT detection was established. Once established, the stimulating intensity was then incrementally increased (approximately 20% from this threshold) to decrease the likelihood of stimulation failures of the afferent fibers.

2.5 Estimating release probability:

Several groups (Yuste and Denk 1995, Emptage et al. 1999, Yuste et al. 1999) have provided evidence that the probability of a presynaptic stimulus evoking an EPSCaT in a postsynaptic spine (p_{ca}) is equivalent to p_r, the probability that the stimulus evoked transmitter release from the unlabeled, and thus non-visualized, presynaptic bouton. A reliable estimate of p_r can therefore be achieved by delivering a sufficient number of stimuli (~20-25 trials) to afferent fibers while recording EPSPs and EPSCaTs from the postsynaptic neuron. A failure method similar to classical quantal analysis can be used, where p_r is related to the number of successes within a sample of trials assessed over a given period of time

$$p_r = N_{success} \,/\, N_{trials}$$

where $N_{success}$ is the number of successful transmission events divided by N_{trials}, the total number of trials (failures were unlikely to be due to failure of action potential initiation in the stimulated axons because increasing the stimulus intensity beyond the threshold for evoking EPSCaTs did not lead to any increase

in the observed frequency of EPSCaTs). The standard error, or uncertainty, associated with estimates of p_r is given, under the binomial theorem, as

$$SEM = \sqrt{(1 - p_r)(p_r)/ N_{trials}}$$

The Ca^{2+} transient amplitude was expressed as

$$\%\Delta F/F = 100\ (F_{transient} - F_{initial}) / (F_{initial} - F_{background})$$

where $F_{initial}$ is the mean fluorescence intensity of the imaged spine over a 20-40 msec time window prior to stimulation, $F_{transient}$ is the mean fluorescence intensity after stimulation, and $F_{background}$ is the mean intensity in regions devoid of labeled structures. To improve the signal-to-noise ratio, $F_{transient}$ was measured over a 10-30 msec window encompassing the peak of the Ca^{2+} transient (Enoki et al. 2009). Using this approach, an event was counted as a success if the EPSCaT amplitude exceeded the unstimulated noise amplitude, a threshold that is typically $\%\Delta F/F > 20\%$. Once sufficient recording of EPSCaTs and EPSPs had been obtained, yielding a stable ratio of successes to failures, long-term synaptic plasticity could be induced using appropriate protocols.

2.6 Estimating synaptic potency:

Electrical recording by itself has proven inadequate to resolve unambiguously the magnitude of quantal size *q* from an individual synapse (hereafter called the “potency” of the synapse) that contributes to a compound EPSP. Conjoint EPSCaT recording, however, permits a subtractive analysis that can effectively remove this ambiguity. On average, compound EPSP amplitudes were larger in trials where the imaged synapse releases transmitter than in those where the imaged synapse fails; I therefore subtracted the mean EPSP in failure trials from the mean EPSP in successes to yield an estimate of the mean unitary EPSP (“synaptic potency”) from the EPSCaT-generating synapse.

$$\overline{\mathrm{EPSP}}_{success} - \overline{\mathrm{EPSP}}_{failure} = potency$$

2.7 Estimating spine volume, density, and neck length:

For imaging of dendritic spines, I used a laser set at wavelength 810 nm, with theoretical lateral and axial resolutions described above. Dendritic images (128x128 pixels; 20.93x20.93 μm; 0.22 μm/pixel) were collected after 20-25 trials of electrical or optical stimulation. Individual xy images of active dendritic spines were collected and Kalman filtered (3-5 images to reduce optical noise) separated by z steps of 0.25-0.50 μm. All xy images within the z stack containing the active spine were collapsed using the z project and average intensity functions in ImageJ software (Schneider et al. 2012). Spatial fluorescence profiles were calculated by normalizing the fluorescence profile of a line segment through the center most point of the spine head (**Fig. 2.2A**) and fitted with a Gaussian function of the form,

$$y = y_0 + Ae^{\frac{-(x-x_1)^2}{2\sigma^2}}$$

Full width at half-max (FWHM) was calculated as,

$$FWHM = 2\sqrt{2\ln(2)\sigma}$$

σ is the standard deviation of the fitted Gaussian **(Fig. 2.1B)**. Finally, the radius and estimates of spine volume were calculated as,

$$R = \frac{FWHM}{2} \qquad V = \frac{4}{3}\pi R^3$$

In limited scenarios, when optical noise or technical difficulties in the Alexa 594 channel prevented the use for fluorescence measurements, images from the OGB-1 channel were used as a proxy. We analyzed a subset of spines (n = 9) and found little difference between the two fluorophores in terms of volume

estimates, with mean volumes (in μm^3) of 0.14 ± 0.03 and 0.14 ± 0.02 for Alexa 594 and OGB-1, respectively. The mean difference score per spine was -0.004 ± 0.02 μm^3 (data not shown).

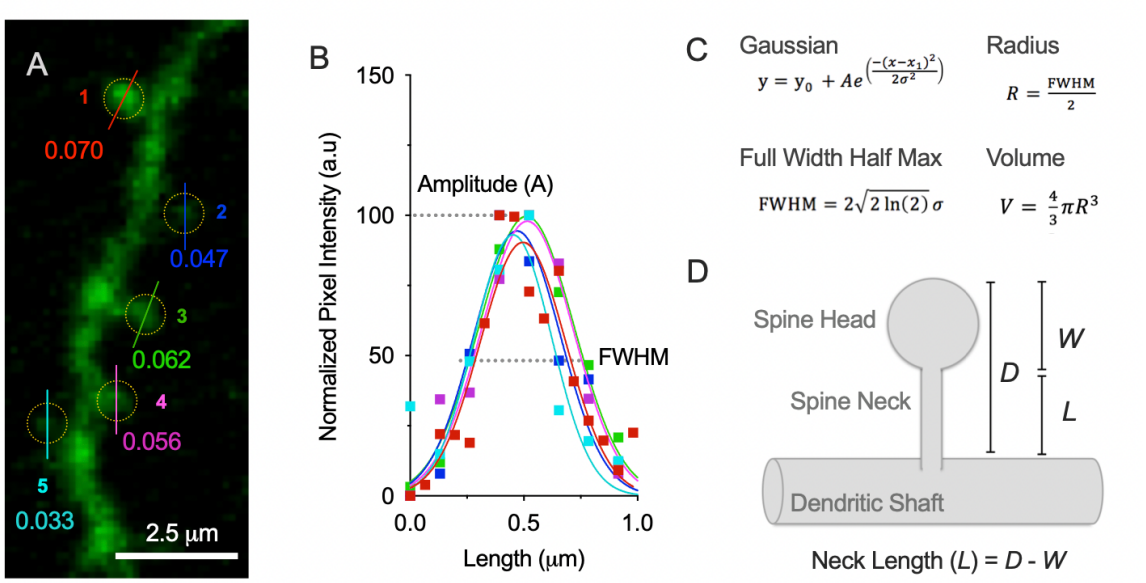

Figure 2.2: *Spatial fluorescence profile of dendritic spines*. A) False colour green fluorescence image (Alexa Fluor 594) of spines on the apical dendrite of a CA1 pyramidal cell. Yellow circles surround the spines of interest and line segments indicate the region of interest for spatial profiles. Spine volumes (in µm3) are indicated below each spine. B) Normalized data (coloured squares) for the spatial profiles of targeted spines with Gaussian fits (coloured lines). (C) Equations used to estimate volume of spines based on normalized fluorescent profiles. (D) Spine neck length, L, was estimated by taking the distance, D, from the tip of the spine head to base of the dendritic shaft and subtracting the width, W, of the spine head. Due to resolution limits of two-photon microscopy, both spine head volume and spine neck length estimates assume spherical spine head morphology.

For spine density measurements, the length of the dendritic branch was traced and measured using ImageJ software. The number of spines across the length of the dendritic branch was then manually counted and divided by the total measured length of the branch segment to give the number of spines per unit length, noting here that this is an underestimate due to spines that would be missed or hidden by the parent dendrite. In addition, I calculated an estimate of spine neck length by taking the total distance from the tip of the spine head to the base of the dendritic branch and subtracted the width of the spine head (**Fig. 2.2D**).

2.8 Induction of long-term potentiation:

Various protocols may be used to induce long-term changes in synaptic efficacy. Here, LTP was induced using a spike-timing dependent plasticity (STDP; Song et al. 2000) protocol, wherein postsynaptic spiking is evoked following a presynaptic stimulus (Markram et al. 1997, Bi and Poo 1998, Nevian and Sakmann 2006). Specifically, each presynaptic stimulus was followed by (Δt = 10 msec) the delivery of 3 pulses (at 100 Hz) of 2-10 msec postsynaptic depolarization (amplitude sufficient to evoke at least one action potential) with 100 repetitions at 0.33 Hz (**Fig. 2.3A**). I also used a high-frequency stimulation (HFS) protocol to induce LTP, where three bursts, at 1.5 sec intervals, of 20-presynaptic pulses at 100 Hz (with, if needed, sufficient simultaneous postsynaptic depolarization such that at least some of the presynaptic stimuli evoke action potentials; Emptage et al. 2003, Enoki et al. 2009; **Fig. 2.3B**). As I observed no difference between the magnitude of LTP between the two induction protocols, the data sets were pooled.

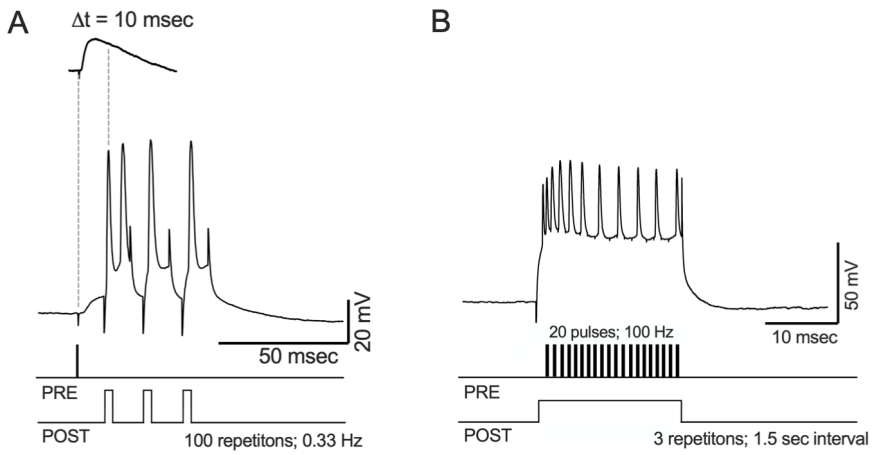

Figure 2.3: *LTP induction protocols*. (**A**) Spike time-dependent plasticity protocol: Each presynaptic stimulus was followed by (Δt = 10 msec) the delivery of 3 pulses (at 100 Hz) of 2-10 msec postsynaptic depolarization with an amplitude sufficient to evoke at least one action potential with100 repetitions at 0.33 Hz. (**B**) High-frequency stimulation protocol: Three bursts, at 1.5 sec intervals, of 20-presynaptic pulses at 100 Hz with, if needed, sufficient simultaneous postsynaptic depolarization such that at least some of the presynaptic stimuli evoke action potentials.

2.9 Glutamate uncaging:

A second Ti:sapphire laser (set at a wavelength of 720 nm) was used for glutamate uncaging with a pulse width of 0.3-0.6 msec and a maximum power of ~14 mW at the back focal plane (Matsuzaki et al. 2004); imaging and uncaging lasers were connected to the laser-scan head and microscope, respectively, through independent optical paths. Prior to two-photon uncaging, images were acquired with the use of a fluorescent slide photobleached at the 720 nm wavelength to establish precise parfocality and parcentricity of the point of photolysis (i.e., uncaging focal spot) with the imaging. MNI-glutamate (3 mM) was added to the perfusate and bath applied to the slices. Uncaging EPSPs (uEPSPs) and, in some experiments, uncaging Ca^{2+} transients (uPSCaTs) were evoked at targeted spines (~0.05 Hz). Laser power and position of the uncaging spot were adjusted until a consistent response was established. For uncaging-induced LTP (uLTP) experiments, the uncaging spot was repositioned to the tip of the spine head for every session, each of which consisted of 5-10 uncaging

pulses repeated every 5 minutes (Lee et al. 2009). uLTP was induced by a pairing procedure with 30 repetitions at 0.33 Hz timed such that the first AP was 10 msec after a presynaptic depolarization (Enoki et al. 2009).

2.10 Monte Carlo simulations:

Monte Carlo simulations were performed using the Monte Carlo cell (MCell) simulation environment (Stiles and Bartol 2001, Kerr et al. 2008), unless otherwise stated. All simulations were run and analyzed on a MacBook Pro (Quadcore 2.5 GHz Intel Core i7) and were performed with a time step of Δt = 1 μsec. Pre and postsynaptic compartments were modeled using simplified cubic geometries (0.5 x 0.5 x 0.5 μm; Zheng and Rusakov 2015) and separated by a cleft height of 20 nm (Savtchenko and Rusakov 2007). The presynaptic vesicular release site was positioned in the center of the upper cube (**Fig. 2.4**). The postsynaptic surface contained a circular disk (diameter of 250 nm) serving as the initial area for the postsynaptic density (PSD). The center most point of the disk was positioned in direct apposition to the presynaptic release site. Five concentric rings (R01-05; 25 nm in width) surrounded the central disk, hereafter referred to as the “core” of the PSD, until reaching the outer walls of the postsynaptic surface (**Fig. 2.4**). The volume of the extracellular space directly above each of the postsynaptic regions (i.e., the shell volume) was calculated as,

$$V = \pi r^2 h$$

where V is the volume, r is the radius of the region, and h is the height of the synaptic cleft. With the exception of the core volume, each shell volume was taken as the cylindrical volume of the extracellular space minus the volume of the preceding neighbouring shell volume.

Table 2.1: Values for parameters used for region and epoch

Region	Radius	Area	Total Area	Volume (L)	AMPARs	p_r
Core	125 nm	0.049 μm^2	0.049 μm^2	$9.82e^{-19}$	36	0.14
R01	150 nm	0.022 μm^2	0.071 μm^2	$4.28e^{-19}$	53	0.21
R02	175 nm	0.025 μm^2	0.096 μm^2	$5.1e^{-19}$	71	0.29
R03	200 nm	0.030 μm^2	0.126 μm^2	$5.9e^{-19}$	93	0.39
R04	225 nm	0.033 μm^2	0.159 μm^2	$6.7e^{-19}$	118	0.50
R05	250 nm	0.037 μm^2	0.196 μm^2	$7.5e^{-19}$	145	0.62

Total area calculated as area of core region plus area of surrounding regions (e.g., R01-05). The number of AMPA receptors randomly embedded within the PSD was determined by the linear approximation (i.e., solving for x given predictor values; Y = 740.4x – 0.01283; Nusser et al. 1998). The release probability for each epoch was similarly determined (Y = 3.27x – 0.02; Holderith et al. 2012).

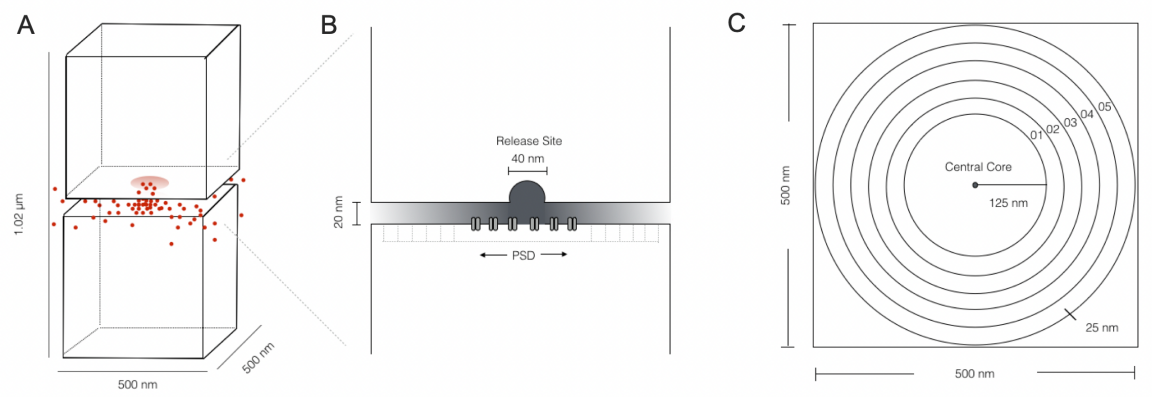

Figure 2.4: *Schematic of synaptic geometries for Monte Carlo simulations*. (**A**) Cubic elements (0.5 X 0.5 X 0.5 µm) made up the pre- and postsynaptic compartments. (**B**) Compartments were separated by a 20 nm synaptic cleft. A hemisphere (40 nm diameter) was aligned to the center of the presynaptic compartment and contained 2700 molecules of glutamate that were simultaneously released (with a 1 µsec delay from trial onset). Molecules diffused freely into synaptic regions with a specified diffusion coefficient and acted upon AMPA- and NMDA-type glutamate receptors embedded within the postsynaptic surface. (**C**) Rendering of the postsynaptic density (PSD): The PSD was divided into distinct regions. A central disk (125 nm radius) region was modeled as the central core of the PSD and was positioned 20 nm below the release site. Concentric rings (width 25 nm) surround the core region and continued outward until reaching the border of the postsynaptic cubic surface. Each region (Core and R01-05) served as putative sites for AMPAR insertion.

Release of glutamate: A total of 2700 molecules of glutamate were released into the cleft center (Savtchenko et al. 2013) in direct apposition to the central core of the PSD and was modeled as an instantaneous point source occurring within a hemispherical vesicle (diameter of 40 nm) to reach the cleft (see Clements 1996, Wahl 1996). A specific release probability (p_r) was assigned to each release site and each epoch (see **Table 2.1**). As surface area of the PSD has been shown to be directly proportional to the surface area of the active zone (Schikorski and Stevens 1997) and p_r scales with active zone size (Holderith et al. 2012), I estimated p_r for each epoch based on the PSD surface area; in simulations where stepwise increments in p_r occurred, the size of the step was estimated based on the area of the PSD (i.e., assumed equal to AZ area) and was determined by linear approximation; Y = 3.27x -0.02 (Holderith et al. 2012), where the predictor value x was the area of the PSD and Y was the expected value of p_r.

Glutamate diffusion and clearance: Based on the suggested values of Rusakov and colleagues (2011) I selected a D_{Glu} value of 0.32 μm^2 $msec^{-1}$, a value well in line with experimental estimates (Nielsen et al. 2004, Zheng et al. 2017). As receptor activation is sensitive to values of D_{Glu} (Holmes 1995) I tested additional lower and upper bounds of 0.22 and 0.42 μm^2 $msec^{-1}$, respectively. Concentric shells were positioned above each region of the PSD and extended the height of the synaptic cleft (20 nm). The number of transmitter molecules within each shell volume per unit time was used to calculate regional molarity. A simplified glial-like diffusion barrier (cubic structure; 0.54 X 0.54 X 1.06 μm; not depicted) was placed around the two synaptic compartments and acted as a sink for freely diffusing glutamate - interaction between glutamate molecules and this surface resulted in the elimination of glutamate from the simulation environment.

Glutamate receptor kinetics and placement: Glutamate receptor kinetics were assigned to both AMPA- (Robert and Howe 2003) and NMDA-type glutamate receptors (Lester and Jahr 1992, Attwell and Gibb 2005). The values for these

kinetic schemes are indicated in Table 2.1. Although conventional AMPAR kinetics schemes with a single open-state (Jonas, Major et al. 1993) are commonly used, I opted for a more representative model employing multiple open-states (Rosenmund et al. 1998, Robert and Howe 2003) with heterogeneous conductance values (Smith and Howe 2000, Smith, Wang et al. 2000). The current (in pA) per open-state for our model was set according to 2, 3, and 4 bound ligands as $O_2 = 0.4$, $O_3 = 0.9$, and $O_4 = 1.4$, respectively (Smith and Howe 2000, Smith, Wang et al. 2000). Current values were then summed for global AMPAR responses. The exact distribution and density of AMPARs within the PSD remains controversial. High-resolution immunogold labeling studies have demonstrated that low-affinity AMPARs may either be uniformly distributed within the PSD (Nusser et al. 1994, Masugi-Tokita and Shigemoto 2007, Masugi-Tokita et al. 2007) or present in an annular-like ring pattern surrounding the center of the PSD (Kharazia et al. 1996, Matsubara et al. 1996, Bernard et al. 1997, Kharazia and Weinberg 1997, Chen et al. 2008). Conversely, high-affinity NMDARs have been shown to be mainly present within the center-most position of the PSD (Racca et al. 2000). Because glutamate bound to receptors may alter the rate of diffusion (Nicholson and Phillips 1981) I included NMDARs in all simulations (data not shown). Importantly, the proportion of AMPARs has been shown to increase throughout postnatal development (Petralia et al. 1999) and following the induction of LTP (Hayashi et al. 2000). For these simulations, 36 AMPARs (Matsuzaki et al. 2001) and 20 NMDARs (Franks 2002) were randomly embedded within the central core of the PSD for initial characterization of baseline efficacy. In simulations involving successive enlargement of PSDs and insertion of new AMPARs, I increased the AMPAR number based on available immunogold labeling $Y = 740.4x - 0.01283$, where x was the PSD area and Y the number of AMPARs (see **Table 2.1**), and placed all new AMPARs within the annular rings surrounding the central core, starting with R01, and I continued to do so following each new epoch until reaching the outer limits of the postsynaptic geometry (i.e., R05). The placement of new AMPAR in the added regions assumes that the central core is at maximal packing density (i.e., that the PDZ

binding “slots” from scaffold proteins were occupied). The number and distribution pattern of NMDARs remained fixed throughout the course of all simulations.

TABLE 2.2: Rate constants describing AMPA and NMDA receptor kinetics

	AMPA Receptor		NMDA Receptor	
Parameters	Symbol	Value	Symbol	Value
On Rate	k_1	$2\times10^7\ M^{-1}\ s^{-1}$	k_1	$2\times5\times10^7\ M^{-1}\ s^{-1}$
Off Rate	k_{-1}	$9000\ s^{-1}$	k_{-1}	$4.7\ s^{-1}$
Open Rate	α	$8000\ s^{-1}$	α	$91.6\ s^{-1}$
Close Rate	β	$3100\ s^{-1}$	β	$46.5\ s^{-1}$
Desensitization Rate	δ_1	$1800\ s^{-1}$	δ_1	$8.4\ s^{-1}$
Resensitization Rate	γ_1	$7.6\ s^{-1}$	γ_1	$1.8\ s^{-1}$

The rate constants above refer to kinetic models used in Monte Carlo simulations. Primary references for rate constants of AMPARs (Robert & Howe, 2003) and NMDARs (Lester & Jahr, 1993).

2.11 Statistical analysis:

All data were tested for normality. Unpaired t-tests were used for independent comparisons between normal random variables while appropriate non-parametric tests were used if and when assumptions of normality or equal variances were not met. For dependent comparisons of normal random variables, paired t-tests were used while the non-parametric Mann-Whitney tests were employed for non-normal data. All comparisons were made with appropriate corrections. Pearson correlation coefficients were used for normal random variables while Spearman rank test was used when one or more random variables being compared were non-normal. Repeated Measures analysis of variance (RM-ANOVA), or the Friedman test, a non-parametric equivalent, were used to compare group effects over the course of LTP and uLTP experiments followed by Dunnet’s or Dunn’s multiple comparisons t-tests (versus baseline) for normal and non-normal data, respectively. In the event of outlier identification (ROUT method: Graphpad Prism 9), mixed-effects analyses were performed with Holm-Šídák's multiple comparisons test. Data were pooled post LTP or uLTP induction if no significant effect of time was found (i.e., at 15 and 30 min) and

mean differences (from baseline) were compared to respective control groups using appropriate t-tests. Univariate normality was assessed using D'Agostino-Pearson omnibus test in Graphpad Prism 9 while multivariate normality was tested using Henze-Kirkler test in R (RStudio, 2020; Korkmaz et al. 2014). Visualization of univariate and multivariate probability density functions (PDFs) was achieved using appropriate scripts in Mathematica (Wolfram Research) and Matlab (Mathworks, 2014B), respectively.

CHAPTER III: EXAMINING PRE AND POSTSYNAPTIC QUANTAL COMPONENTS IN RELATION TO SYNAPSE SIZE AT CA3-CA1 SYNAPSES IN RAT HIPPOCAMPUS UNDER LOW BASAL STIMULATING FREQUENCIES

3. Introduction

Central synapses are important sites of information processing and signal transduction within the mammalian brain. The functional properties of quantal transmission are such that vesicles fuse to the presynaptic membrane at a probabilistic rate following the invasion of an action potential, chemical transmitter enters and diffuses throughout the synaptic cleft, interacting stochastically with receptors embedded in the postsynaptic membrane. The small glutamatergic synapses in area CA1 of the hippocampus display remarkable variation in structure (Harris and Stevens 1989, Harris, Jensen et al. 1992) and functional states (Montgomery and Madison 2004). However, several structural and functional aspects within individual synapses show highly correlated relationships: in presynaptic boutons, for example, the number of docked vesicles and release probability (p_r) scale with active zone (AZ) size (Schikorski and Stevens 1997, Murthy et al. 2001, Holderith et al. 2012), postsynaptic spine volume scales with the size of the postsynaptic density (PSD; Harris and Stevens 1989, Bartol et al. 2015), responsiveness to photo-released transmitter scales with spine volume (Matsuzaki et al. 2001), the total AMPA receptor (AMPAR) number scales with the size of the PSD (Baude et al. 1995, Nusser et al. 1998), and the size of the presynaptic AZ scales with the size of the PSD (Schikorski and Stevens 1997).

Understanding the relationship between synaptic structure and function has been difficult due to a lack of methods capable of routinely monitoring presynaptic p_r, postsynaptic potency, and synapse size simultaneously at individually active synapses (Lisman 2017). I therefore used optical quantal analyses with conjoint morphological characterization of dendritic spines to understand how pre and postsynaptic quantal components scale in relation to morphological aspects of optically-confirmed active synapses. I found that at individual mature synapses, increase in synaptic size is associated with a corresponding increase in p_r while changes in synaptic potency do not scale for mature synaptic systems. These data conflict with the popular notion that larger synapses are made stronger via a greater number of AMPARs. Indeed, these data provide compelling experimental

support to the contrary, and support an alternative view of synaptic physiology that proposes a small central zone or “hotspot” of receptor activity within synapses (Rusakov and Kullmann 1998, Lisman and Raghavachari 2006, MacDougall and Fine 2014); larger synapses with a supposed greater number of AMPARs (Baude et al. 1995, Nusser et al. 1998, Takumi et al. 1999), would then not have a larger synaptic weight as the majority of membrane bound AMPARs would be too distant from the presynaptic release site to be sufficiently activated by cleft glutamate. Rather, these data suggest that as mature synaptic systems become larger, they efficiently modulate synaptic efficacy via an enhanced reliability of transmitter release (MacDougall and Fine 2014). I corroborate this view through Monte Carlo simulations and demonstrate that the effective size of PSD is limited to a central zone of 250-300 nm diameter and that AMPARs added at distances greater than this contribute negligibly to synaptic strength, at least for low frequency synaptic transmission.

3.1 Results

I recorded from individual CA1 pyramidal neurons in acute transverse slices of hippocampus using sharp microelectrodes filled with the fluorescent Ca^{2+} indicator Oregon Green 488 BAPTA-1 and the red-fluorescent morphological indicator Alexa 594 (note the use of false colour LUTs as indicated in Methods). Synaptic responses were evoked by remote (>50 μm) extracellular stimulation in Stratum Radiatum to activate Schaffer collateral afferents without risk of direct postsynaptic depolarization (**Fig. 3.1A**). Using two-photon fluorescence microscopy, I then systematically searched the apical dendrites for dendritic spines responsive to square-pulse stimulation of afferent fibers (see Chapter two). After locating an active spine, I carried out line-scan imaging of the responding synapse during stimulation at low frequencies and recorded the associated EPSPs and EPSCaTs or EPSCaT failures as previously described (Emptage et al. 1999, Reid et al. 2001, Enoki et al. 2009, MacDougall and Fine 2019). The xy image in Figure 3.1B shows the dendritic branch loaded with OGB-

1 (shown in red) with the active synapse surrounded by a white dashed box while the upper right image shows the same synapse with morphological marker (shown in green) from which estimates of synapse size are derived. Vertical xt image in Figure 3.1B (OGB-1) shows a red streak of fluorescence in response to synaptic stimulation (white line indicated time of stimulation), the precise timing of which was recorded by computer during data acquisition. The averaged EPSCaT trace monitored during successful transmission (%ΔF/F = 92.53 ± 6.22%) is shown in red and the average response of synaptic failures (%ΔF/F = -2.37 ± 2.94%) is shown in black (**Fig. 3.1D**). While monitoring EPSCaTs, I simultaneously recorded EPSPs from the somatic microelectrode (**Fig. 3.1C**). As EPSP responses tend to be, on average, larger for events that result in successful transmission (red trace in **Fig. 3.1F**) than those that result in synaptic failures (black trace in **Figure 3.1F**), I employed a subtractive procedure (Enoki et al. 2009, MacDougall and Fine 2019) to expose the mean unitary response to released transmitter at the imaged synapses (green trace in **Fig. 3.1F**). These optical quantal analyses in association with morphological characterization of spines allow for structure-function relationships to be discerned for individually active synapses.

3.1.1 Presynaptic release probability, but not postsynaptic potency, scales with spine size:

Despite considerable variability, the majority of excitatory connections between CA3 and CA1 pyramidal neurons are made by presynaptic boutons that form singular synapses onto dendritic spines, with single active zones (AZs) and postsynaptic densities (PSDs) of closely correlated surface areas (Schikorski and Stevens 1997). I reasoned that spine volume should serve as a good predictor of p_r based on the following rationale: *i.* spine volume serves as a good predictor of PSD size (Harris and Stevens 1989); *ii*. PSD surface area is directly proportional to the surface area of the AZ (Schikorski and Stevens 1997); *iii*. the number of docked vesicles scales with AZ area (Schikorski and Stevens 1997) and is

functionally correlated with transmitter release (Holderith et al. 2012). Indeed, p_r, probed via optically-detectable synaptic failure rates, varied across our sampled synapses from 0.043 ± 0.002 to 0.89 ± 0.032 (mean: 0.38 ± 0.03; n = 42) as did spine volume from 0.05 to 0.66 μm^3 (mean: 0.25 ± 0.02 μm^3) and p_r showed a positive linear correlation with volume (R = 0.60; y = 0.72x + 0.19; **Fig. 3.0E**). This result is consistent with data from Holderith et al. (2012), showing that p_r scales with AZ size, the number of docked vesicles, and voltage-gated Ca^{2+} channel (e.g., Cav2.1) number in boutons. Here, I show that spine volume is a reliable predictor of basal synaptic reliability.

Because total AMPAR number scales in relation to the size of the PSD (Baude et al. 1995, Nusser et al. 1998) and AMPAR currents scale in relation to spine volume during two-photon glutamate uncaging (Matsuzaki et al. 2001), synaptic potency in our experiments with physiological release of glutamate was expected to scale with spine size. Synaptic potency, probed via our subtractive procedure, varied across a wide range from 0.16 mV to 0.93 mV (mean of 0.45 ± 0.04; n = 36), falling within the range of amplitudes reported

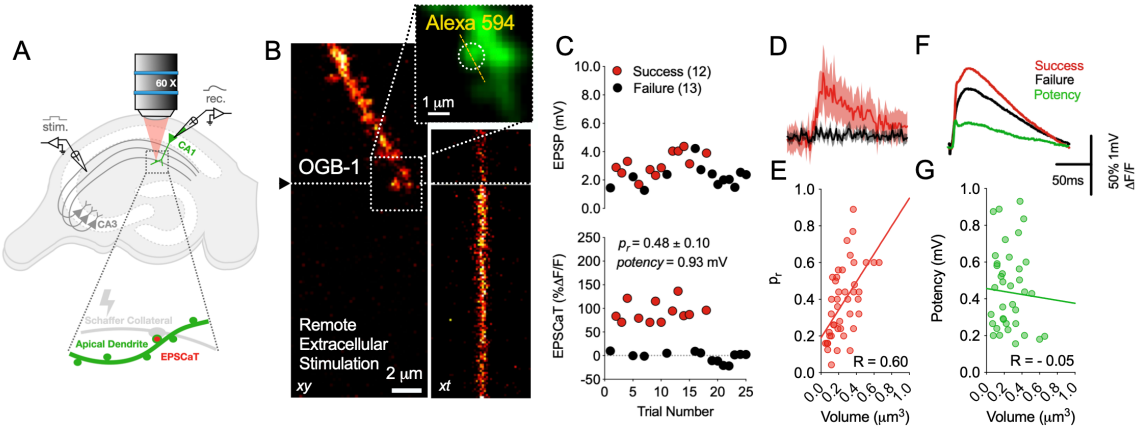

Figure 3.1: *Presynaptic release probability, but not postsynaptic potency, scales with spine size*: (**A**) Schematic of optical and electrical recording of CA1 pyramidal cells. An extracellular electrode is placed remotely (>50 µm from the target cell) in the stratum radiatum. Square pulses were delivered to evoked subthreshold EPSPs in the target cell while optically searching for spines that exhibit a stimulus evoked excitatory postsynaptic Ca^{2+} transient (EPSCaT). (**B**) Fluorescence images of dendritic branch with calcium indicator (OGB-1 shown in red). Dotted box indicates area of the active spine shown in inset with morphological marker Alexa 594 (shown in green). Black arrow indicates position along the xy image where the line scan through the spine was made. xt image reveals a line scan through the spine with EPSCaT. Dotted line in the xt image indicated time of electrical stimulation. (**C**) Scatter plot of EPSPs (above) measured in CA1 pyramidal cells with sharp microelectrode recordings with successes and failures determined via optical monitoring of EPSCaTs (below); trials that resulted in an EPSCaT were deemed successes (red circles) and those that did not were deemed failures (black circles). (**D**) Optically monitored successes of the synapse shown in B (red trace; %ΔF/F = 92.53 ± 6.22%) and failures (black trace; mean %ΔF/F = -2.37 ± 2.94%). (**E**) Presynaptic efficacy (p_r) and spine head volume show positive linear correlation (R = 0.60; ****p < 0.0001). Regression line indicated in red (Y = 0.76x + 0.19). (**F**) Mean EPSP traces that resulted in failure (black trace) were subtracted from mean EPSP of successes (red trace) to reveal potency (green trace). (**G**) Postsynaptic efficacy (potency) and spine head volumes show no significant correlation (R = -0.05; p = 0.77). Regression line indicated in green (Y – 0.08X).

during minimal stimulation experiments for CA1 pyramidal neurons (Turner 1988, Sayer et al. 1989, Friedlander et al. 1990, Sayer et al. 1990). Interestingly, and contrary to glutamate uncaging-elicited scaling of synaptic currents (Matsuzaki et al. 2001), potency, under these experimental conditions, showed no such scaling with spine volume ($R = -0.05$; $p = 0.77$). These data are at odds with commonly held views on the strengthening mechanisms of synaptic weight and will be discussed in relation to alternative viewpoints in subsequent sections.

3.1.2 Examining the range of influences on synaptic potency measurements

Because the distribution of potency values was broad and apparently multimodal (see **Fig. 3.6B**), I questioned the cause of such variance. Using a K-means clustering algorithm (Mathematica 12, Wolfram Research) I determined that our potency values could be grouped into three distinct clusters (in mV); a low group of 0.26 ± 0.02, a medium group of 0.53 ± 0.02; and a high group of 0.85 ± 0.07; **Fig. 3.2A**). Importantly, as with the group data, none of the three subgroups showed a correlation between spine volume (**Fig. 3.2B)**. Such clustering prompted questions related to the number of quanta released per synapse. I reasoned that if larger potency clusters were the result of multiple quanta summing, then I ought to be able to simulate the observed distribution of data based on multiple integers of the mean and variance from the lowest observed potency cluster (**Fig. 3.2B-D**), factoring in appropriate noise (~0.061 mV; data not shown). I simulated expected potency values using the same sample size as the experimental sample (**Fig. 3.2C, D**) as well as using 500 trials (**Fig. 3.2Ci and Di**). Both simulated potency distributions yielded peak amplitudes that did not differ significantly from the observed potency values (**Fig. 3.2E-G**), consistent with the possibility that the observed potency clusters (see **Fig. 3.6B**) could arise from the linear summation of evoked release of multiple quanta of transmitter at one or more sites presynaptic to the imaged synapse.

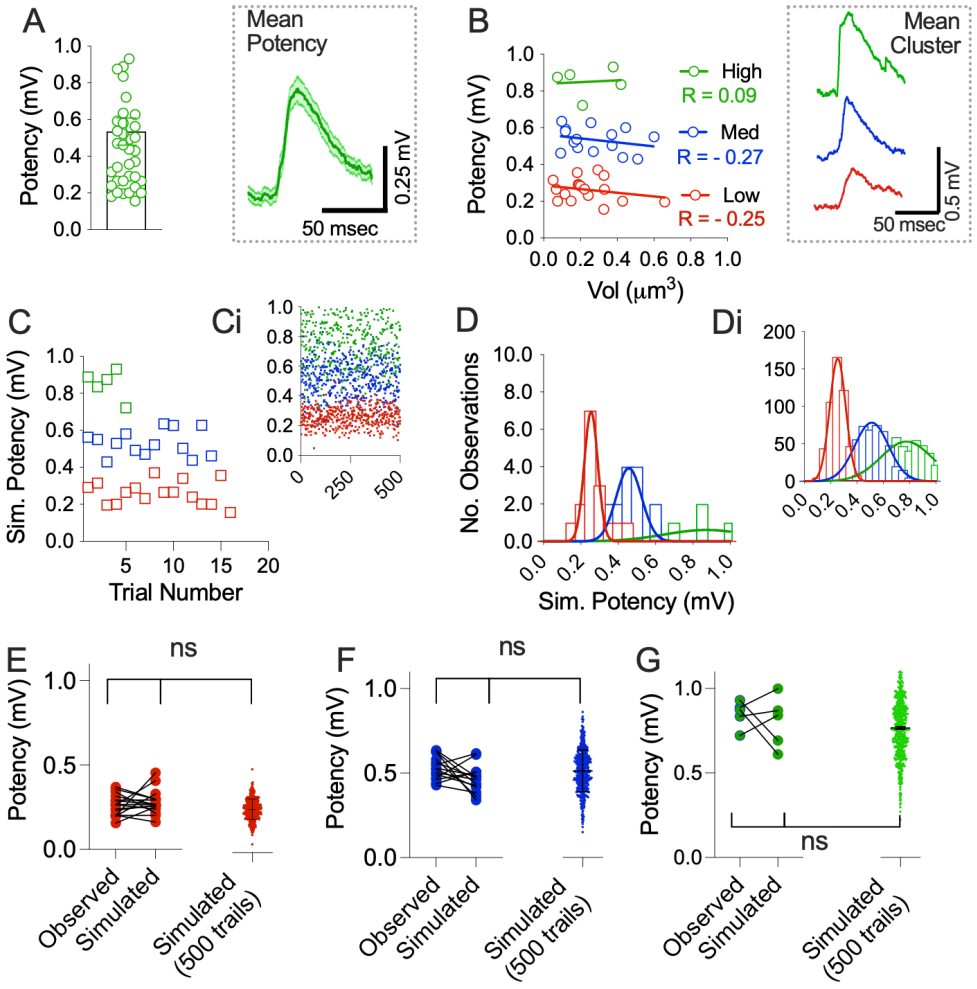

Figure 3.2: *K-means clustering of observed potency and simulations of potency based on multiple integers of lowest cluster mean and variance supports idea of multi-release events*. **(A)** Mean and spread of extracted potency values for all optical quantal analyses (n = 36). Mean potency trace for all imaged synapse is shown in dotted box. (**B**) k-means clustering of potency values reveals three distinct clusters; low (shown in red), medium (shown in blue), and high (shown in green). Each cluster shows no correlation with spine volume. Respective Pearson correlation coefficients shown in legend. Mean potency traces for each potency cluster shown in dotted box. (**C**) Simulated potency values based on multiple integers of the mean and variance of low potency cluster for 36 trials and (**Ci**) 500 trials. Histograms for simulated potency values for (**D**) 36 trials and (**Di**) 500 trials. Comparisons between observed and simulated potency values reveal no significant differences for (**E**) low (F = 1.40; ns; p = 0.25), (**F**) med (F = 1.20; ns; p = 0.30), and (**G**) high (F = 0.62; ns; p = 0.54) groupings. Dunn's multiple comparisons (all p > 0.05).

I next reasoned that if higher potency values were in fact due to multi-release events, then one might expect increases in postsynaptic Ca^{2+} response from the EPSCaT-generating spines, mediated presumably by an increase in the non-saturated NMDAR component (Mainen et al. 1999) and/or an enhanced release from internal Ca^{2+} stores (Emptage et al. 1999). Mean EPSCaT amplitudes were normally distributed (p = 0.20; not shown), and I observed a weak positive linear correlation (R = 0.35; p = 0.038) between EPSCaT amplitudes and potency values (**Fig. 3.3B**). When grouped according to potency cluster, mean EPSCaT amplitudes did not differ significantly between groupings (F = 2.56; ns; p = 0.9), though a weak but significant linear trend was evident (p = 0.03) with mean EPSCaT amplitudes increasing (in %ΔF/F) from 65.30 ± 5.69, 80.81 ± 8.71, and 94.82 ± 12.06 for low, medium, and high potency groupings, respectively (**Fig. 3.3C**). It is worth noting in this context that the ~15% increase in EPSCaT responses between groups is similar in magnitude to the average difference between single and double stimulus evoked Ca^{2+} responses shown by others (Mainen et al. 1999).

I next used fluorescence fluctuation analysis (Conti and Lisman 2003) of EPSCaTs to determine if synapses with higher potency values displayed higher variation. According to the uniquantal release model, each synapse releases at most a single vesicle thereby generating a stereotyped response with low (<0.2) CV (Stricker, Field et al. 1996). Alternatively, according to the multiquantal release model, a single synapse may release multiple vesicles; responses at a single synapse will thus show greater variability with the number of vesicles released and higher resultant CV (Conti and Lisman 2003), where

$$CV = \frac{\left(\sigma^2_{success} - \sigma^2_{failure}\right)^{0.5}}{\overline{EPSP}_{success}}$$

However, I found no significant difference between EPSCaT CV across potency clusters (p > 0.05; **Fig. 3.3C**).

Definitive conclusions of muli-release events based

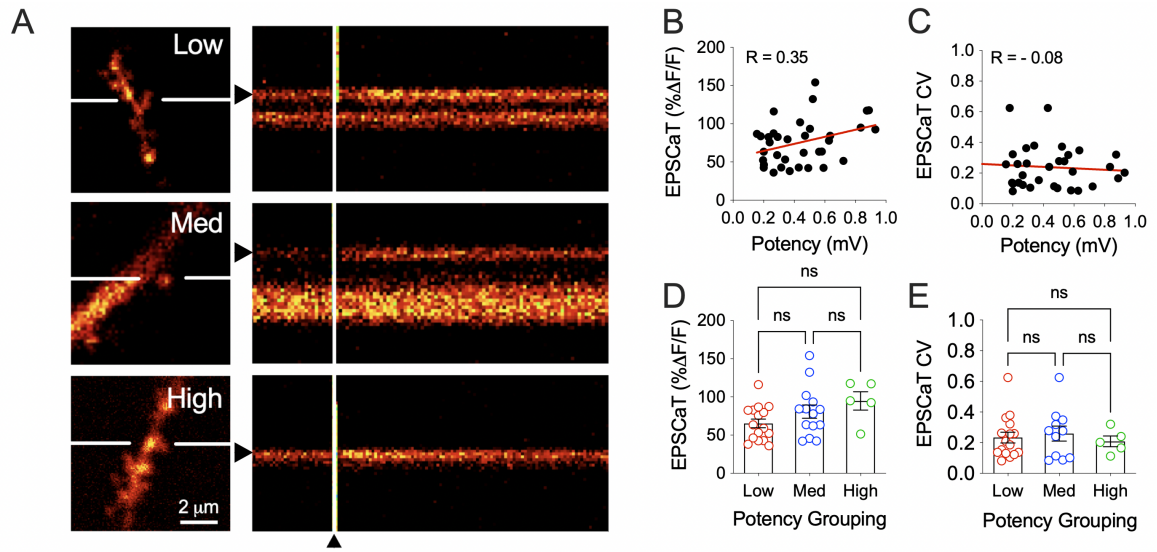

Figure 3.3: *EPSCaT amplitude and fluorescence fluctuation analyses across potency:* (**A**) Representative spines (left) and corresponding line scans (right) for successful transmission events for each potency grouping. White horizontal lines across spine images show region of line scans and black arrow head and white vertical line in line scan images indicates timing of extracellular stimulation. All initial line scans (up to stimulation) were 50 msec (**B**) Mean EPSCaT amplitudes and potency values show weak, albeit significant, positive correlation (R = 0.35, *p = 0.038). (**C**) EPSCaT coefficient of variation (CV) shows no correlation with observed potency values (R = -0.08, p > 0.05). (**D**) EPSCaT amplitudes for potency groupings show a modest linear trend (*p = 0.03), increasing with potency group. (**E**) EPSCaT CV shows no difference across potency groupings. Error bars indicate s.e.m.

on spine Ca^{2+} dynamics, however, may not be possible due to the dominant contribution of store release to the Ca^{2+} transients (Emptage et al. 1999). I therefore sought to explore alternative factors such as cable attenuation along the dendritic arbour (Rall 1960, Jack et al. 1981, Stuart and Spruston 1998) and spine neck geometry (Araya et al. 2006, Araya et al. 2014, Tonnesen et al. 2014) that might influence measurements of potency. I first explored the possibility that cable attenuation along the dendritic arbour and the positioning of the active synapses, relative to the somatically-placed recording electrode, posed an influence on the measurements of potency. As I did not routinely measure the distance of the imaged spine from the soma, I instead examined the amplitude and waveform characteristics of the compound EPSPs (Turner 1988) that were optically confirmed to have resulted in successful transmission (i.e., those responses that resulted in an EPSCaT). Since proximal synapses are generally observed to be more efficacious than distal ones (Turner 1988, Sayer et al. 1980; although see Andrasfalvy and Magee 2001) I reasoned if cable attenuation were responsible for the observed potency distribution, then I should see distinct waveform patterns per potency grouping, as proximal and distal synapses are known to have distinct waveform properties discernible even with small compound EPSPs (Rall 1967, Turner 1988). I found no evidence of significant variation in amplitude or waveform characteristics for compound EPSPs that resulted in an EPSCaT at the imaged spines and thus in the location of the monitored synapses along the proximal-distal axis of the dendritic arbour (**Fig. 3.4B-F**). I conclude therefore that the sampled synapses are likely drawn from a similar population of spines along the dendritic tree.

Lastly, the attenuation of synaptic potentials may be brought about by resistivity of the spine neck (Koch and Poggio 1983, Araya et al. 2006, Tonnesen et al. 2014). I therefore estimated spine neck length by calculating the distance from the tip of spine head to the base of the dendritic shaft and subtracting out the width of the spine head (see chapter 2). Estimates of spine neck length varied across imaged synapses (**Fig. 3.5A**) and was normally distributed within the sample. Interestingly, I found that potency values display a significant negative

correlation with spine neck length (R = - 0.48; *p* = 0.004; **Fig. 3.5B**), decreasing across potency clusters (Low: 0.66 ± 0.6 ; Med: 0.42 ± 0.07 High: 0.14 ± 0.10 µm; **Fig. 3.5D**), suggesting that the

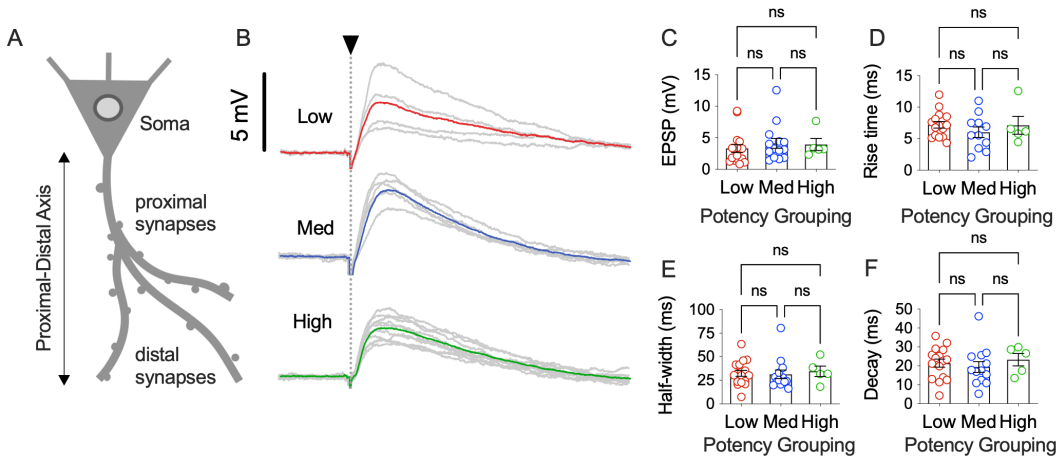

Figure 3.4: *Amplitude and waveform characteristics of small compound EPSPs suggest similar population and loci of synaptic contacts for each potency cluster*: (**A**) Schematic of experimental rationale depicting a pyramidal neuron with proximal and distal synapses. (**B**) Representative compound EPSP traces from different potency (i.e., unitary EPSP) clusters during successful transmission events (EPSCaT-generating events) at the imaged spine; individual trials that resulted in a success (gray traces) and the corresponding mean (coloured trace). Traces are 150 msec in length. (**C**) Mean peak amplitude of compound EPSPs that resulted in a success across potency clusters. (**D**) 10-90% rise times, (**E**) half-width, (**F**) and decay times for compound EPSPs that resulted in success. All comparisons were not significantly different across potency groupings ($p > 0.05$). Error bars indicate s.e.m.

range and groupings of our potency measurements were indeed influenced, at least in part, by this aspect of spine neck geometry. It is worth mentioning here that the correlation between spine volume and spine neck length was not significant ($R = -0.29$, $p = 0.06$; data not shown). It will be interesting to examine the contribution of spine neck width to the observed attenuation in future analyses.

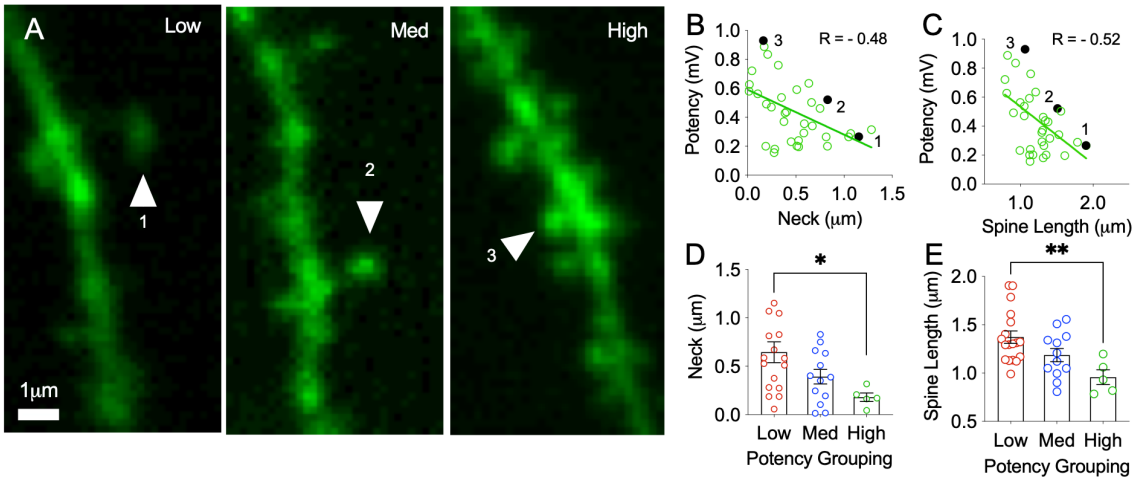

Figure 3.5: *Spine neck length influences potency measures*: (**A**) Representative morphological (Alexa 594; false colour) images of dendritic branches with responsive spines (indicated by arrow head) grouped according to potency cluster. (**B**) Potency and spine neck length show a significant negative linear correlation (R = - 0.48; **p* = 0.004). Regression line shown in green (Y= 0.31x + 0.59). (**C**) Potency and total spine length, measured as the distance from the tip of the spine head to base of the dendritic shaft, show a significant negative linear correlation (R = - 0.52; ***p* = 0.002). Regression line shown in green (Y= 0.39x + 0.92). (**D**) Bar graph of all spine neck lengths clustered according to potency grouping. Spine neck length showed significant linear trend with potency grouping (*p* = 0.0046), decreasing with potency cluster. ANOVA revealed significant difference in groupings (F = 2.232; **p* = 0.029) and Dunnet's corrected t-tests revealed a significant difference between low and high groupings (**p* = 0.01). (**E**) Bar graph of all spine lengths clustered according to potency grouping. ANOVA revealed a significant difference in total spine length in grouping (F = 5.95; ** *p* = 0.006) and corrected t-tests revealed a significant difference between low and high groupings (***p* = 0.008). Black data points 1,2, and 3 (black circles in B and C) correspond to the spines shown in A.

3.1.3 Release probability and potency are independent quantal components at CA3-CA1 synapses

I next examined the functional relationship between pre and postsynaptic quantal components. Both p_r and potency were tested for univariate normality using the D'Agostino-Pearson omnibus test (**Fig. 3.6A, B**). Both quantal components were univariate normal: for pr, $p = 0.41$ and for potency $p = 0.18$; quantile-quantile (QQ) plots were generated to graphically visualize normality of each quantal component against theoretical normal distributions with the same means and variances of the observed data (**Fig. 3.6Ai-ii, Bi-Bii**). Pearson's correlation coefficient was used to assess the relationship between pre and postsynaptic components. Interestingly, I found no functional correlation between p_r and potency (R = -0.11; ns; y = -0.1284x + 0.4115; **Fig. 3.6C**). Henze-Zirkler test was performed (Korkmaz et al. 2014) to assess multivariate "joint" normality of p_r and potency, which were shown to be jointly normal (HZ = 0.44; $p = 0.50$; **Fig. 3.6D**). The results here indicate, importantly, that this uncorrelated bivariate data set passes tests of marginal and joint normality and thus that the quantal components of transmission at CA3-CA1 synapses may be said to be functionally uncoupled or independent (Lancaster 1963, Pierce and Dykstra 1969, Henze and Zirkler 1990). These results are compatible with those of other hippocampal excitatory synapses (Biro et al. 2005) but are at odds with the functional correlation between pre and postsynaptic efficacies found at neocortical synapses (Hardingham et al. 2010). Overall, the results of these optical quantal analyses in association with morphological estimates of synapse size, indicate that variations in basal synaptic strength at excitatory synapses onto CA1 pyramidal cells primarily reflects differences in reliability of synaptic transmitter release, coupled with an effect of spine neck length restricting or augmenting responsiveness to released transmitter.

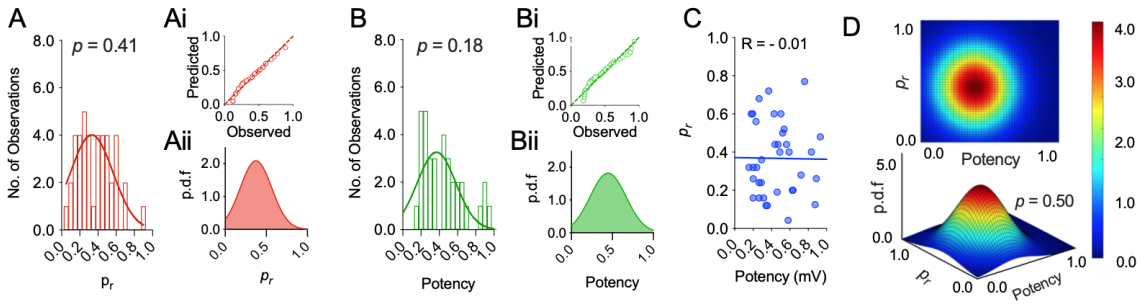

Figure 3.6: *p_r and potency are independent quantal components at CA3-CA1 synapses*: (**A**) Sample distribution of p_r with Gaussian fit. p_r was univariate normal (D'Agostino-Pearson; p = 0.41). (**Ai**) QQ plot and (**Aii**) probability density function for observed p_r. (**B**) Sample distribution of observed potency values with Gaussian fit. Potency was univariate normal (D'Agostino-Pearson; p = 0.18). (**Bi**) QQ plot and (**Bii**) probability density function for observed potency. (**C**) p_r and potency are uncorrelated normal random variables (R = -0.01). (**D**) 2- (top) and 3D (bottom) probability density functions of p_r and potency showing multivariate normality (Henze-Zirkler: p = 0.50).

3.1.4 Monte Carlo model of mature synaptic architectures reveals hotspot of receptor activity opposite functional release sites.

To better understand the scaling of p_r and potency in relation to synapse size I performed Monte Carlo simulations of synaptic transmission, relying upon previously published ultrastructural (Harris and Stevens 1989, Harris et al. 1992, Nusser et al. 1994, Baude et al. 1995, Schikorski and Stevens 1997, Nusser et al. 1998, Shepherd and Harris 1998) and functional (Ward et al. 2006, Enoki et al. 2009, Holderith et al. 2012) data for relationships between pre- and postsynaptic sites (see Chapter 2). Such simulations complement the experimental findings here and extend previous models used to explore the spatiotemporal relationship between diffusible transmitter and receptor activation at radial distances from sites of transmitter release (Rusakov and Kullmann 1998, Raghavachari and Lisman 2004). For these simulations I relied on simplistic cubic geometries (Zheng and Rusakov 2015) for our pre and postsynaptic structures (**Fig. 3.7A**) and complex AMPAR kinetics with multiple open states and heterogenous current values (**Fig. 3.7B-C**). I set presynaptic p_r to values expected for a given PSD/AZ size (Holderith et al. 2012) and ran through several epochs (see table 2 in chapter 2), adjusting both pre and postsynaptic variables every 20 trials. The total amount of glutamate released was held constant and glutamate concentration measured at distinct regions of the synaptic cleft (**Fig. 3.7D).** All simulations were repeated using different effective glutamate diffusion coefficients (**Fig. 3.7**; results summarized in **Tables 3.1** and **3.2**).

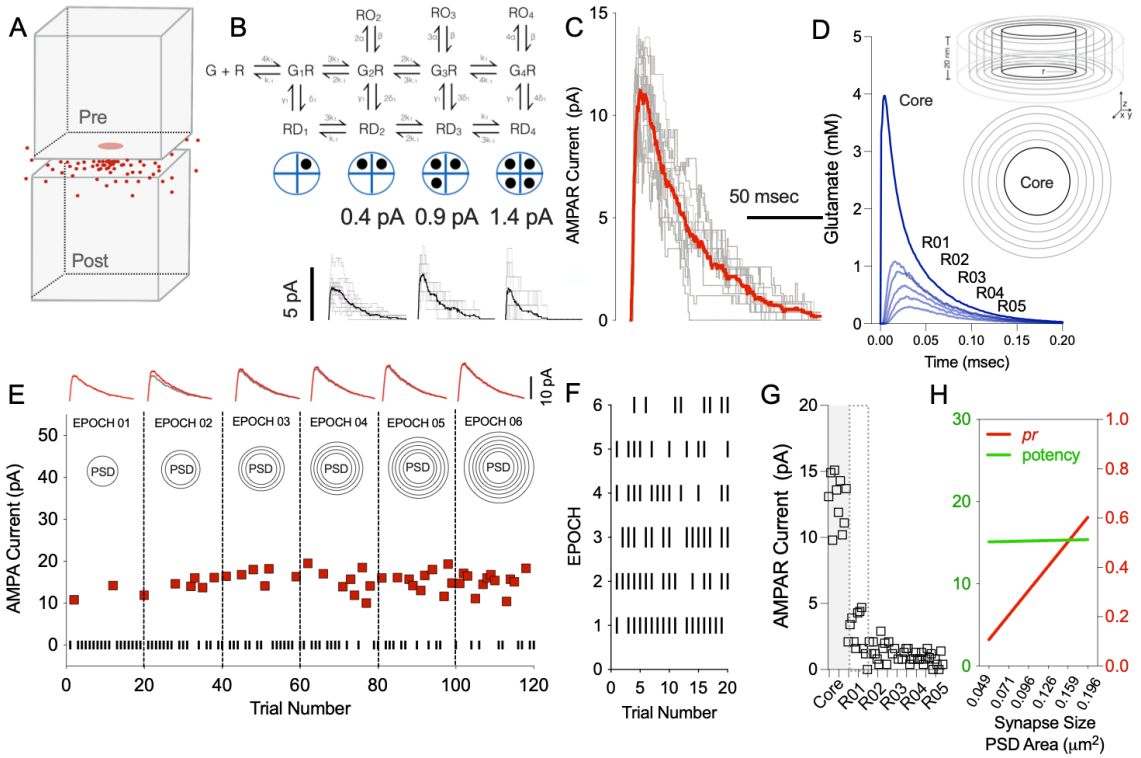

Figure 3.7: *Monte Carlo simulations of pre and postsynaptic efficacies*: (**A**) Schematic of cubic geometries used for pre and postsynaptic compartments. (**B**) AMPA receptor kinetics with multiple open states and heterogenous current values. Schematic of tetrameric AMPAR with number of bound ligand (black circles) and associated current values shown below. Individual trials (gray traces) and mean (black traces) are shown. (**C**) Average AMPAR current within the core region at D_{GLU} = 0.32; individual traces (gray) and mean trace (shown in red) demonstrate typical AMPAR current responses (**D**) Glutamate profile for regions within the synaptic cleft. Inset shows cylindrical shells (top) from which molecular count and glutamate concentration was determined and birds eye view of the boundaries within the PSD for each region (bottom). (**E**) A representative scatter plot of AMPAR current (red squares) and failures (black squares) following the stepwise increases in synaptic elements in accordance with Table 2. Average AMPAR current traces (red) for each epoch is shown above for each epoch with previous epoch traces (grey) superimposed. Note the contribution of new AMPARs becomes negligible at distances greater than 300 nm (i.e., beyond R01) from the central release site. (**F**) Synaptic failures (black lines) per epoch. (**G**) Comparisons of AMPAR current across regions of the PSD reveal core region is a hotspot of receptor activation. (**H**) Linear predictors of p_r (right y axis) and potency (left y axis; in pA) for mature synaptic systems with PSDs greater than 300 nm.

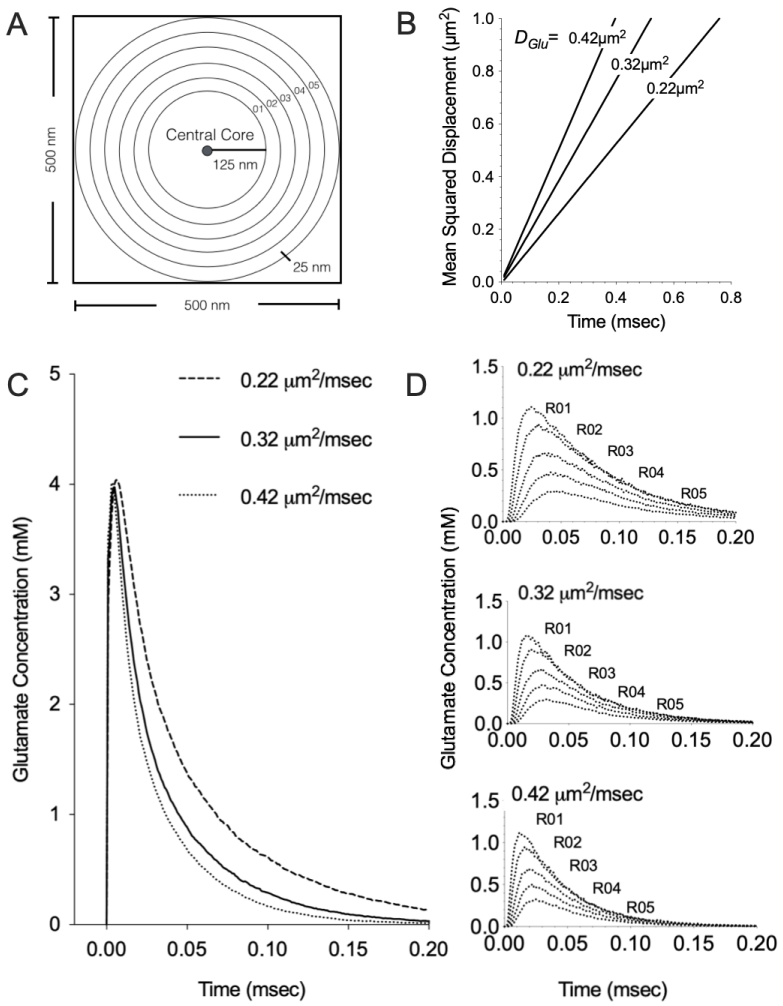

Figure 3.8: *Glutamate profiles in Monte Carlo simulations*: (**A**) Schematic rendering of the postsynaptic density. Regions were subdivided into a central core (125 nm radius) and peripheral regions (R01-05) with 25 nm radial increments per region. The height of the synaptic cleft (not shown) was set at 20 nm (**B**) Theoretical mean square displacement profiles of glutamate molecules for each effective diffusion coefficient. (**C**) Glutamate concentration (in mM) within the central core of the cleft across values of D_{GLU}. (**D**) Glutamate concentration (in mM) within each peripheral region across values of D_{GLU}.

Open State	Core	R01	R02	R03	R04	R05
Double Bound						
0.22μm^2 ms^{-1}	0.34 ± 0.02	0.22 ± 0.03	0.21 ± 0.03	0.17 ± 0.02	0.12 ± 0.02	0.05 ± 0.02
0.32μm^2 ms^{-1}	0.27 ± 0.02	0.15 ± 0.03	0.15 ± 0.02	0.14 ± 0.02	0.08 ± 0.02	0.04 ± 0.01
0.42μm^2 ms^{-1}	0.25 ± 0.02	0.15 ± 0.01	0.12 ± 0.30	0.10 ± 0.01	0.07 ± 0.01	0.04 ± 0.01
Triple Bound						
0.22μm^2 ms^{-1}	0.25 ± 0.03	0.08 ± 0.02	0.07 ± 0.02	0.03 ± 0.02	0.01 ± 0.01	0.01 ± 0.01
0.32μm^2 ms^{-1}	0.21 ± 0.02	0.06 ± 0.01	0.02 ± 0.01	0.02 ± 0.01	0.01 ± 0.01	0.00 ± 0.00
0.42μm^2 ms^{-1}	0.16 ± 0.02	0.04 ± 0.01	0.02 ± 0.01	0.01 ± 0.01	0.00 ± 0.00	0.00 ± 0.00
Quad Bound						
0.22μm^2 ms^{-1}	0.13 ± 0.02	0.01 ± 0.00	0.01 ± 0.00	0.0 ± 0.0	0.0 ± 0.0	0.0 ± 0.0
0.32μm^2 ms^{-1}	0.09 ± 0.02	0.01 ± 0.00	0.00 ± 0.00	0.0 ± 0.0	0.0 ± 0.0	0.0 ± 0.0
0.42μm^2 ms^{-1}	0.02 ± 0.01	0.01 ± 0.01	0.01 ± 0.00	0.0 ± 0.0	0.0 ± 0.0	0.0 ± 0.0

Table 3.1: Open probabilities across regions and diffusion coefficients for AMPARs: measured during the first 10-1000 μsec of each run (10 trials). Peak values that occurred outside this window were not included in the analysis. All data shown as mean ± s.e.m.

Open State	Core	R01	R02	R03	R04	R05
Double Bound						
0.22μm^2 ms^{-1}	4.68 ± 0.27	2.48 ± 0.37	1.47 ± 0.16	1.46 ± 0.16	1.16 ±0.16	0.76 ± 0.20
0.32μm^2 ms^{-1}	3.56 ± 0.33	1.60 ± 0.12	1.16 ± 0.20	0.85 ± 0.12	0.92 ± 0.13	0.40 ± 0.15
0.42μm^2 ms^{-1}	3.70 ± 0.16	1.56 ± 0.20	1.20 ± 0.14	1.00 ± 0.13	0.68 ± 0.12	0.32 ± 0.14
Triple Bound						
0.22μm^2 ms^{-1}	7.47 ± 0.73	1.89 ± 0.34	0.63 ± 0.23	0.56 ± 0.16	0.10 ± 0.10	0.10 ± 0.10
0.32μm^2 ms^{-1}	6.66 ± 0.67	1.35 ± 0.30	0.27 ±0.14	0.30 ± 0.15	0.18 ± 0.12	0.09 ± 0.09
0.42μm^2 ms^{-1}	4.05 ± 0.36	0.81 ± 0.21	0.36 ± 0.15	0.39 ± 0.18	0.36 ± 0.15	0.18 ±0.12
Quad Bound						
0.22μm^2 ms^{-1}	4.06 ± 0.57	0.42 ± 0.21	0.0 ± 0.0	0.0 ± 0.0	0.0 ± 0.0	0.0 ± 0.0
0.32μm^2 ms^{-1}	3.08 ± 0.62	0.28 ± 0.19	0.0 ± 0.0	0.0 ± 0.0	0.0 ± 0.0	0.0 ± 0.0
0.42μm^2 ms^{-1}	2.10 ± 0.43	0.14 ± 0.14	0.0 ± 0.0	0.0 ± 0.0	0.0 ± 0.0	0.0 ± 0.0

Table 3.2: AMPAR currents across synaptic regions and effective diffusion coefficients: Averaged peak AMPAR currents (in pA) measured during the first 10-1000 μsec of each run (10 trials). Peak values that occurred outside this window were not included in the analysis. All data shown as mean ± s.e.m.

A representative trace of AMPAR current is shown for the central core region (**Fig. 3.7C**) and a plot of AMPAR current (red squares) as well as synaptic failures (black lines) across epochs is shown in Figure 3.7E. It is clear from our simulations that as the area of synaptic specializations increase, synaptic failures rates decrease (**Fig. 3.7D**) and although the number of embedded AMPARs also increases, the change in AMPAR open probability (**Table 3.1**) and thus current (**Table 3.2**) was negligible at distances >300 nm (**Fig. 3.7E**). Figure 3.7H shows the linear trends for the expected p_r and potency values for mature synaptic systems, results that complement the experimental findings and help explain why the potency values did not scale with the size of synapses: *AMPARs added to newly available slots of an expanding PSD are too far from the presynaptic release site to sense the millimolar concentrations of glutamate necessary for opening and thus do not contribute significantly to synaptic potency*, at least for low frequency transmission.

3.2 Discussion

I investigated the relationship between pre and postsynaptic quantal components of transmission in relation to synapse size for individually active CA3-CA1 glutamatergic connections in acute hippocampal slice preparations. I demonstrated that *i.* p_r scales with spine volume (see **Fig. 3.1E**)*, ii*. potency and spine volume are uncorrelated (see **Fig. 3.1G**), *iii*. p_r and potency are independent quantal components of transmission across the population of synapses under investigation (see **Fig. 3.6C-D**), and *iv.* potency is influenced by spine neck length (see **Fig. 3.5**). I further demonstrated, using Monte Carlo simulations, that the likely reason potency does not scale with synapse size at mature synapses is that the effective radius of AMPAR activation is limited to a small central zone or “hotspot” of glutamate activity opposed to functional release sites. These results are discussed in relation to the glutamate hotspot hypothesis and their implications for forms of long-term synaptic plasticity.

p_r scales with estimates of spine size and affords an efficient gain control mechanism for mature synaptic systems

Minimal stimulation of Schaffer collaterals results in activation of a few synapses at most or, in some cases, a unitary synaptic response, on postsynaptic CA1 neurons (Turner 1988, Sayer et al. 1989, Sayer et al. 1990, Stevens and Wang 1995, Enoki et al. 2009). Serial electron micrographs indicate that dendritic spines of CA1 pyramidal cells contain, on average, a single "macular" PSD and receive synaptic input from a single presynaptic bouton (Sorra and Harris 1993), typically containing a single active zone (Harris and Stevens 1989, Shepherd and Harris 1998). The p_r at individual synapses can be reliably established by optical readout of successful and failed transmission events (Denk et al. 1996, Emptage et al. 1999), thereby reducing ambiguities and interpretations of the evoked responses. Here, I show heterogeneity in p_r across the sampled EPSCaT-generating synapses and that average p_r shows a positive linear correlation with spine size, and by inference, with synapse size. These observation are in line with a previous accounts of p_r scaling with aspects of the presynaptic microenvironment (e.g., size of the AZ and number of VGCCs; Holderith et al. 2012). Although I attempted to determine *n*, defined here as the number of vesicles released at each imaged synapse, ambiguities prevented definite conclusions of multi-release events. It remains to be determined whether the selection of synapses is biased toward larger spines with ER stores (Spacek and Harris 1997), whether our activated synapses have perforated PSDs and/or AZs with more than one functional release site per bouton (Sorra and Harris 1993), or whether EPSCaT-generating synapses behave like other mature synapses that lack the necessary machinery for optical detection. Regardless of their ubiquity, the contribution of EPSCaT-generating synapses to the multisynaptic evoked responses of CA3-CA1 connections is substantial (Enoki et al. 2009). The exact mechanism by which this presynaptic scaling phenomenon occurs remains to be determined but our data nevertheless demonstrate that p_r is a major determinant of basal synaptic strength and could afford an efficient gain

control mechanism for mature synaptic systems and their plasticity when postsynaptic efficacies saturate or are limited.

CHAPTER IV: EXAMINING STRUCTURE-FUNCTION RELATIONSHIPS OF INDIVIDUALLY ACTIVE SYNAPSES DURING THE EXPRESSION OF LONG-TERM POTENTIATION AT HIPPOCAMPAL CA3-CA1 SYNAPSES

4. Introduction

Long-term modifications of synaptic connectivity, such as the growth of new synapses (Ramón y Cajal 1893) or the modification of pre-existing synapses (Tanzi 1893, Hebb 1949), have long been thought to underlie information storage in the mammalian brain. Functional alterations in synaptic connectivity in the form of long-term potentiation (LTP; Bliss and Lømo 1973) and depression (LTD; Dudek and Bear 1992) remain the leading cellular candidates of mnemonic processing, providing synapses with a functional means to strengthen or weaken their efficacies, respectively. Pinpointing the locus of functional expression, be it pre or postsynaptic, remains an important and elusive task (Bliss and Collingridge 2013, MacDougall and Fine 2014). Long-term structural changes associated with LTP, such as persistent enlargement of spine head volume (Van Harreveld and Fifkova 1975, Fifkova and Van Harreveld 1977, Matsuzaki et al. 2004, Tanaka et al. 2008, Bosch et al. 2014, Meyer et al. 2014) increases in spine density (Engert and Bonhoeffer 1999, Maletic-Savatic 1999, Toni et al. 1999, Jourdain et al. 2003, Nagerl et al. 2004), and alterations in spine neck geometry (Araya et al. 2014), also remain contested (Hosokawa et al. 1995, Sorra and Harris 1998, Lang et al. 2004, Popov et al. 2004, Bagal et al. 2005). Despite much progress, it remains unclear whether the primary strengthening mechanism of LTP is pre or postsynaptic and whether these so-called morphological correlates are necessary components to the functional expression of LTP. Considerable efforts have thus been undertaken in recent years to understand how individual synapses respond, both functionally and structurally, during the expression of long-term synaptic plasticity (Yuste and Bonhoeffer 2001). Resolution of these issues is possible by combining optical quantal analyses (MacDougall and Fine 2019, Padamsey et al. 2019) with morphological characterization of individually active synapses (Matsuzaki et al. 2004) before and after plasticity.

Here, I demonstrate that when LTP is induced under the physiological release of glutamate via remote synaptic stimulation there is a persistent increase in the average p_r at individual synapses while the average postsynaptic potency, or responsiveness to released glutamate, remains unchanged. Moreover, I could

find no evidence of new spine growth or persistent spine enlargement following LTP. I do observe an “on average” transient increase in spine volume immediately following LTP induction as seen by others (Lang et al. 2004). I note, however, that similar enlargement was evident in a subset of experiments in which potentiation failed to occur but not in those experiments in which no induction protocol was administered, suggesting that enlargement may be independent of potentiation. In contrast, when LTP is induced via photolytic-release of glutamate (uLTP) I observe a persistent increase in responsiveness to ectopic glutamate, a sustained enlargement of spine volume, and a reduction in spine neck length. Comparisons of baseline functional and structural data reveal no difference in the selection criteria for the sampled synapses, suggesting that the difference in results is due to differences inherent in the methodology of synaptic stimulation. Such data supports previous literature on the presynaptic expression of LTP (Bolshakov and Siegelbaum 1994, Emptage et al. 2003, Ahmed and Siegelbaum 2009, Enoki et al. 2009) while casting considerable doubt on suggestions of functional postsynaptic strengthening mechanisms and the necessity of structural correlates of LTP (Matsuzaki et al. 2004, Harvey and Svoboda 2007, Lee et al. 2009), and provides insights into the temporal aspects of the morphological changes of spines. This combined approach is a powerful experimental strategy for assessing the dynamics of synaptic form and function during activity-dependent synaptic modification.

4.1 Results

4.1.1 LTP is associated with a persistent increase in presynaptic release probability and transient enlargement of spine head volume.

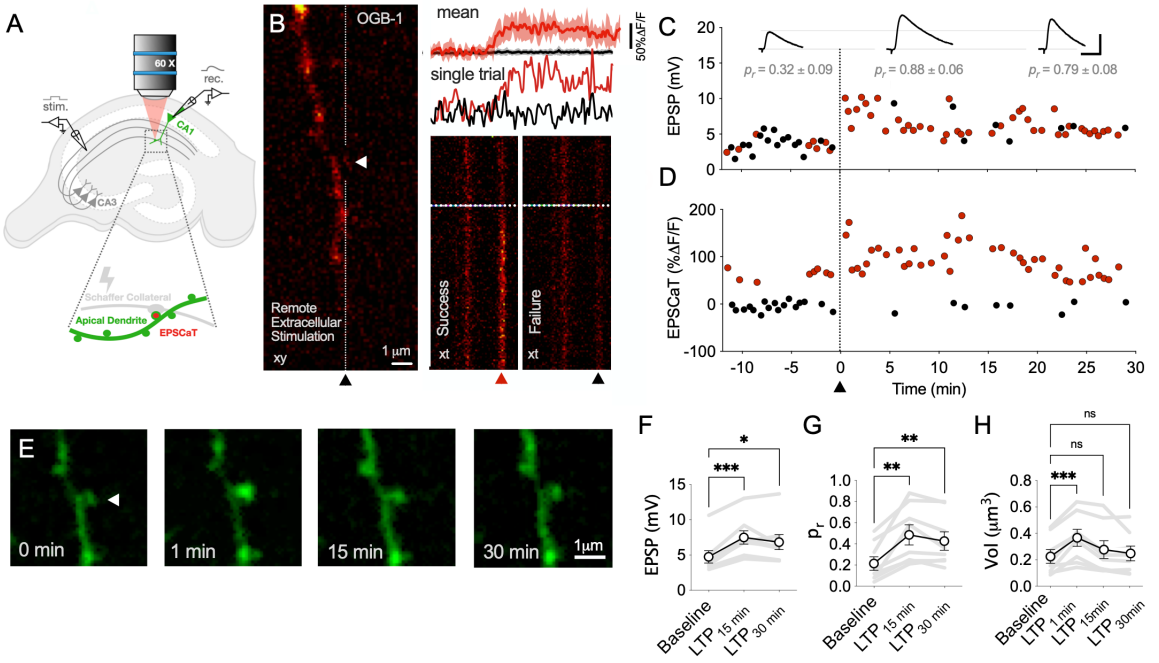

Figure 4.1: *LTP is associated with a persistent increase in presynaptic release probability and transient enlargement of dendritic spines*: (**A**) Schematic of experimental conditions (as in Chapter 2). (**B**) Representative fluorescence image of a dendritic branch with an active spine indicated by white arrow head. EPSCaTs were monitored via line-scan imaging of OGB-1 fluorescence across the spine and dendritic branch (trajectory indicated by vertical white line. Timing of the extracellular stimulation is indicated by dotted horizontal line across each line scan image. Successful synaptic transmission (left xt image) can be clearly distinguished from transmission failures (right xt image). Mean fluorescence traces from this spine during successful transmissions (red) and transmission failures (black) are shown above (top) with individual single trial fluorescence traces for the corresponding line scan images shown below. (**C**) EPSP amplitudes plotted for each stimulus before and after LTP induction (indicated by black arrow and dotted line) with successful transmission and failures marked by red and black circles, respectively. Average EPSP traces of baseline and at 15 and 30 minutes after LTP induction are shown above with the corresponding p_r values for each epoch (25 trials) shown below. (**D**) EPSCaT amplitudes plotted for each stimulus before and after LTP induction with red and black circles indicating successes and failures as above. (**E**) Fluorescent morphological image of dendritic spine (as in A) before and at distinct time points after LTP induction. (**F**) Individual and mean EPSPs across epochs (F = 13.00, ***p = 0.003) at baseline (4.79 ± 1.01), 15 min (7.61 ± 1.07; ***p = 0.0009), and 30 min (6.75 ± 1.20; *p = 0.025) post LTP induction. Persistent increases in EPSP amplitude are indicative of increases in synaptic efficacy of the stimulated pathway. (**G**) Individual and mean p_r across epochs (F = 14.00, ****p < 0.0001) at baseline (0.22 ± 0.07), 15 min (0.49 ± 0.11; ***p = 0.006), and 30 min (0.43 ± 0.10; *p = 0.035) post LTP induction. (**H**) Individual and mean volume measurement for spines across epochs (F = 13.95, ** p = 0.003) at baseline (0.21 ± 0.07), 1 min

(0.39 ± 0.08; ***p = 0.0007), 15 min (0.31 ± 0.08; ns; p = 0.16), and 30 min (0.28 ± 0.07; ns; p = 0.52) post LTP induction. Error bars indicate s.e.m.

I recorded from individual CA1 pyramidal neurons in acute transverse slices of hippocampus using sharp microelectrodes filled with the fluorescent Ca^{2+} indicator Oregon Green 488 BAPTA-1 and morphological indicator Alexa 594, as described previously (see chapters 2 and 3; **Fig. 4.1A**). Optical detection of transmission events in association with morphological characterization of synapses allowed for a detailed structure-function analysis during activity-dependent changes in synaptic strength. Figure 4.1B shows a typical raster scan of an OGB-1 loaded dendrite with an EPSCaT-generating spine (arrow head). The dotted white line indicates area through which line scans were taken. The corresponding line scans for successful transmission events (left) as well as failures (right) show discernible detection of transmitter release (dotted line indicating timing of extracellular stimulation (**Fig. 4.1B**). Individual Ca^{2+} traces during a success (red trace) and a failure (black trace) as well as the mean responses across trials are shown above. Representative scatter plots for EPSP (**Fig. 4.1C**) and EPSCaT (**Fig. 4.1D**) amplitudes for the imaged synapse in Fig. 4.1B show a significant increase in amplitude and proportion of successful events, respectively, post LTP induction. The dotted black line indicates the time at which an LTP-inducing protocol was administered: either a spike-timing dependent plasticity (STDP) protocol or a standard high-frequency stimulation (HFS) protocol was used to induce LTP – as there was no difference on the magnitude of our responses between protocols (data not show) the data were pooled. We performed morphological imaging of spines for baseline and at different times after the induction of LTP (**Fig. 4.1E**). LTP is indicated by significant increases in the mean EPSP following induction from 4.71 ± 0.90 mV to 7.50 ± 0.90 mV and 6.90 ± 1.0 mV at times 15 (p = 0.001) and 30 minutes (p = 0.02; **Fig. 4.1F**); LTP at these imaged synapses was associated with a sustained increase in p_r, with a baseline average of 0.22 ± 0.06 to 0.49 ± 0.10 and 0.43 ± 0.09 at times 15 (p = 0.005) and 30 minutes (p = 0.005),respectively, post LTP induction (**Fig. 4.1G**) as indicated by a decrease in optically confirmed failure rates (n = 8); this increase in synaptic reliability was not associated with significant increases in the amplitude of EPSCaT responses post LTP (see **Fig.**

4.2). I also observed a near doubling of spine volume from (in μm^3) 0.21 $\pm$ 0.07 at baseline to 0.39 $\pm$ 0.08 1 minute after LTP induction (p = 0.001), but this swelling was transient, with spines then shrinking to volumes not significantly different from baseline within 15-30 minutes (**Fig.4.1H**).

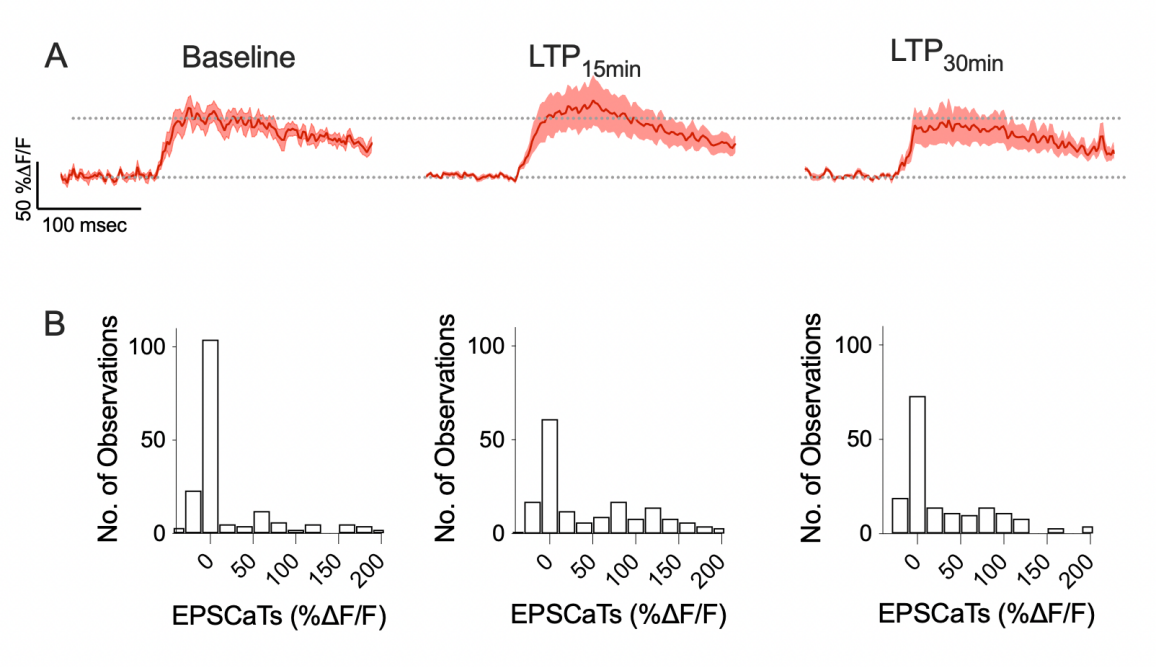

Figure 4.2: *EPSCaT amplitudes before and after LTP induction*: **(A)** Mean EPSCaT traces across experiments (n = 8). Mean EPSCaT amplitudes did not change appreciably after LTP induction (F = 0.44; ns; p = 0.54), though see (Emptage et al. 2003). Shaded area above and below mean traces represents s.e.m. (**B**) Frequency distributions of all optical recordings including successes and failures before and after LTP induction. Note the decrease in failures (i.e., ~0% amplitude events) after LTP induction, indicative of increases in p_r across all imaged synapses.

4.1.2 LTP-inducing stimuli promote a transient enlargement of dendritic spines even in the absence of potentiation.

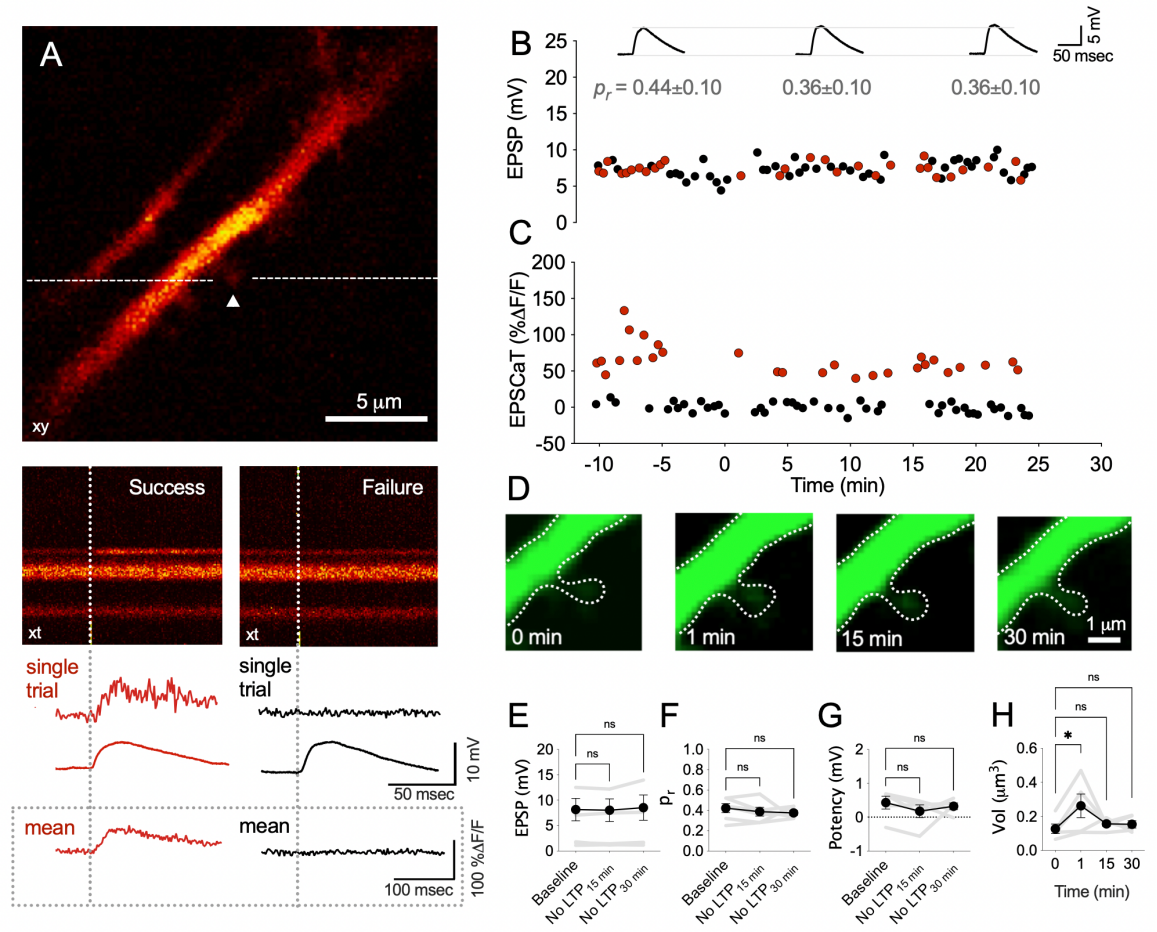

Figure 4.3: *Spine enlargement evident in subset of synapses in which LTP failed to occur*: (**A**) Representative fluorescence image of a dendritic branch with an active spine indicated by white arrow head. EPSCaTs were monitored via line-scan imaging across the spine and dendritic branch (trajectory indicated by horizontal white line in the upper image of (**A**). Timing of the extracellular stimulation is indicated by dotted vertical line across each line scan image. Successful synaptic transmission (left) can be clearly distinguished from transmission failures (right), with corresponding single trial fluorescence and voltage traces shown below. Mean fluorescence traces from this spine during successful transmissions (left) and transmission failures (right) are shown in the lower traces enclosed by dotted box. (**B**) EPSP amplitudes plotted for each stimulus before and after LTP induction protocol (indicated by black arrow) with successful transmission and failures marked by red and black circles, respectively. Average EPSP traces of baseline and 15 and 30 minutes after LTP induction are show above with the corresponding p_r values for each epoch (25 trials) shown below. (**C**) EPSCaT amplitudes plotted for each stimulus before and after the LTP induction protocol with red and black circles indicating successes and failures as above. (**D**) Fluorescent image of dendritic spine (as in A) before

and at distinct time points after the LTP induction protocol. (**E**) Average EPSPs for each epoch (~25 trials) across experiments (n = 5) before (4.82 ± 2.21), 15 min (4.71 ± 2.22; p > 0.05), and 30 min (5.21 ± 2.49; p > 0.05) after the LTP protocol. No increases in compound EPSP amplitude is indicative of LTP induction failure of the stimulated pathway (F = 2.8; ns; p = 0.37). (**F**) Average p_r for each epoch across experiments; baseline (0.44 ± 0.04), 15 min (0.40 ± 0.05; p > 0.05), and 30 min (0.35 ± 0.02; p > 0.05) after the LTP induction protocol. p_r remained unchanged when LTP failed to occur (F = 4.11; ns; p = 0.16). (**G**) Average potency measurements for each epoch across experiments at baseline (0.41 ± 0.19), 15 min (0.16 ± 0.19; p > 0.05), and 30 min (0.30 ± 0.10; p > 0.05) after LTP protocol. Potency remained unchanged when LTP failed to occur (F = 1.6; ns; p = 0.52). (**H**) Average volume measurement for each spine across experiments. Spine volume increased immediately following LTP inducing stimuli even in the absence of potentiation; from baseline (0.13 ± 0.03), 1 min (0.26 ± 0.07; *p = 0.02), (15 min: 0.16 ± 0.01; p > 0.05) and 30 min (0.15 ± 0.02; p > 0.05) post LTP protocol. Friedman's non-parametric repeated measure ANOVA with Dunn's multiple comparisons t-tests.

The induction of LTP in tissue preparations is not always successful (Debanne et al. 1999, Dhanrajan et al. 2004), and there were instances (n = 5) in which LTP-inducing stimuli failed to significantly potentiate aggregate synaptic responses with mean baseline EPSP amplitude of 4.8 ± 2.2 mV to 4.7 ± 2.2 mV and 5.2 ± 2.5 mV at 15- and 30-min post induction protocol, respectively (**Fig. 4.3E)**. In this subset of experiments, I observed no significant change in either pre or postsynaptic efficacies when EPSP amplitudes were unchanged; average p_r was 0.45 ± 0.04 pre- versus 0.40 ± 0.05 at 15 min post-stimuli and 0.35 ± 0.02 at 30 min post-stimuli ($p > 0.05$; **Fig. 4.3F**) while average potency at baseline was (in mV) 0.40 ± 0.20, 0.16 ± 0.20, and 0.30 ± 0.10 ($p > 0.05$; **Fig. 4.3G**) at the imaged synapses. However, I did observe, in 3 of the 5 experiments yeilding no LTP, a similar transient enlargement of spines as seen in our potentiated synapses with average volumes (in μm^3) of 0.13 ± 0.03, 0.26 ± 0.07, 0.16 ± 0.01,0.15 ± 0.02, for baseline and time points 1, 15, and 30 minutes post stimuli, respectively (**Fig. 4.3H**). Initial mean quantal and structural values of these 5 synapses did not differ significantly between those that underwent LTP (data not shown). These data will be discussed and summarized in relation to LTP experiments in section 4.15.

4.1.3 LTP is not associated with increases in postsynaptic responsiveness to released glutamate

It is possible to estimate the responsivness to released glutamate (i.e., potency) using a subtractive procedure (**Fig. 4.4A**), whereby the mean EPSP of trials that resulted in synaptic failures is smaller than, and subtracted from, the mean EPSP during successful transmission events at the imaged synapse (Enoki et al. 2009, see Chapters 2 and 3). I reasoned that if AMPARs laterally diffuse into the synapse to increase synaptic efficacy, I ought to be able to detect changes in synaptic potency after the induction of LTP. I therefore performed this subtractive procedure before and after induction of LTP. I observed no net change in potency following the induction of LTP (from 0.51 ± 0.32 to 0.52 ± 0.23

and 0.49 ± 0.14 mV; **Fig. 4.4B**). These data are in keeping with those of Enoki et al. 2009 demonstrating no net increase in the subtracted or optically-confirmed unitary EPSP 60 minutes post LTP induction, and extend those observations to earlier time points examined here, i.e., at 15 and 30 minutes after LTP induction.

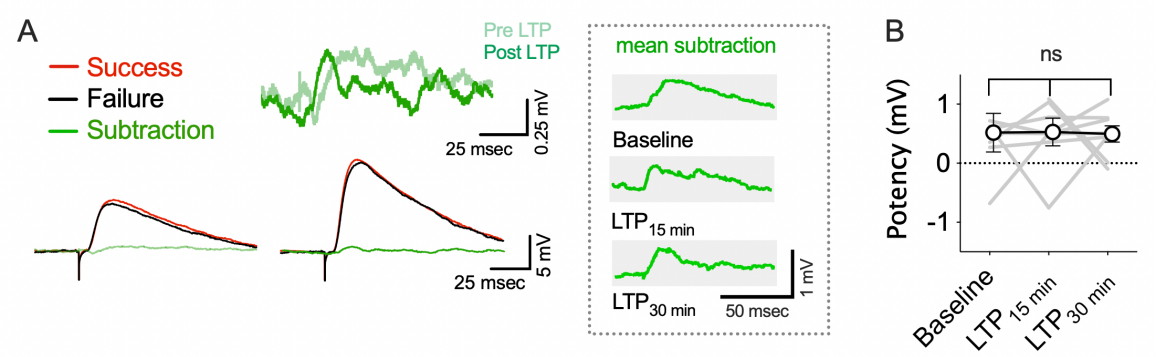

Figure 4.4: *LTP is not associated with increases in postsynaptic responsiveness to released glutamate*: (**A**) Representative voltage traces before and after LTP induction (from synapse shown in Fig.1A) with averaged successful events shown in red and failures in black. Subtracting the average failures from successes provides an estimate of the average potency value, shown in green. The same potency traces for this experiment are shown superimposed in the upper inset as pre (light green) and post (dark green) LTP. Mean subtracted potency traces across all experiments (n = 8) for each epoch before and after LTP are shown in dotted black box. (**B**) Individual (grey lines) and mean (white circles) potency values across epochs (F = 0.01, ns; p = 0.95) at baseline (0.51 ± 0.07), 15 min (0.52 ± 0.23; ns; p = 0.98), and 30 min (0.49 ± 0.14; ns; p = 0.98) post LTP induction. No significant differences in mean potency values (versus baseline) were evident post LTP induction. Of the 24 potency measurements across 8 synapses, 3 were identified as outliers (i.e., >2 standard deiviations from group mean) and removed for analysis and graphing; mixed-effects analysis with Holm-Šídák's multiple comparisons test. Without removal mean potency values were (in mV) 0.63 ± 0.32, 0.16 ± 0.41, 0.48 ± 0.14 for baseline, 15 min, and 30 min post LTP induction, respectively. Standard repeated measures ANOVA of full data set without outlier removal also yielded no significant difference (F = 0.58; ns; p = 0.57) with all multiple comparisons (versus baseline) yielding p > 0.05. Error bars indicate s.e.m.

4.1.4 LTP is not associated with changes in spine density or spine neck length.

Two additional and controversial morphological correlates thought to be associated with changes in synaptic efficacy are *i.* the addition of new synapses and/or *ii*. a reduction in spine neck length of potentiated synapses. The emergence of small filopodia-like protrusions and/or the growth of new spines have been reported in the hippocampus following spatial learning (Moser et al. 1994) and after a variety of LTP-inducing protocols (Engert and Bonhoeffer 1999, Maletic-Savatic 1999, Toni et al. 1999, Jourdain et al. 2003, Nagerl et al. 2004). In addition, two-photon fluorescence imaging has revealed reductions in spine neck length following glutamate uncaging induced LTP (uLTP) induction (Araya et al. 2014). Others however have failed to observe such morphological changes (Hosokawa et al. 1995, Sorra and Harris 1998). I therefore probed measurements of spine density and spine neck length before and after LTP under our experimental conditions, in an attempt to reveal any morphological changes in these measures that may accompany the observed functional increases in p_r (**Fig. 4.5**). Specifically, I used our collapsed stack of morphological images (i.e., Alexa 594-fluorescence) of the dendritic branch before LTP induction (shown in false-coulor green) as a baseline measure, measuring volume of the activated spine and counting the number of protrusions per unit length over the imaged dendritic segment, with subsequent images taken at times 1, 15, and 30 minutes after LTP induction (overlaid in false-colour red fluorescence) to reveal any observable changes. As shown in Fig.4.5A (and in agreement with data shown in Fig.4.1), there is a transient increase in spine volume at the potentiated synapse (dotted box) 1 minute after LTP induction (indicated by increases in red in the overlaid images) but this enlargement returns to baseline levels 30 minutes after LTP induction. Importantly, I saw no evidence of any net changes in spine density within the vicinity of newly potentiated synapses from baseline (0.66 ± 08 μm^{-1}) to 30 min (0.68 ± 0.8 μm^{-1}) nor did I see, using estimates of spine neck length, any significant changes associated with neck length of imaged spines from (in μm) 0.43 ± 0.24 at baseline to 0.40 ± 0.23 by 30 min post LTP (**Fig. 4.5C**). Together, I report here no evidence for any persistent postsynaptic functional or

morphological modifications during LTP expression. These data are consistent with previous accounts of visualized enhancements of transmitter release accompanying LTP (Zakharenko et al. 2001, Emptage et al. 2003, Ward et al. 2006, Enoki et al. 2009) and extend our understanding to rule out any significant morphological changes during the earliest time points of LTP expression; early LTP may therefore be adequately described as a functional redistribution of synaptic weight mediated primarily through an enhancement of transmitter release at pre-existing synapses.

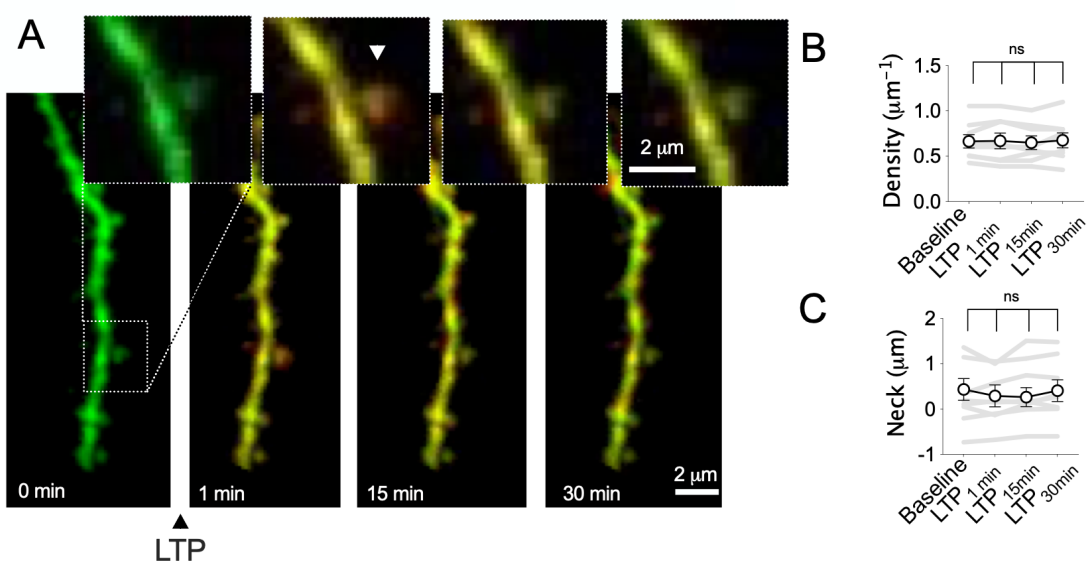

Figure 4.5: *LTP is not associated with net changes in spine density or spine neck length*: (**A**) Representative morphological (Alexa-594) images of a dendritic branch with an EPSCaT-generating spine indicated by dotted white box, enlarged above at distinct time points for clarity. Black arrow head below indicates time of LTP induction. Baseline image (0 min) is shown in false-colour green with post LTP images in red superimposed to reveal changes in spine count. Arrow in the second upper inset (1 min post LTP induction) reveals the transient nature of enlargement of the imaged spine. (**B)** Individual (grey lines) and mean (white circles) spine density measurements (expressed as spines per micrometer) across epochs ($F = 1.03$; ns; $p = 0.79$) at baseline (0.66 ± 0.07), 1 min (0.67 ± 0.08; ns; $p > 0.99$), 15 min (0.65 ± 0.08; ns; $p > 0.99$), and 30 min (0.68 ± 0.08; ns; $p > 0.99$) post LTP induction. (**C**) Individual (grey lines) and mean (white circles) spine neck length measurements across epochs ($F = 9.15$, $^*p = 0.027$) at baseline (0.43 ± 0.24), 1 min (0.28 ± 0.24; ns; $p = 0.10$), 15 min (0.25 ± 0.21; ns; $p > 0.06$), and 30 min (0.40 ± 0.24; ns; $p > 0.99$) post LTP induction. Dunn's multiple comparisons tests (versus baseline) reveal no significant differences in mean density (all $p > 0.99$) or spine neck length (all $p < 0.05$) at all time points post LTP induction. Error bars indicate s.e.m.

4.1.5 Summary of functional and structural components associated with LTP

As mentioned above, the induction of LTP in tissue preparations is not always successful (Dhanrajan et al. 2004) and there were instances in which LTP-inducing stimuli failed to potentiate synaptic responses (No LTP), yet a similar transient enlargement of spine volume was evident in a subset of those experiments (see **Fig. 4.3**). Statistical comparisons across the quantal and morphological measurements were thus carried between LTP and No LTP groups (**Fig. 4.6A-F**). Because a transient enlargement of spine volume occurred even in the absence of LTP, I carried out similar repeated imaging of spines in the absence of afferent extracellular stimulation as a secondary control measure (**Fig. 4.6G**). Imaging of these unstimulated synapses revealed no net change in spine volume, transient or otherwise, over similar time periods: average volumes (in μm^3) were initially 0.11 ± 0.01 and then 0.10 ± 0.01, 0.12 ± 0.01, and 0.14 ± 0.02 after intervals of 1, 15, and 30 minutes ($p > 0.05$). Because control experiments that pharmacologically antagonize glutamate receptors may alter pre and/or postsynaptic efficacies and synapse size (Murthy et al. 2001), these fortuitous experiments in which LTP induction failed to occur allowed for an unambiguous comparison between potentiated (LTP) and unpotentiated (No LTP) synapses that have undergone identical treatment (Dhanrajan et al. 2004; **Fig. 4.6A-F)**. Taken together, these data provide compelling evidence that transient enlargement of spine head volume is not necessary for early LTP but may instead be epiphenomenal, perhaps an osmotic or biochemical concomitant of ion influx during repetitive stimulation (Rungta et al. 2015). An increase in p_r was the only consistent and persistent change specifically associated with LTP at the imaged synapses.

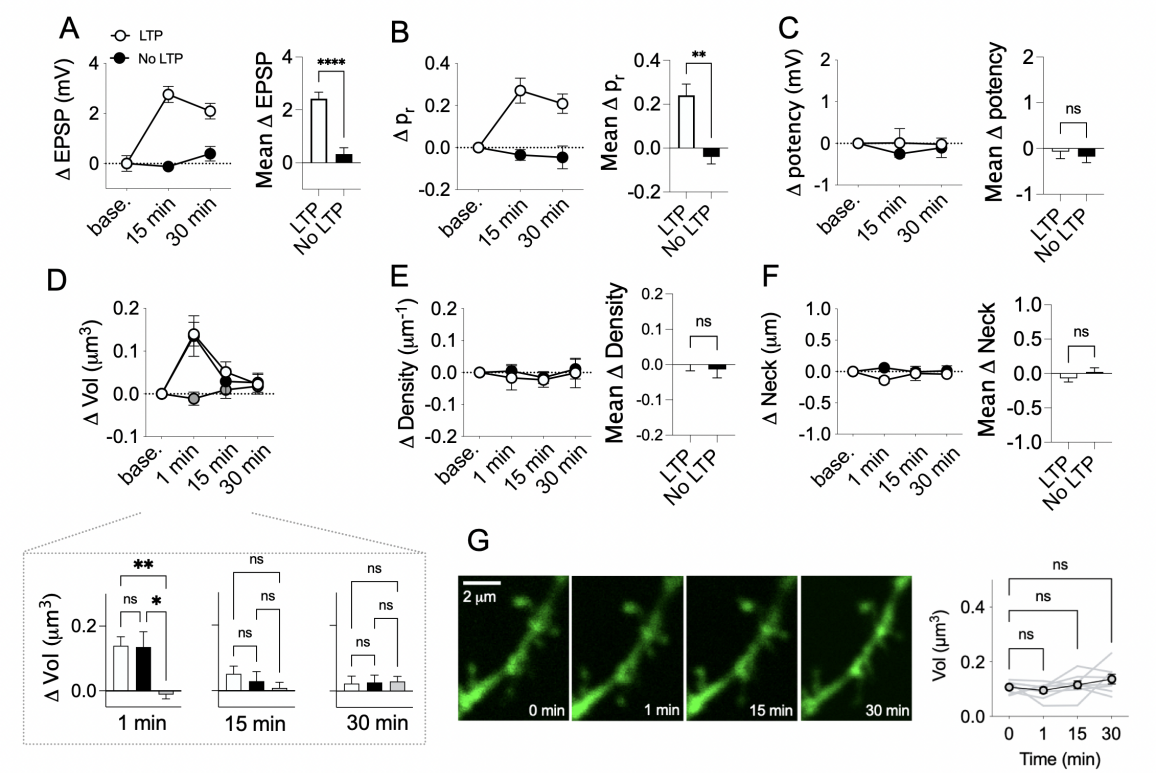

Figure 4.6: *Functional and structural comparisons between synapses that exhibited LTP and those that displayed No LTP*. (**A**) Mean ΔEPSPs for LTP at 15 min and 30 min were significantly different than the No LTP group (mean difference 2.87 ± 0.37 and 1.699 ± 0.43 mV; $p < 0.001$). (**B**) Mean Δp_r for LTP ($n = 8$) at 15 and 30 min were significantly different than No LTP ($n = 5$) mean difference 0.31 ± 0.08 and 0.26 ± 0.07; $p < 0.001$). (**C**) Mean potency did not differ significantly between LTP and No LTP groups across time ($p > 0.05$). (**D**) Mean volume: No significant differences in spine volume were found between LTP and No LTP experiments ($p > 0.05$). By contrast, significant differences were evident between LTP and an unstimulated CTRL group (grey circles and bars; $n = 9$; $p = 0.0006$) immediately after LTP induction but no other time points. (**E**) Mean spine density did not differ significantly between LTP and No LTP groups across time ($p > 0.05$). (**F**) Mean spine neck length did not differ significantly between LTP and No LTP groups across time ($p > 0.05$). The second control (grey data points in D), a repeated imaging of non-stimulated dendritic spines, was undertaken to assess dynamics of individual spine volumes over time. No significant interaction of time and volume was evident in these optical recordings ($p = 0.44$). (**G**) Representative repeated imaging (Alexa 595 fluorescence) of unstimulated dendritic spines as mophological control (data shown in D). Individual (grey lines) and mean (grey circles) time course of volume estimates for unstimulated spines. Despite intrinsic fluctuations (mean standard deviation = 0.031 ± 0.007), no significant differences were observed over the reported time frame for unstimulated spines ($F = 2.06$; ns; $p = 0.17$). Error bars indicate s.e.m.

4.1.6 Estimating the contribution of Δp_r to LTP expression

Because our small compound EPSPs were similar in amplitude to those reported previously (Enoki et al. 2009), I estimated the contribution of Δp_r from a pool of eight EPSCaT-generating synapses, the mean number of active synapses previously found in exhaustive searches of the apical dendrite of CA1 cells (Enoki et al. 2009), to ΔEPSP amplitudes after LTP induction. Here, I assume that each of the expected EPSCaT-generating synapses have values comparable to the mean values of p_r and potency as determined via optical quantal analyses across epochs (i.e., baseline, LTP_{15min}, LTP_{30min}). I performed Monte Carlo simulations (Mathematica 12; Wolfram Research) using binomial events with parameters *n* and *p* set to 8 and the observed mean p_r across each experimental epoch, respectively. A total of 25 trials, with eight repetitions, was performed for each epoch, corresponding to baseline, LTP_{15min}, LTP_{30min} of our experimental time points. The number of simulated binomial successes was scaled by the average potency per epoch plus or minus σ, which was taken as the average quantal variability (CV) for each epoch with standard deviation of channel noise (0.061 mV). **Figure 4.7A** shows the scatter plot of the results of these simulations along with the averaged experimental LTP results with histograms for each epoch shown in **Figure 4.7B.** I estimate that the observed Δp_r, at only eight such synapses, could alone account for 36.61 ± 5.60 to 32.07 ± 6.70% of the observed potentiation (**Fig. 4.7C**), noting that this contribution is likely the lowest bound estimate due to the difficulty in locating these synapses (Enoki et al. 2009). It remains to be determined whether EPSCaT-generating synapses, and their loci of expression during LTP, are representative of the total pool of stimulated synapses or whether they represent a distinct subclass unto themselves. Regardless of their prevalence (Spacek and Harris 1997), it is clear from the above simulations, and in keeping with previous literature (Enoki et al. 2009), that the increase in p_r at these synapses contributes a substantial component to the expression of LTP at CA3-CA1 synapses in the hippocampus. An important

question then is, why have other groups reported exclusively postsynaptic functional and structural components to LTP expression?

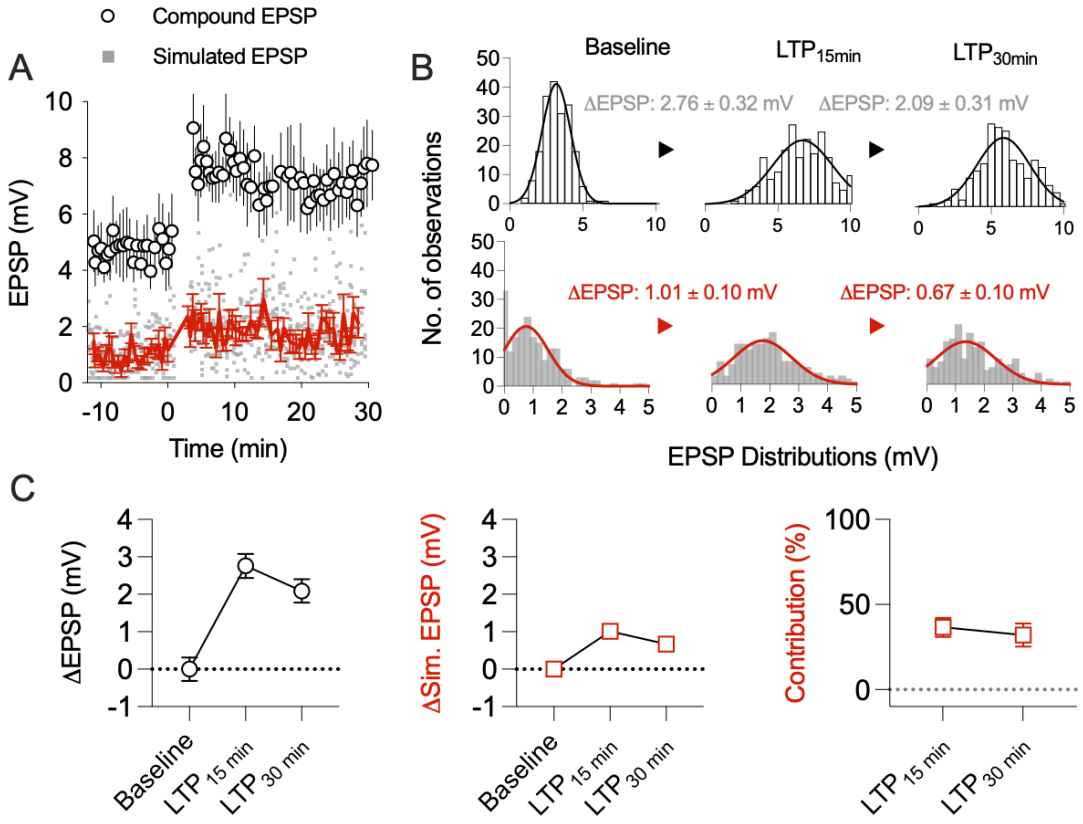

Figure 4.7: *Lower bound estimates for the contribution of Δp_r to LTP expression*: (**A**) Time and voltage averaged scatter plot of all long-term potentiation (LTP) experiments (white circles; n = 8). Simulated EPSPs (grey squares) with means and s.d. (red line) for eight theoretical EPSCaT-generating synapses with mean p_r and potency values equal to those determined empirically via optical quantal analyses before and after LTP induction. (**B**) EPSP histograms across epochs for observed compound EPSPs (top white bars) and averaged simulated EPSPs of eight theoretical EPSCaT-generating synapses (grey bars). Gaussian fits indicated by black and red lines in compound EPSP and simulated EPSP histograms, respectively. (**C**) Changes in EPSP (left) and simulated EPSP (middle) amplitudes (from baseline) after LTP. The contribution of Δp_r to the magnitude of LTP for the eight modeled synapses was taken to be the mean Δsim. EPSP/ΔEPSP (right). Approximately one third of the observed potentiation can be explained by Δp_r at as few as eight synapses.

4.1.7 Two-photon glutamate uncaging at individual spines confirms relationship with spine head volume and responsiveness to photo-released glutamate

To date, much of the support for the notion of postsynaptic expression of LTP (including changes in spine volume) stems from experiments stimulating a targeted spine by two-photon photolysis of caged-glutamate (Matsuzaki et al. 2001, Matsuzaki et al. 2004, Lee et al. 2009, Granger and Nicoll 2014, Ucar et al. 2021). I therefore adopted this approach to corroborate changes seen by other groups. I recorded from indicator-loaded pyramidal cells in area CA1 (**Fig. 4.8A-B**) as previously described (see Chapter 2) but with bath-applied caged glutamate (MNI-glutamate; 3 mM; Tocris) and an additional femtosecond infrared laser (720 nm, duration controlled by acousto-optic modulator) for focal two-photon photolysis. Uncaging-evoked EPSPs (uEPSPs), elicited by 0.3 msec light pulses, were stable over time (**Figs. 4.8C** and **E**). I initially recorded uncaging-evoked Ca^{2+} transients (uPSCaTs; **Figs. 4.8D** and **E**) but found that the amplitude of uPSCaTs consistently dissipated over time (see Chapter 5 for discussion) and as it was not pertinent to monitor uPSCaTs for these experiments (i.e., success/failure information is not applicatable to photolytic stimulation), Ca^{2+} imaging was discontinued. uEPSP amplitudes were variable both within and across synapses (**Fig. 4.8F**) but mean amplitudes showed a significant positive linear correlation with spine size (R = 0.62; **Fig.4.8G**).

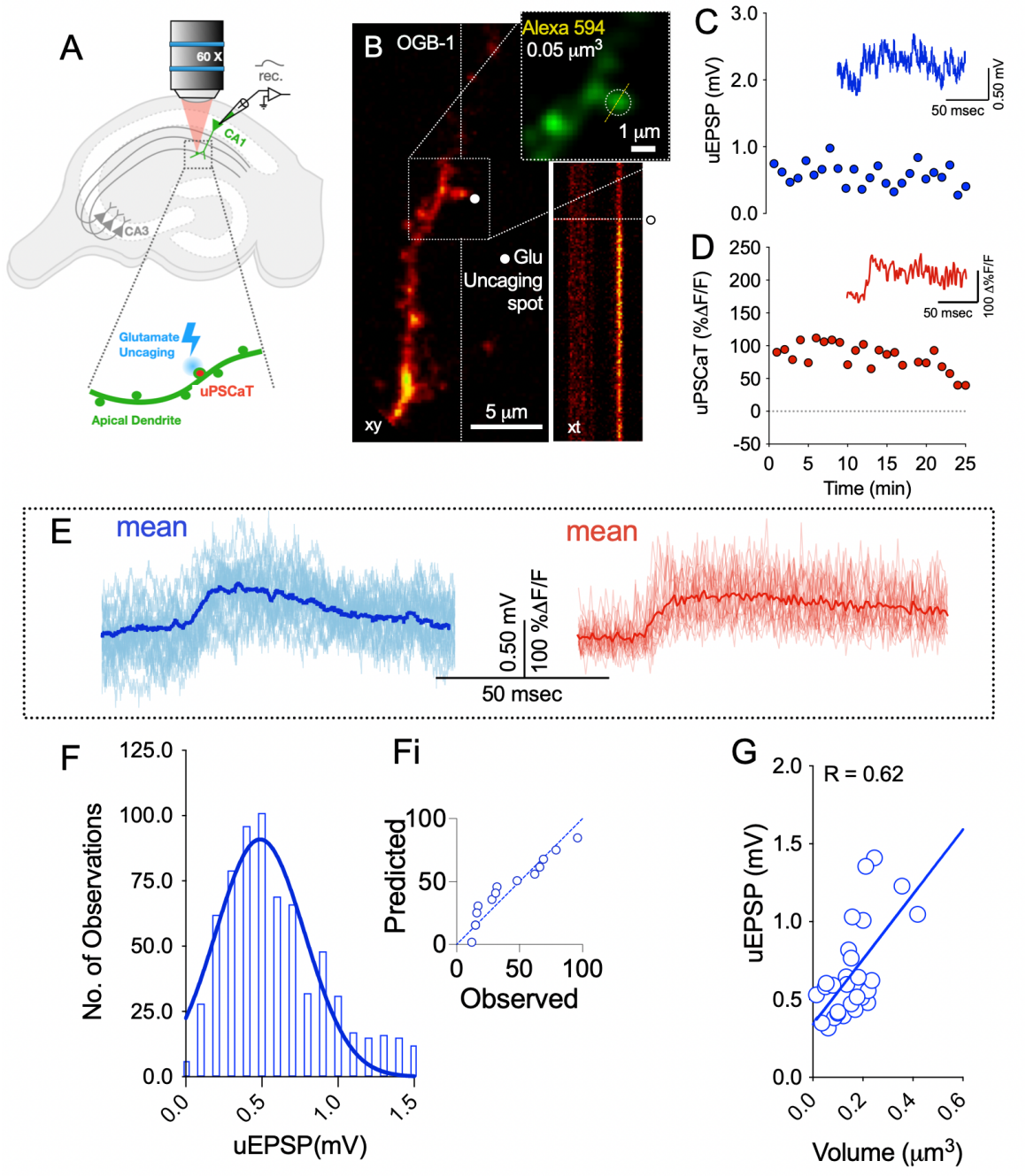

Figure 4.8: *Glutamate uncaging confirms correlation between spine head volume and amplitude of voltage transients evoked by photo-released glutamate*: (**A**) Schematic of experimental conditions; A CA1 pyramidal neuron is impaled and loaded with Ca^{2+} (Oregon Green BAPTA-1; 0.5-1mM) and morphological (Alexa 594; 0.25 mM) fluorescent dyes. Light pulses (720 nm; 0.3 msec) in the presence of MNI-glutamate (3.0 mM) produce glutamate uncaging-evoked EPSPs (uEPSPs) and uncaging-evoked postsynaptic Ca^{2+} transients (uPSCaTs) at targeted spines. (**B**) Representative fluorescence Ca^{2+} image of a dendritic branch with targeted spine enclosed in dotted box. White dot indicates point of photolysis (i.e., glutamate

uncaging spot). Inset shows same spine with morphological marker Alexa 594. uPSCaTs were monitored via line-scan imaging across the spine and dendritic branch (trajectory indicated by vertical white line). Timing of the two-photon glutamate uncaging is indicated by dotted horizontal line across the line scan image. (**C**) Scatter plot of uEPSP amplitudes plotted for each uncaging event at the spine shown in B. Representative uEPSP trace (shown above in blue) for the trial depicted in B. (**D**) Scatter plot of the corresponding uPSCaTs for the uEPSPs shown in C. Representative uPSCaT trace (shown above in red) for the line scan shown in B. (**E**) Superimposed individual uEPSP (blue) traces and uPSCaT (red), along with mean responses in bold, for trials shown in scatter plots C and D, respectively. (**F**) Sample distribution of uEPSPs with Gaussian fit (blue line). uEPSP amplitudes were univariate normal (D'Agostino-Pearson; $p = 0.30$). (**Fi**) QQ plot for observed uEPSP amplitudes (in mV) plotted against a predicted normally distributed data set to visualize and support the assumption of normality. (**G**) mean uEPSP amplitudes show positive linear correlation with spine head volume ($R = 0.62$; $p = 0.0004$). Solid blue line is regression line ($Y = 2.085*X + 0.3405$).

4.1.8 uLTP is associated with a persistent increase in responsiveness to photo-released glutamate, a persistant enlargment of spine head volume, and a persistent decrease in spine neck length

uEPSPs could be reliably evoked in these preparations and remained stable over time in the control experiments where no pairing protocol was administered (uCTRL; from 0.54 ± 0.06 mV at baseline to 0.50 ± 0.05 and 0.52 ± 0.06 mV at 15 and 30 min, respectively; n = 6). uLTP was induced by a pairing procedure (see Methods, Chapter 2) and resulted in an increase in reponsiveness to photo-released glutamate from (in mV) 0.45 ± 0.06 at baseline to 0.78 ± 0.15 and 0.67 ± 0.10 at 15 and 30 min, respectively. **Figure 4.9B** shows mean uEPSP amplitude over time for these uLTP experiments (n = 6). In all cases, morphological parameters were not significantly different from baseline levels in control experiments (**Fig. 4.9A** and **C**; $p > 0.05$). In contrast to controls and the above observations on LTP induced via the endogenous release of glutamate (e.g., **Fig 4.6D**), spine volumes showed *persistent* enlargement, increasing from (in μm^3) 0.15 ± 0.04 at baseline to 0.24 ± 0.05, 0.24 ± 0.06, and 0.25 ± 0.06, at time points 1 min, 15 min, 30 min after uLTP induction. I did not see the gross transient phase of enlargement (~200-400% change) reported by other groups (Matsuzaki et al. 2004, Harvey and Svoboda 2007, Lee et al. 2009), presumably due to the mode of induction, the presence of Mg^{2+} in the perfusate, the duration of the uncaging pulse, or other experimental factors (Kruijssen and Wierenga 2019). Spine necks were significantly reduced in length, from (in μm) 0.47 ± 0.13 at baseline to 0.25 ± 0.11, 0.29 ± 0.14, and 0.26 ± 0.14 at time points 1 min, 15 min, and 30 min after uLTP induction, respectively (**Fig. 4.9D**). These experiments confirm that uLTP, in marked contrast to LTP induced via the endogenous release of glutamate, results in postsynaptic changes including increased responsiveness to photo-released glutamate and persistent changes in spine morphology.

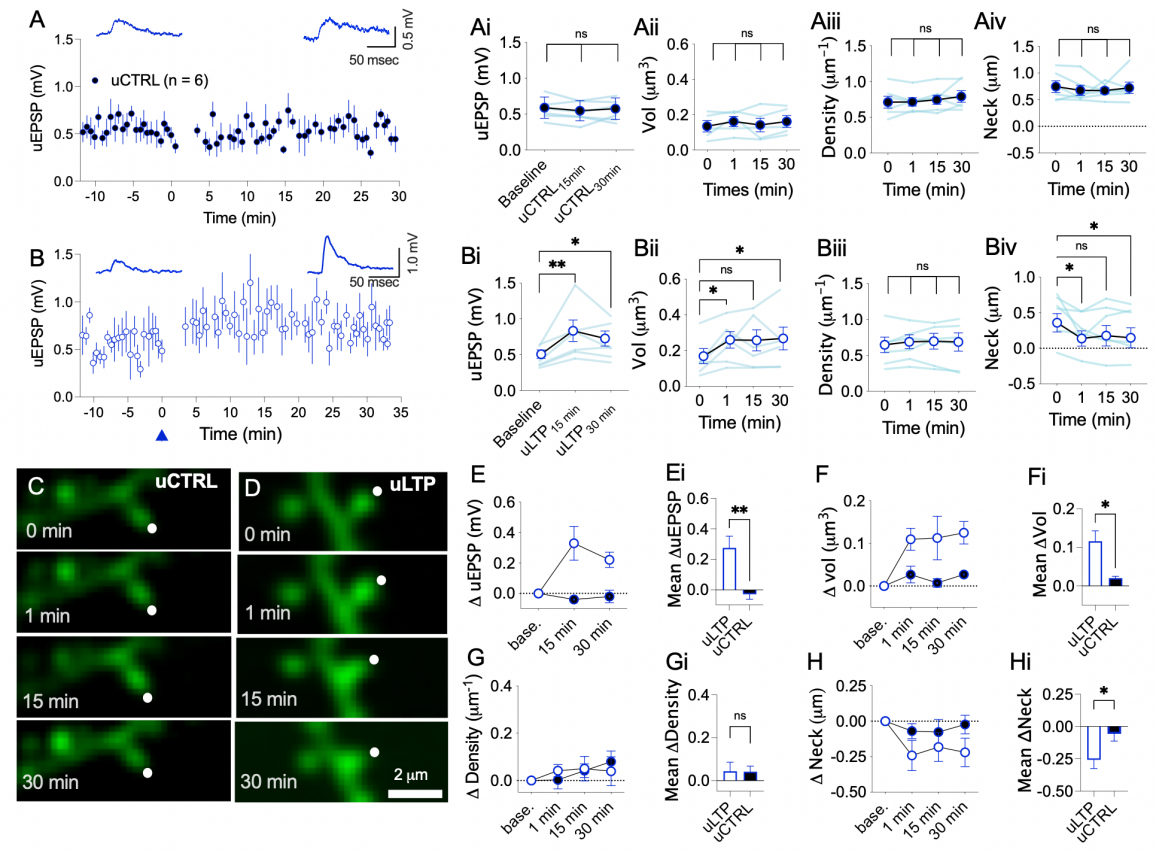

Figure 4.9: *uLTP is associated with persistent increases in responsiveness to photo-released glutamate, persistent enlargement of spine head volume, and persistent reductions in spine neck length*: (**A**) Time and voltage averaged uEPSPs for control experiments (uCTRL; n = 6) in which no plasticity protocol was administered and (**B**) uncaging-induced LTP experiments (uLTP; n = 6) in which pairing protocol was administered at time 0 (blue arrowhead). Individual (blue lines) and mean (black circles) values for (**Ai**) uEPSP amplitude (**Aii**) spine head volume, (**Aiii**) spine density, and (**Aiv**) spine neck length across time for uCTRL groups. Individual (blue lines) and mean (white circles) values for (**Bi**) uEPSPS (**Bii**) spine head volume, (**Biii**) spine density, and (**Biv**) spine neck length across time for uLTP groups. Representative morphological (Alexa 594 fluorescence) images of targeted spines for uCTRL (**C**) and uLTP (**D**) groups. Mean time course comparisons of changes (from baseline) in (**E**) uEPSP amplitude, (**F**) spine head volume, (**G**) spine density, and (**H**) spine neck length between uCTRL and uLTP groups. Mean response comparisons (averaged across time) for (**Ei**) uEPSP amplitude, (**Fi**) spine head volume, (**Gi**) spine density, and (**Hi**) spine neck length between uCTRL and uLTP groups. Error bars indicate s.e.m.

4.1.9 Sampled synapses for remote stimulation and uncaging experiments come from a functionally and morphologically similar population of inputs.

The observed differences between the consequences, both functional and morphological, of LTP vs. uLTP led me to compare the synapses examined in the two groups (**Fig. 4.10A-G**). Initial mean unitary responses to stimulation were similar in both groups: 0.46 ± 0.08 mV for remote stimulation vs. 0.50 ± 0.04 mV for uncaging (**Fig. 4.10B**; $p > 0.05$). Mean amplitudes for initial Ca^{2+} responses were also comparable (in %ΔF/F) at 82.06 ± 17.78 for remote stimulation vs. 72.32 ± 16.04 for uncaging (**Fig. 4.10C**; $p > 0.05$), as were spine head volumes (0.17 ± 0.04 μm^3 for remote stimulation vs. 0.14 ± 0.03 μm^3 for uncaging; **Fig. 4.10D**; $p > 0.05$) and spine density (0.72 ± 0.06 μm^{-1} for remote stimulation vs. 0.66 ± 0.007 μm^{-1} for uncaging; **Fig. 4.10E**; $p > 0.05$). Mean spine neck length showed the greatest divergence among morphological characteristics (0.31 ± 0.16 μm for remote stimulation vs. 0.61 ± 0.09 μm for uncaging) but was not significantly different by conventional statistical criteria (**Fig. 4.10F**; $p > 0.05$). Importantly, upon closer inspection of the data, this difference was largely brought about by our control groups – mean differences between synapses that underwent plasticity were (in μm) 0.43 ± 0.24 for remote stimulation vs. 0.47 ± 0.13 for uLTP ($p > 0.05$). Thus, preexisting differences in the studied spines (at baseline) are unlikely to have caused the discordant results between groups. Lastly, and as mentioned previously, the release of a single quantum of transmitter produces stereotyped responses with minimal variation (Stricker et al. 1996). Our measures of EPSP amplitude variance (coefficient of variation; CV) differed remarkablely between groups; 0.17 ± 0.03 for remote stimulation vs. 0.56 ± 0.08 for uncaging (**Fig. 4.10G**; $p < 0.001$). The high CV for uncaging has been previously reported to reflect stochastic responses of AMPAR activation (Matsuzaki et al. 2001). If this were indeed the sole cause of such variance, then it would imply that uncaging of glutamate activates a divergent pool of AMPARs than endogenous release events. Other factors associated with photolytic release of glutamate, such as local cage concentration and replenishment rate, diffusion of released glutamate in the cleft, and position and variation of the uncaging spot

relative to the postsynaptic density, (Kruijssen and Wierenga 2019) may however also contribute to the excess variance with uncaging. Together, these data suggest that the spines and synapses examined here were initially both functionally and morphologically similar, and that differences in LTP and uLTP expression result from differences in the mode of synaptic activation.

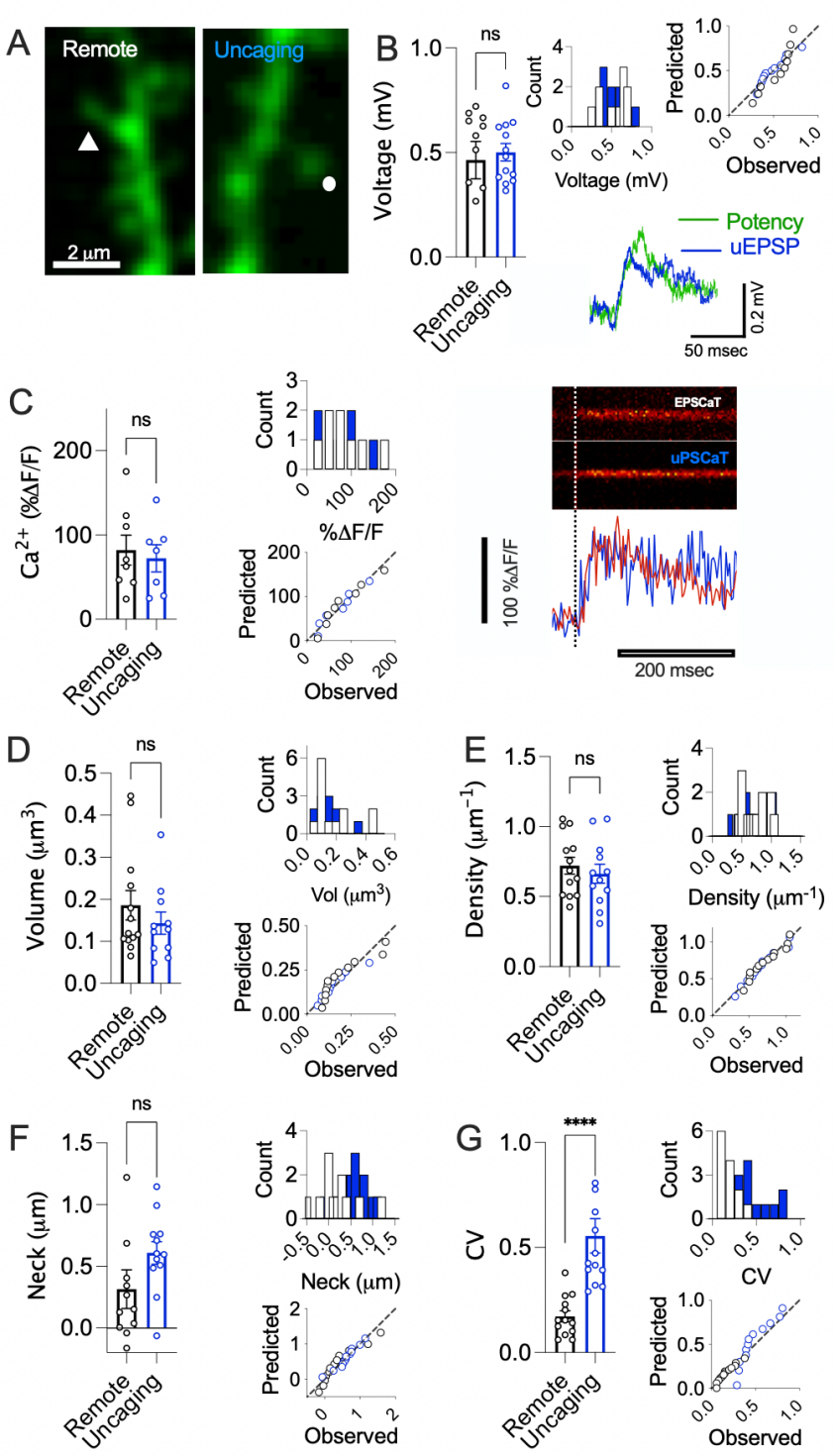

Figure 4.10: *Comparisons between synapse selection for remote extracellular synaptic stimulation and two-photon glutamate uncaging experiments*: (**A**) Representative Alexa 594 fluorescence images of an EPSCaT-generating spine (left) and a spine targeted for two-photon glutamate uncaging (right). White arrowhead indicates spine activated by remote stimulation and white circle indicates point of photolysis for glutamate uncaging. (**B**) Remote extracellular

stimulation and focal 2P uncaging evoke comparable mean voltages at sampled synapses (Mann-Whitney, $p > 0.05$). Upper insets show (left) frequency distributions and (right) QQ-plots for visualization of normality. Potency values were non-normal (D'Agostino & Pearson; $p < 0.001$). Lower inset shows representative voltage traces for the imaged synapses depicted in A; mean unitary synaptic responses (as revealed by subtraction analysis; see Fig 3.0) to remote stimulation is shown in green (for consistency with Fig. 4.3) and mean uEPSP is shown in blue. (**C**) Mean amplitudes of baseline Ca^{2+} transients evoked by remote synaptic stimulation (black) vs. uncaging (blue). Upper insets show frequency distributions, and lower insets show QQ plots for visualization of normality here and in (D-G). Both data sets were normal ($p > 0.05$). Right panel shows representative line scan images (top) and the corresponding evoked-Ca^{2+} transients are shown below with EPSCaT in red and uPSCaT in blue. Vertical dotted line indicates time of electrical or photolytic stimulation. (**D-F**) Morphological comparisons between mean volume (**D**) and spine density (**E**) for remote vs. uncaging data show no significant difference in volume (Mann-Whitney, $p > 0.05$) or density ($p > 0.05$) of spines sampled in the different stimulation experiments. (**F**) Mean spine neck length estimates for remote stimulation vs. uncaging experiments. Estimates of mean spine neck length were not significantly different between the two groups ($p > 0.05$). (**G**) Mean unitary electrical response variance (coefficient of variation; CV) differed between remote and uncaging experiments (Mann-Whitney; $p < 0.0001$). All data points taken from baseline recordings of experimental and control groups.

4.1.10 Glutamate uncaging-induced LTP (uLTP) artifactually enhances resting Ca^{2+} load in dendritic spines.

As the synapses under investigation showed remarkable similarity in both structure and function, I questioned the cause of divergence between remote synaptic stimulation and uncaging-induced potentiation of single synapses. Both remote stimulation and glutamate uncaging-induced potentiation showed similar levels of potentiation (**Fig. 4.11A-Ai**) and because I collected both Ca^{2+} and morphological fluorescence images at distinct time points before and after potentiation, it was possible to examine the Green/Red fluorescence ratios (i.e., resting Ca^{2+} load) within single spines at the time points examined (**Fig. 4.11B**). Resting spine Ca^{2+} load was not significantly different after baseline recordings (i.e., time 0) between remote and uncaging groups (**Fig. 4.11C**) and LTP did not significantly alter resting spine Ca^{2+} levels from baseline (**Fig. 4.11D-Di**); by contrast, glutamate uncaging-induced potentiation produced a significantly increased resting spine Ca^{2+} load immediately after uLTP induction (**Fig. 4.11E-Ei**). Between group comparison of changes in spine Ca^{2+} load one minute after induction (i.e., between LTP and uLTP groups) revealed significantly elevated levels when potentiation was brought about via glutamate uncaging ($p < 0.05$; **Fig. 4.11F**). uLTP therefore seems to artificially increase resting spine Ca^{2+} levels above and beyond the threshold necessary for LTP induction and thereby recruits/maintains excessive signalling cascades (not recruited to the same extent during LTP induction methods that make use of the endogenous and stochastic release of glutamate) that may contribute to long lasting enlargement of spine head volume and/or other synaptic phenotypes. Taken together, these data highlight fundamental differences between the modes of synaptic stimulation and their resultant forms of activity-induced plasticity.

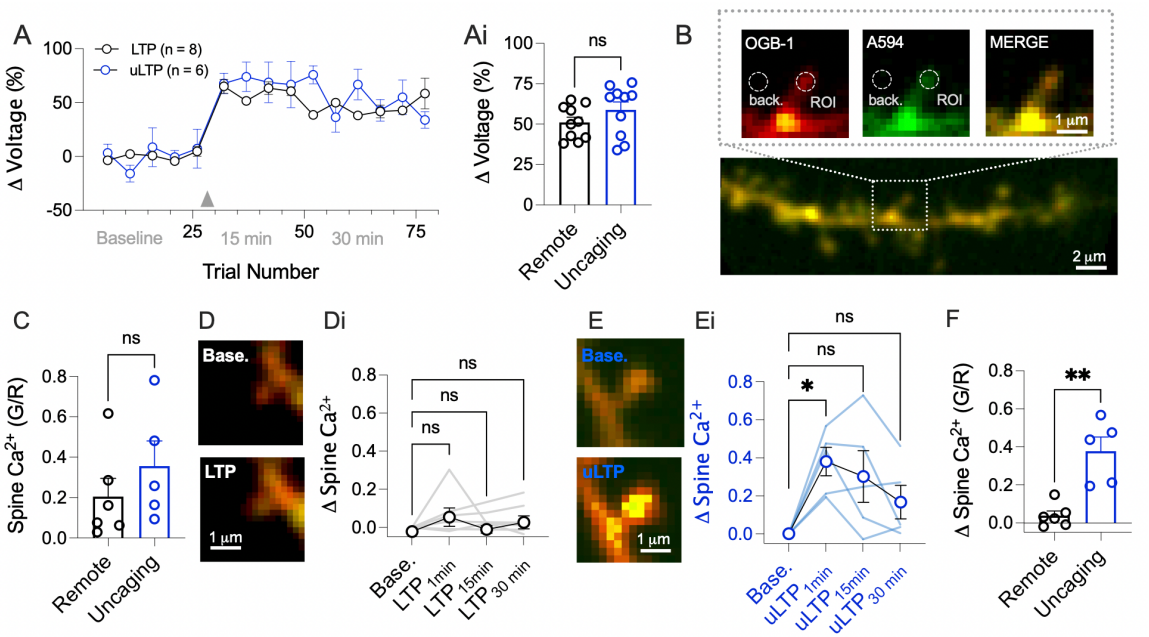

Figure 4.11: *Resting spine Ca^{2+} before and after LTP and uLTP*: (**A**) Mean scatter plots for LTP and uLTP experiments. Each point represents the average of 5 trials. Arrowhead indicates plasticity-inducing protocol (after 25 trial baseline). (**Ai**) Comparison of magnitude of potentiation (computed as % change of mean of all data points post-induction versus mean of all data points pre-induction) reveals no significant difference between the for compound EPSPs during remote stimulation induced LTP and uEPSPs during uLTP. (**B**) Total corrected fluorescence of spine heads was calculated for green (OGB-1; upper left image shown with red LUT for consistency throughout this thesis) and Alexa 594 (A594; upper middle image shown in green for consistency throughout this thesis) with the merger of the two channels (Merge; upper right image). Bottom image shows full dendritic branch with active spine. (**C**) Baseline G/R ratios for 6/8 LTP experiments and 5/6 uLTP experiments. Baseline images captured after 25 trials of remote extracellular stimulation or two-photon glutamate uncaging pulses. No significant difference in spine Ca^{2+} evident at baseline (Mann-Whitney U = 5; ns; p = 0.08). (**D**) Representative green (OGB-1) and red (Alexa 594) superimposed image of a dendritic spine before (upper image) and 1 minute after (lower image) LTP induction revealing the transient enlargement of spine head volume. (**Di**) Individual (grey lines) and mean (circles) time course of G/R values, plotted as spine Ca^{2+} change from baseline show no significant increase post LTP (F = 2.4; ns; p = 0.54); see C for remote baseline value. (**E**) Representative image of a dendritic spine before (upper image) and after (lower image) uLTP induction. (**Ei**) Individual (blue lines) and mean (blue circles) time course of G/R values, plotted as spine Ca^{2+} change from baseline (F = 7.8; *p = 0.04); see A for uncaging baseline value. Dunn's multiple comparison t-tests revealed a significant difference in G/R value (versus baseline) 1 min after uLTP (*p = 0.02). (**F**) Comparison between remote and uncaging G/R values immediately (1 min) after plasticity induction revealed a significant difference (Mann-Whitney U = 0;

**p = 0.004) between remote stimulation (0.04 ± 0.02) and uncaging (0.38 ± 0.08).

4.2 Discussion

The loci of synaptic expression mechanisms in LTP and their putative structural correlates have been contentious issues (Bliss and Collingridge 2013, Nicoll and Roche 2013, MacDougall and Fine 2014). It is often asserted that LTP at CA3-CA1 synapses is solely or chiefly expressed postsynaptically, by the insertion or modification of AMPARs (Nicoll 2003, Granger and Nicoll 2014, Nicoll 2017). Increases in responsiveness to exogenous glutamate and associated changes in spine morphology after two-photon glutamate uncaging induced LTP (uLTP) have been adduced as evidence of this postsynaptic locus of LTP expression. Presynaptic mechanisms of LTP expression have generally been discounted, or deemed to play a less significant role. Here, I have used optical quantal analyses as well as glutamate uncaging experiments, along with morphological characterization of individually activated synapses, to examine the locus of LTP expression and the putative underlying structural modifications.

Changes in synaptic reliability

Optical monitoring of transmission at single synapses described here provides a clear demonstration that, within the confines of the current study, LTP expression is associated with a persistent increase in p_r, consistent with previous electrophysiological (Malinow and Tsien 1990, Stevens and Wang 1994, Bolshakov and Siegelbaum 1995) and optical observations (Emptage et al. 2003, Ward et al. 2006, Enoki et al. 2009). Using Monte Carlo simulations, I could provide a lower bound estimate demonstrating that the observed changes in p_r alone, via a small number of similarly weighted synapses, can account for a large percentage of the observed potentiation. It is important to note here that I was unable to monitor observed changes in p_r during glutamate uncaging as this method solely probes postsynaptic function. Nevertheless, notwithstanding

claims of minimal presynaptic involvement (Granger and Nicoll 2014) or an exclusive postsynaptic locus based on uncaging-induced LTP, recent work has shown that uncaging-induced spine enlargement may enhance presynaptic vesicle release (Ucar et al. 2021). Combining optical quantal analyses with glutamate uncaging at single synapses would help resolve this issue. Because we have shown previously (Chapter 3) that p_r scales with spine size, it is reasonable to hypothesize that persistent changes in p_r at individual synapses, as reported here, would promote, or be associated with, slow homeostatic growth processes (i.e., non-Hebbian plasticity) at later (i.e., >2 hrs) post-induction times (Sorra and Harris 1998). Because I was not able to maintain these recordings for these extended times, I could not investigate such slow growth.

Changes in potency

The delivery of new AMPARs into synapses has been observed in spines following LTP-inducing protocols (Makino and Malinow 2009) and during forms of learning (Matsuo et al. 2008). When LTP is induced via remote synaptic stimulation the amplitude of the compound EPSP increased by 47.70 ± 7.10%. However, postsynaptic responsiveness to released glutamate (i.e., potency) at individually monitored synapses remains largely unchanged (4.35 ± 29.90% decrease 30 min after LTP induction). By contrast, uLTP is characterized by a robust increase in responsiveness to photo-released glutamate (48.90 ± 7.10% increase 30 min after uLTP induction). The degree to which the increased uEPSP amplitudes during uLTP result from recruitment of new AMPARs, modifications of existing AMPARs, reduced spine neck length, or other causes remains to be determined. These contrasting findings with LTP induced via the endogenous release of glutamate do not exclude recruitment or modification of existing AMPARs at potentiated synapses with LTP; rather they indicate that if these modifications occur, they do not contribute significantly to postsynaptic efficacy. The findings are consistent with the glutamate hotspot hypothesis (Rusakov and Kullmann 1998, Raghavachari and Lisman 2004) and recent indications that the

delivery of new AMPARs into synapses does not alter postsynaptic strength (Sinnen et al. 2017), and supports our working model of LTP expression at mature synaptic structures (see MacDougall and Fine 2014 and Chapter 1).

Morphological changes

I also examined aspects of synaptic morphology that have been suggested to change in association with LTP expression, including spine head volume, spine density, and spine neck length. I observed transient increases in spine volume immediately after LTP-inducing stimulation, as reported by others (Lang et al. 2004); these increases were also present in a subset of experiments in which potentiation failed to occur but not in those experiments where spines were not stimulated. Thus, spine enlargement appears to be a transient consequence of synaptic activation, but not an essential component of long-lasting synaptic potentiation. The transitory nature of spine enlargement may reflect local changes in ionic concentrations within spines during induction and/or activation of enzymatic pathways independent of LTP, possibly with negligible functional consequences. I also observed no persistent changes in spine density, in agreement with several reports (Lee et al. 1980, Geinisman et al. 1991, Hosokawa et al. 1995, Sorra and Harris 1998). Lastly, I observed no persistent change in spine neck length at potentiated synapses when LTP is induced by remote synaptic stimulation. In contrast, after uLTP I observed a persistent increase in spine head volume, along with a persistent decrease in spine neck length. Importantly, I have ruled out the possibility of biases in synapse selection between the two experimental groups by demonstrating statistically similar baseline levels of postsynaptic strength, evoked Ca^{2+} responses, and all morphological parameters between spines subjected to LTP vs. uLTP. I cannot rule out the possibility of new synapse formation at later time points after LTP induction or changes, such as altered protein synthesis (Bolshakov et al. 1997, Bozdagi et al. 2000), pre- or postsynaptic unsilencing of unimaged synapses (Isaac et al. 1995, Voronin et al. 2004), nor can I rule out the formation of new

axo-dendritic (i.e., shaft synapses) connections (Chang and Greenough 1984) that would be undetected with these methods, limited in time and restricted to small dendritic segments containing our visualized and potentiated synapses.

Taken together the findings reported here demonstrate that LTP induced by remote stimulation is expressed very differently from uLTP induced by glutamate uncaging. Ongoing work, combining these two experimental approaches at single synapses while monitoring, for example, the spatiotemporal profile of endogenously-released and/or photo-released glutamate with appropriate optical sensors (Marvin et al. 2013, Jensen et al. 2017, Kopach et al. 2020) will help elucidate the precise mechanisms underlying these discordant results and provide a clearer framework for understanding the physiological and necessary components of LTP expression.

CHAPTER V: GENERAL DISCUSSION

5. Introduction

The research described in this thesis was undertaken to establish the quantal components of transmission and associated morphological characteristics of individually active synapses in their basal state and during plasticity in order to elucidate structure-function relationships of these important units and resolve discordant results among laboratories. To this end, I used ; electrophysiological recording, with morphological classifications of synapses, Monte Carlo modelling, and postsynaptic stimulation by two-photon glutamate uncaging. I find evidence of presynaptic, but not postsynaptic, scaling of synaptic efficacy with synapse size under basal states of transmission, as well as an enhancement of presynaptic, but not postsynaptic, efficacy underlying the expression of long-term potentiation (LTP). I find no evidence of persistent morphological changes associated with LTP during the early time points examined, but consistently observe such changes associated with uncaging-induced LTP (uLTP). These observations help resolve several outstanding issues regarding the essential aspects of LTP expression. What follows is a general discussion on the gain control mechanisms of mature synaptic systems and the different effects of glutamate release at the level of single synapses during remote vs. uncaging synaptic stimulation.

5.1 Reliability as the primary basis for gain control of mature synapses

As hippocampal glutamatergic synapses grow in size, the reliability of their transmitter release appears generally to be enhanced, even as new postsynaptic AMPARs are likely added too far from the release site to be significantly activated (this thesis). Thus, as we have proposed (Chapter 1; MacDougall and Fine 2014), the addition of new AMPARs would make little contribution to the efficacy of mature synapses, at least for low frequency transmission. As postsynaptic AMPAR activation appears to be limited at distances greater than ~0.25-0.30 μm from the release site, modifications to p_r afford more effective gain control of

synaptic efficacy for mature synapses, extending the dynamic range and permitting multiple bouts of plasticity (Enoki et al. 2009). The results of this thesis provide a strong challenge to prevalent views of postsynaptic gain control, as depending upon “AMPAfication” of synapses and instead highlight the limitations imposed on postsynaptic alterations to mature synapses and thus on their contribution to synaptic efficacy. Larger synapses, may in general be stronger synapses, but their strength is modulated primarily by changes in the reliability of presynaptic transmitter release and is largely independent of postsynaptic potency. Although potency is not related to a synapse’s size, taken here to mean the generally matched size of pre and postsynaptic specializations, it can be influenced by spine neck length (see **Fig. 3.5**), providing a means by which postsynaptic weight may be influenced by morphology. It remains to be determined whether presynaptic scaling occurs to the same extent at smaller synapses than those studied here. Nevertheless, the data presented here make a compelling case for a significant shift in our thinking about the basis of synaptic strength and information storage during activity-dependent synaptic modification.

The issue of pre vs. postsynaptic modification underlying the expression of LTP is far from trivial: the locus of expression is key to understanding the molecular mechanisms of LTP, the dominant model of learning and memory. Of the synapses that underwent LTP (n = 8) in the experiments of Chapter 4, all demonstrated a persistent increase in p_r with negligible changes in potency or morphology 30 minutes after induction. In contrast, only synapses undergoing uncaging-induced LTP (uLTP; n = 7) showed persistent postsynaptic changes, both functional and structural. Importantly, this contrast was evident even between synapses that were both functionally and structurally similar before the induction of plasticity. Thus, under experimental conditions where LTP is induced by the release of glutamate via the normal endogenous release machinery, presynaptic modifications are the primary means of LTP expression. In contrast, postsynaptic modifications seem to predominate when LTP is induced photolytic release of caged glutamate. Conclusions regarding the locus of early LTP expression based on glutamate uncaging (Matsuzaki et al. 2004, Bagal et al

2005, Harvey and Svoboda 2007, Lee et al. 2009, Ucar et al. 2021; reviewed in Granger and Nicoll 2014, Kruijssen and Wierenga 2019), may be undermined by methodological artifact. Understanding the exact presynaptic molecular determinants of LTP expression and the extent to which these results may be extended to different synapses (e.g., inhibitory synapses or synapses lacking internal Ca^{2+} stores), other forms of plasticity such as long-term depression (LTD), and longer time points are now central tasks.

5.2 The spatiotemporal profile of glutamate during vesicular and photo-release

The tightly controlled time course and level of released glutamate at central synapses, and thus the precision of excitatory transmission, serves to maximize signal transmission while minimizing crosstalk and the excitotoxic effects of excessive glutamate. Indeed, synapses and their associated astroglia have the necessary machinery to rapidly release, buffer, and recycle glutamate at physiological levels. The photolytic release of exogenous glutamate, however, has a spatiotemporal profile significantly different from that of endogenous synaptic release, and results in different and artifactual synaptic behaviour.

Spatiotemporal levels of free glutamate concentration in the synaptic cleft upon photolysis of caged glutamate (the uncaging hotspot or “uHotspot”), and thus of glutamate receptor activation, may be sufficient to account for uncaging-associated scaling of AMPAR currents with spine head volume under basal states (Matsuzaki et al. 2001) and during uLTP (Matsuzaki et al. 2004). Due to the large uncaging volume (~1 μm^3) and time course (0.3 – 4.0 msec pulses used throughout the literature) of the uHotspot, extrasynaptic AMPARs that would normally be too far from vesicular release sites to be activated by the endogenous release of glutamate may be artifactually activated following the photolytic release of caged glutamate. Thus, larger synapses with an inferred greater number of extrasynaptic AMPARs would display a greater response to photolytic glutamate release compared to the response to endogenous release of glutamate reported and predicted in this thesis and elsewhere (Rusakov and Kullmann 1998, Raghavachari and Lisman 2004,

Cathala et al. 2005). During uLTP, as AMPARs are added to peripheral regions of the PSD the newly incorporated receptors may thus contribute to and artificially enhance, the photolysis-evoked response. The same synapses, would show no such scaling of evoked responses to synaptically (i.e., endogenous) released glutamate during basal states and LTP, due to a much smaller glutamate hotspot not activating extrasynaptic receptors. This explanation fits well with the observations reported here.

5.3 The ionic burden of glutamate uncaging

Significant differences in the frequency, and thus the ionic burden, of single spine activation between remote vs. uncaging regimes must also be considered. If, for example, 10 stimuli are delivered over a period of time with remote activation, a synapse would experience fewer than 10 transmission events due to the stochastic nature of release, the exact number reflecting the p_r at that particular synapse. In contrast, glutamate uncaging, with the same 10 trials over the same time course and at the same stimulating frequencies would result in 10 transmission-like events. Uncaging of glutamate, both at low frequency and during plasticity-inducing stimuli, is thus expected to impose a substantially larger ionic burden upon the postsynaptic spines than does remote synaptic stimulation at the corresponding frequencies. This increased postsynaptic loading of Ca^{2+} and Na^{+} ions, along with differences in the spatiotemporal profile of photolysis-released glutamate, may well explain the transient and persistent differences in spine head morphology during LTP and uLTP. To this point, I have demonstrated that photolytic release of glutamate with uLTP-inducing stimuli boosts and maintains resting spine Ca^{2+} levels, above and beyond those seen during remote stimulation and the needed threshold for LTP induction. Indeed, differences in degree and duration of spine Ca^{2+} elevation have previously been shown to regulate the magnitude of LTP at hippocampal synapses (Simons et al. 2009). The consequences of this excessive uncaging-induced postsynaptic Ca^{2+} loading may therefore involve artifactual recruitment of

Ca^{2+}-dependent enzymes promoting long-term reorganization of key cytoskeletal elements resulting in the persistence of spine head enlargement (Lee et al. 2009, Bosch et al. 2014). By this reasoning, NMDAR-dependent LTP induction, via remote synaptic stimulation, would display only a transient spine head enlargement, presumably mediated by osmotic factors, but not sustained enlargement. Furthermore, NMDAR-dependent uLTP would display both transient and sustained enlargements via both osmotic pressure and artifactual activation of Ca^{2+}-dependent processes due to the excessive spine Ca^{2+} loading. Moreover, selective NMDAR antagonists (e.g., AP5) would invariably block both the transient and persistent phases of enlargement by preventing Na^{+} (Rose and Konnerth 2001) and Ca^{2+} accumulation (Emptage et al. 1999) in spines, and therefore block LTP and uLTP induction. Finally, inhibiting Ca^{2+}-dependent processes while leaving NMDARs unperturbed during uLTP would permit the transient changes but prevent the Ca^{2+}-dependent sustained changes. All of these, indeed, seem to be the case (Matsuzaki et al. 2004, Yang et al. 2008, Lee et al. 2009). I hypothesize therefore that the volume, timing, and positioning of the focal uncaging spot produces a broadened profile of postsynaptic glutamate receptor activation and thus an enhanced sensitivity to extrasynaptic vs. focal synaptic receptors at the PSD. A consequence of this increased receptor activation is the imposition of an increased ionic burden (i.e., Na^{+} and Ca^{2+} overload) on the postsynaptic spines during and after uLTP induction, leading not only to increased transient spine swelling (as seen in experiments with full or partial Mg^{2+} relief of NMDARs; e.g., Matsuzaki et al. 2004, Lee et al. 2009, Harvey & Svoboda, 2007) but also to an artifactual persistent enlargement of spines via Ca^{2+}-dependent processes.

5.4 Concluding remarks

Research into the mechanisms of LTP induction and expression has provided remarkable insights into the synaptic basis of memory (Nicoll 2017). Although the history of this research is rife with controversies involving discordant results and interpretational disputes (reviewed in Bliss and Collingridge 2013,

MacDougall and Fine 2014), progress continues to be made in elucidating LTP's cellular and molecular underpinnings at the level of single synapses (Kruijssen and Wierenga 2019, Sanderson et al. 2020). Notwithstanding the elegance and technical sophistication of glutamate uncaging experiments (Matsuzaki et al. 2001, Matsuzaki et al. 2004, Bagal et al. 2005, Noguchi et al. 2005, Harvey and Svoboda 2007, Tanaka et al. 2008, Lee et al. 2009, Kwon and Sabatini 2011, Bosch et al. 2014, Kwon et al. 2017, Ucar et al. 2021), the physiological relevance to synaptic form and function, such as but not limited to the expression of LTP, must now be questioned. It also remains a challenge to understand the relationship between the fast Hebbian processes reported here and slower mechanisms stabilizing or normalizing modified synaptic connections. How these important processes play out over time remains crucial to understanding the relationship between synaptic form and function in the activity-dependent plasticity subserving learning and memory.

APPENDIX

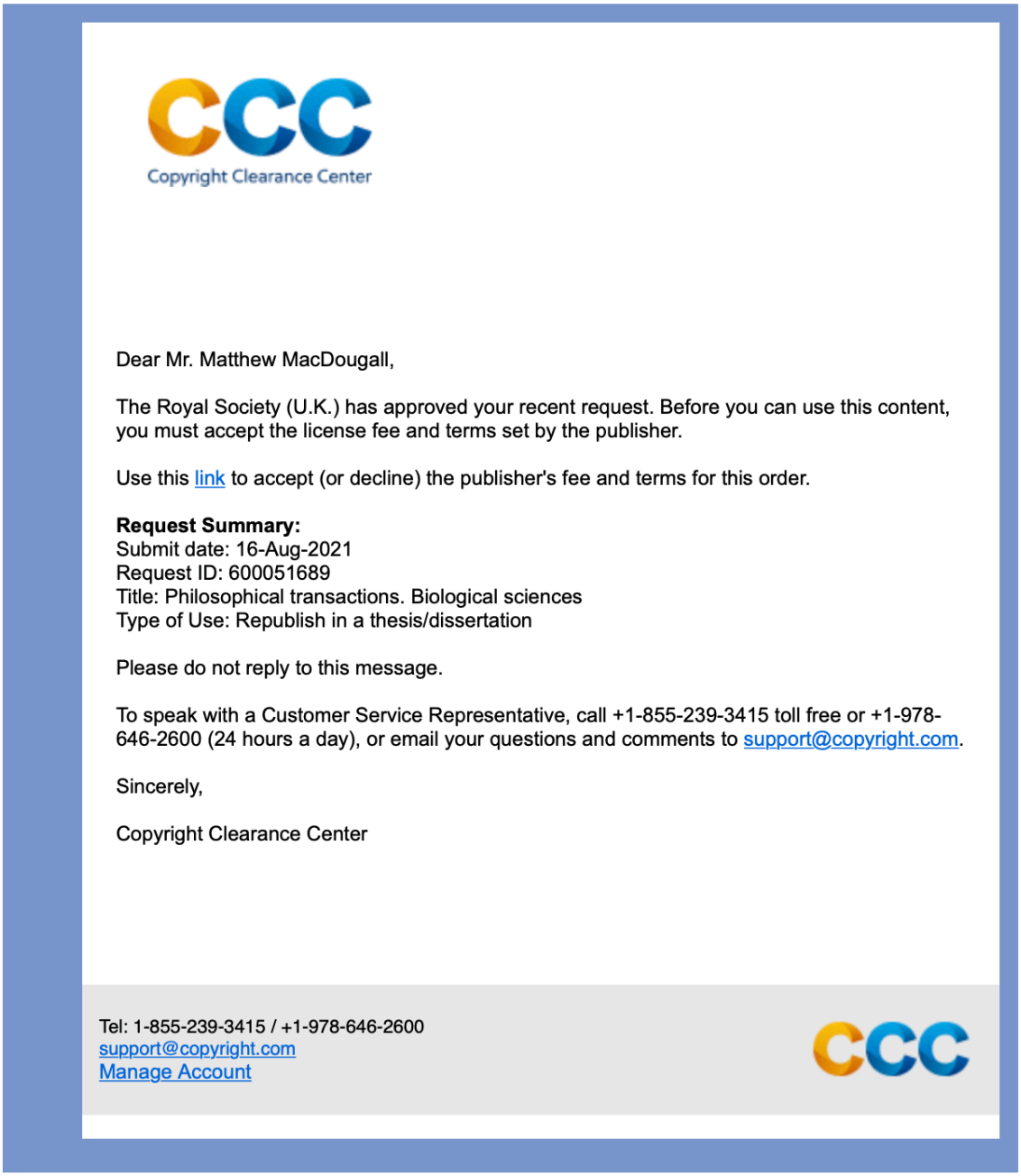

Copyright Clearance Center

Dear Mr. Matthew MacDougall,

The Royal Society (U.K.) has approved your recent request. Before you can use this content, you must accept the license fee and terms set by the publisher.

Use this link to accept (or decline) the publisher's fee and terms for this order.

Request Summary:
Submit date: 16-Aug-2021
Request ID: 600051689
Title: Philosophical transactions. Biological sciences
Type of Use: Republish in a thesis/dissertation

Please do not reply to this message.

To speak with a Customer Service Representative, call +1-855-239-3415 toll free or +1-978-646-2600 (24 hours a day), or email your questions and comments to support@copyright.com.

Sincerely,

Copyright Clearance Center

Tel: 1-855-239-3415 / +1-978-646-2600
support@copyright.com
Manage Account

Frontiers in Synaptic Neuroscience - Peer Re... August 16, 2021 at 11:43 AM

RE: Permission to use in PhD thesis

To: matthew.j.macdougall@gmail.com

Dear Dr MacDougall,

Thank you for your email.

I would like to confirm that all Frontiers articles are Open Access and distributed under the terms of the Creative Commons Attribution License (CC-BY), which permits the re-use, distribution and reproduction of material from published articles, provided the original authors / copyright owner(s) are credited and that the original publication in this journal is cited, in accordance with accepted academic practice. No use, distribution or reproduction is permitted which does not comply with these terms.

Please keep in mind that if anything in the paper was already under copyright restriction from any other third party, then you would have to seek permission to reuse the item from that third party.

Best wishes,
Anshu

--
Anshu Uppal
Review Operations Manager
he / his

Frontiers | Editorial Office | Collaborative Peer Review Team
Avenue du Tribunal Fédéral 34
1005 Lausanne, Switzerland
Office T +41 21 510 1793
www.frontiersin.org

REFERENCES

Ahmed, M. S. and S. A. Siegelbaum (2009). "Recruitment of N-Type Ca(2+) channels during LTP enhances low release efficacy of hippocampal CA1 perforant path synapses." Neuron **63**(3): 372-385.

Aitken, P. G., G. R. Breese, F. F. Dudek, F. Edwards, M. T. Espanol, P. M. Larkman, P. Lipton, G. C. Newman, T. S. Nowak, Jr., K. L. Panizzon and et al. (1995). "Preparative methods for brain slices: a discussion." J Neurosci Methods **59**(1): 139-149.

Andersen, P., R. Morris, D. Amaral, T. V. P. Bliss and J. O'Keefe (2006). The hippocampus book, Oxford University Press.

Andrasfalvy, B. K. and J. C. Magee (2001). "Distance-dependent increase in AMPA receptor number in the dendrites of adult hippocampal CA1 pyramidal neurons." J Neurosci **21**(23): 9151-9159.

Araya, R., J. Jiang, K. B. Eisenthal and R. Yuste (2006). "The spine neck filters membrane potentials." Proc Natl Acad Sci U S A **103**(47): 17961-17966.

Araya, R., T. P. Vogels and R. Yuste (2014). "Activity-dependent dendritic spine neck changes are correlated with synaptic strength." Proc Natl Acad Sci U S A **111**(28): E2895-2904.

Attwell, D. and A. Gibb (2005). "Neuroenergetics and the kinetic design of excitatory synapses." Nat Rev Neurosci **6**(11): 841-849.

Bagal, A. A., J. P. Kao, C. M. Tang and S. M. Thompson (2005). "Long-term potentiation of exogenous glutamate responses at single dendritic spines." Proc Natl Acad Sci U S A **102**(40): 14434-14439.

Bartol, T. M., C. Bromer, J. Kinney, M. A. Chirillo, J. N. Bourne, K. M. Harris and T. J. Sejnowski (2015). "Nanoconnectomic upper bound on the variability of synaptic plasticity." Elife **4**: e10778.

Bashir, Z. I., S. Alford, S. N. Davies, A. D. Randall and G. L. Collingridge (1991). "Long-term potentiation of NMDA receptor-mediated synaptic transmission in the hippocampus." Nature **349**(6305): 156-158.

Baude, A., Z. Nusser, E. Molnar, R. A. McIlhinney and P. Somogyi (1995). "High-resolution immunogold localization of AMPA type glutamate receptor subunits at

synaptic and non-synaptic sites in rat hippocampus." Neuroscience **69**(4): 1031-1055.
Beique, J. C. and R. Andrade (2002). "PSD-95 regulates synaptic transmission and plasticity in rat cerebral cortex." The Journal of Physiology **546**(3): 859-867.
Bekkers, J. M. and C. F. Stevens (1990). "Presynaptic mechanism for long-term potentiation in the hippocampus." Nature **346**(6286): 724-729.
Bernard, V., P. Somogyi and J. P. Bolam (1997). "Cellular, Subcellular, and Subsynaptic Distribution of AMPA-Type Glutamate Receptor Subunits in the Neostriatum of the Rat." J Neuroscience **17**(2): 819-833.
Betz, W. J. and G. S. Bewick (1992). "Optical analysis of synaptic vesicle recycling at the frog neuromuscular-junction." Science **255**(5041): 200-203.
Bi, G. Q. and M. M. Poo (1998). "Synaptic modifications in cultured hippocampal neurons: dependence on spike timing, synaptic strength, and postsynaptic cell type." J Neurosci **18**(24): 10464-10472.
Biro, A. A., N. B. Holderith and Z. Nusser (2005). "Quantal size is independent of the release probability at hippocampal excitatory synapses." J Neurosci **25**(1): 223-232.
Bischofberger, J., D. Engel, L. Li, J. R. Geiger and P. Jonas (2006). "Patch-clamp recording from mossy fiber terminals in hippocampal slices." Nat Protoc **1**(4): 2075-2081.
Bliss, T. V. and G. L. Collingridge (2013). "Expression of NMDA receptor-dependent LTP in the hippocampus: bridging the divide." Mol Brain **6**(5): 5.
Bliss, T. V., M. L. Errington, S. Laroche and M. A. Lynch (1987). "Increase in K+-stimulated, Ca2+-dependent release of [3H]glutamate from rat dentate gyrus three days after induction of long-term potentiation." Neurosci Lett **83**(1-2): 107-112.
Bliss, T. V. and T. Lømo (1973). "Long-lasting potentiation of synaptic transmission in the dentate area of the anaesthetized rabbit following stimulation of the perforant path." J Physiol **232**(2): 331-356.

Bliss, T. V. P. and A. R. Gardner-Medwin (1973). "Long-lasting potentiation of synaptic transmission in the dentate area of the unanaesthtized rabbit following stimulation of the perforant path." Journal of Physiology **232**: 357-374.
Bolshakov, V. Y., H. Golan, E. R. Kandel and S. A. Siegelbaum (1997). "Recruitment of new sites of synaptic transmission during the cAMP-dependent late phase of LTP at CA3-CA1 synapses in the hippocampus." Neuron **19**(3): 635-651.
Bolshakov, V. Y. and S. A. Siegelbaum (1994). "Postsynaptic induction and presynaptic expression of hippocampal long-term depression." Science **264**(5162): 1148-1152.
Bolshakov, V. Y. and S. A. Siegelbaum (1995). "Regulation of hippocampal transmitter release during development and long-term potentiation." Science **269**(5231): 1730-1734.
Bosch, M., J. Castro, T. Saneyoshi, H. Matsuno, M. Sur and Y. Hayashi (2014). "Structural and molecular remodeling of dendritic spine substructures during long-term potentiation." Neuron **82**(2): 444-459.
Bozdagi, O., W. Shan, H. Tanaka, D. L. Benson and G. W. Huntley (2000). "Increasing numbers of synaptic puncta during late-phase LTP: N-cadherin is synthesized, recruited to synaptic sites, and required for potentiation." Neuron **28**(1): 245-259.
Busetto, G., M. J. Higley and B. L. Sabatini (2008). "Developmental presence and disappearance of postsynaptically silent synapses on dendritic spines of rat layer 2/3 pyramidal neurons." J Physiol **586**(6): 1519-1527.
Cathala, L., N. B. Holderith, Z. Nusser, D. A. DiGregorio and S. G. Cull-Candy (2005). "Changes in synaptic structure underlie the developmental speeding of AMPA receptor-mediated EPSCs." Nat Neurosci **8**(10): 1310-1318.
Chang, F. L. and W. T. Greenough (1984). "Transient and enduring morphological correlates of synaptic activity and efficacy change in the rat hippocampal slice." Brain Res **309**(1): 35-46.
Chen, L., D. M. Chetkovich, R. S. Petralia, N. T. Sweeney, Y. Kawasaki, R. J. Wenthold, D. S. Bredt and R. A. Nicoll (2000). "Stargazin regulates synaptic

targeting of AMPA receptors by two distinct mechanisms." Nature **408**(6815): 936-943.
Chen, X., C. D. Nelson, X. Li, C. A. Winters, R. Azzam, A. A. Sousa, R. D. Leapman, H. Gainer, M. Sheng and T. S. Reese (2011). "PSD-95 is required to sustain the molecular organization of the postsynaptic density." J Neurosci **31**(17): 6329-6338.
Chen, X., C. Winters, R. Azzam, X. Li, J. A. Galbraith, R. D. Leapman and T. S. Reese (2008). "Organization of the core structure of the postsynaptic density." Proc Natl Acad Sci U S A **105**(11): 4453-4458.
Clark, K. A. and G. L. Collingridge (1995). "Synaptic potentiation of dual-component excitatory postsynaptic currents in the rat hippocampus." J Physiol **482 (Pt 1)**: 39-52.
Clements, J. D. (1996). "Transmitter timecourse in the synaptic cleft: its role in central synaptic function." Trends Neurosci **19**(5): 163-171.
Collingridge, G. L., J. T. Isaac and Y. T. Wang (2004). "Receptor trafficking and synaptic plasticity." Nat Rev Neurosci **5**(12): 952-962.
Conti, R. and J. Lisman (2003). "The high variance of AMPA receptor- and NMDA receptor-mediated responses at single hippocampal synapses: evidence for multiquantal release." Proc Natl Acad Sci U S A **100**(8): 4885-4890.
Dean, C., F. G. Scholl, J. Choih, S. DeMaria, J. Berger, E. Isacoff and P. Scheiffele (2003). "Neurexin mediates the assembly of presynaptic terminals." Nat Neurosci **6**(7): 708-716.
Debanne, D., B. H. Gahwiler and S. M. Thompson (1999). "Heterogeneity of synaptic plasticity at unitary CA3-CA1 and CA3-CA3 connections in rat hippocampal slice cultures." J Neurosci **19**(24): 10664-10671.
Del Castillo, J. and B. Katz (1954). "Quantal components of the end-plate potential." J Physiol **124**(3): 560-573.
Denk, W., R. Yuste, K. Svoboda and D. W. Tank (1996). "Imaging calcium dynamics in dendritic spines." Curr Opin Neurobiol **6**(3): 372-378.
Dhanrajan, T. M., M. A. Lynch, A. Kelly, V. I. Popov, D. A. Rusakov and M. G. Stewart (2004). "Expression of long-term potentiation in aged rats involves

perforated synapses but dendritic spine branching results from high-frequency stimulation alone." Hippocampus **14**(2): 255-264.
Diamond, J. S., D. E. Bergles and C. E. Jahr (1998). "Glutamate release monitored with astrocyte transporter currents during LTP." Neuron **21**(2): 425-433.
Dolphin, A. C., M. L. Errington and T. V. P. Bliss (1982). "Long-term potentiation of the perforant path in vivo is associated with increased glutamate release." Nature **297**: 496-497.
Dudek, S. M. and M. F. Bear (1992). "Homosynaptic long-term depression in area CA1 of hippocampus and effects of N-methyl-D-aspartate receptor blockade." Proc Natl Acad Sci U S A **89**(10): 4363-4367.
Durand, G. M., Y. Kovalchuk and A. Konnerth (1996). "Long-term potentiation and functional synapse induction in developing hippocampus." Nature **381**(2): 71-75.
Edwards, F. (1991). "Neurobiology - LTP is a long-term problem." Nature **350**(6316): 271-272.
Ehlers, M. D., M. Heine, L. Groc, M. C. Lee and D. Choquet (2007). "Diffusional trapping of GluR1 AMPA receptors by input-specific synaptic activity." Neuron **54**(3): 447-460.
Ehrlich, I., M. Klein, S. Rumpel and R. Malinow (2007). "PSD-95 is required for activity-driven synapse stabilization." Proc Natl Acad Sci U S A **104**(10): 4176-4181.
Ehrlich, I. and R. Malinow (2004). "Postsynaptic density 95 controls AMPA receptor incorporation during long-term potentiation and experience-driven synaptic plasticity." J Neurosci **24**(4): 916-927.
El-Husseini, A. E., E. Schnell, D. M. Chetkovich, R. A. Nicoll and D. S. Bredt (2000). "PSD-95 involvement in maturation of excitatory synapses." Science **290**(5495): 1364-1368.
Emptage, N., T. V. Bliss and A. Fine (1999). "Single synaptic events evoke NMDA receptor-mediated release of calcium from internal stores in hippocampal dendritic spines." Neuron **22**(1): 115-124.

Emptage, N. J., C. A. Reid, A. Fine and T. V. P. Bliss (2003). "Optical quantal analysis reveals a presynaptic component of LTP at hippocampal Schaffer-associational synapses." Neuron **38**(5): 797-804.
Engert, F. and T. Bonhoeffer (1999). "Dendritic spine changes associated with hippocampal long-term synaptic plasticity." Nature **399**(6731): 66-70.
Enoki, R., Y. L. Hu, D. Hamilton and A. Fine (2009). "Expression of long-term plasticity at individual synapses in hippocampus is graded, bidirectional, and mainly presynaptic: optical quantal analysis." Neuron **62**(2): 242-253.
Errington, M. L., P. T. Galley and T. V. Bliss (2003). "Long-term potentiation in the dentate gyrus of the anaesthetized rat is accompanied by an increase in extracellular glutamate: real-time measurements using a novel dialysis electrode." Philos Trans R Soc Lond B Biol Sci **358**(1432): 675-687.
Faber, D. S. and H. Korn (1991). "Applicability of the coefficient of variation method for analyzing synaptic plasticity." Biophys J **60**(5): 1288-1294.
Fifkova, E. and A. Van Harreveld (1977). "Long-lasting morphological changes in dendritic spines of dentate granular cells following stimulation of the entorhinal area." J Neurocytol **6**(2): 211-230.
Franks (2002). "A Monte Carlo model reveals independent signaling at central glutamatergic synapses." Biophys J **83**(5): 2333-2348.
Friedlander, M. J., R. J. Sayer and S. J. Redman (1990). "Evaluation of long-term potentiation of small compound and unitary EPSPs at the hippocampal CA3-CA1 synapse." J Neurosci **10**(3): 814-825.
Geiger, J. R., J. Bischofberger, I. Vida, U. Frobe, S. Pfitzinger, H. J. Weber, K. Haverkampf and P. Jonas (2002). "Patch-clamp recording in brain slices with improved slicer technology." Pflugers Arch **443**(3): 491-501.
Geinisman, Y., L. deToledo-Morrell and F. Morrell (1991). "Induction of long-term potentiation is associated with an increase in the number of axospinous synapses with segmented postsynaptic densities." Brain Res **566**(1-2): 77-88.
Granger, A. J. and R. A. Nicoll (2014). "Expression mechanisms underlying long-term potentiation: a postsynaptic view, 10 years on." Philos Trans R Soc Lond B Biol Sci **369**(1633): 20130136.

Granger, A. J., Y. Shi, W. Lu, M. Cerpas and R. A. Nicoll (2013). "LTP requires a reserve pool of glutamate receptors independent of subunit type." Nature **493**(7433): 495-500.
Grosshans, D. R., D. A. Clayton, S. J. Coultrap and M. D. Browning (2002). "LTP leads to rapid surface expression of NMDA but not AMPA receptors in adult rat CA1." Nat Neurosci **5**(1): 27-33.
Hardingham, N. R., J. C. Read, A. J. Trevelyan, J. C. Nelson, J. J. Jack and N. J. Bannister (2010). "Quantal analysis reveals a functional correlation between presynaptic and postsynaptic efficacy in excitatory connections from rat neocortex." J Neurosci **30**(4): 1441-1451.
Harris, K. M., F. E. Jensen and B. Tsao (1992). "Three-dimensional structure of dendritic spines and synapses in rat hippocampus (CA1) at postnatal day 15 and adult ages: implications for the maturation of synaptic physiology and long-term potentiation." J Neurosci **12**(7): 2685-2705.
Harris, K. M. and J. K. Stevens (1989). "Dendritic spines of CA1 pyramidal cells in the rat hippocampus: serial electron microscopy with reference to their biophysical characteristics." J Neurosci **9**(8): 2982-2997.
Harvey, C. D. and K. Svoboda (2007). "Locally dynamic synaptic learning rules in pyramidal neuron dendrites." Nature **450**(7173): 1195-1200.
Harvey, J. and G. L. Collingridge (1992). "Thapsigargin blocks the induction of long-term potentiation in rat hippocampal slices." Neurosci Lett **139**(2): 197-200.
Hayashi, Y., S. H. Shi, J. A. Esteban, A. Piccini, J. C. Poncer and R. Malinow (2000). "Driving AMPA receptors into synapses by LTP and CaMKII: Requirement for GluR1 and PDZ domain interaction." Science **287**(5461): 2262-2267.
Hebb (1949). The organization of behavior: A Neuropsychological Theory. New York, Wiley.
Heine, M., L. Groc, R. Frischknecht, J. C. Beique, B. Lounis, G. Rumbaugh, R. L. Huganir, L. Cognet and D. Choquet (2008). "Surface mobility of postsynaptic AMPARs tunes synaptic transmission." Science **320**(5873): 201-205.

Henze, N. and B. Zirkler (1990). "A class of invariant consistent tests for multivariate normality." Communications in Statistics - Theory and Methods **19**(10): 3595-3617.
Holderith, N., A. Lorincz, G. Katona, B. Rozsa, A. Kulik, M. Watanabe and Z. Nusser (2012). "Release probability of hippocampal glutamatergic terminals scales with the size of the active zone." Nat Neurosci **15**(7): 988-997.
Holmes, W. R. (1995). "Modeling the effect of glutamate diffusion and uptake on NMDA and non-NMDA receptor saturation." Biophys J **69**(5): 1734-1747.
Hosokawa, T., D. A. Rusakov, T. V. P. Bliss and A. Fine (1995). "Repeated confocal imaging of individual dendritic spines in the living hippocampal slice - evidence for changes in length and orientation associated with chemically-induced LTP." Journal of Neuroscience **15**(8): 5560-5573.
Isaac, J. T., R. A. Nicoll and R. C. Malenka (1995). "Evidence for silent synapses: implications for the expression of LTP." Neuron **15**(2): 427-434.
Jack, J. J., S. J. Redman and K. Wong (1981). "The components of synaptic potentials evoked in cat spinal motoneurones by impulses in single group Ia afferents." J Physiol **321**: 65-96.
Jensen, T. P., K. Zheng, O. Tyurikova, J. P. Reynolds and D. A. Rusakov (2017). "Monitoring single-synapse glutamate release and presynaptic calcium concentration in organised brain tissue." Cell Calcium **64**: 102-108.
Jonas, P., G. Major and B. Sakmann (1993). "Quantal components of unitary EPSCs at the mossy fibre synapse on CA3 pyramidal cells of rat hippocampus." J Physiol **472**: 615-663.
Jourdain, P., K. Fukunaga and D. Muller (2003). "Calcium/calmodulin-dependent protein kinase II contributes to activity-dependent filopodia growth and spine formation." J Neurosci **23**(33): 10645-10649.
Kauer, J. A., R. C. Malenka and R. A. Nicoll (1988). "A persistent postsynaptic modification mediates long-term potentiation in the hippocampus." Neuron **1**(10): 911-917.
Kerchner, G. A. and R. A. Nicoll (2008). "Silent synapses and the emergence of a postsynaptic mechanism for LTP." Nat Rev Neurosci **9**(11): 813-825.

Kerr, R. A., T. M. Bartol, B. Kaminsky, M. Dittrich, J. C. Chang, S. B. Baden, T. J. Sejnowski and J. R. Stiles (2008). "Fast Monte Carlo simulation methods for biological reaction-diffusion systems in solution and on surfaces." SIAM J Sci Comput **30**(6): 3126.

Kessels, H. W., C. D. Kopec, M. E. Klein and R. Malinow (2009). "Roles of stargazin and phosphorylation in the control of AMPA receptor subcellular distribution." Nat Neurosci **12**(7): 888-896.

Kessels, H. W. and R. Malinow (2009). "Synaptic AMPA receptor plasticity and behavior." Neuron **61**(3): 340-350.

Kharazia, V. N., K. D. Phend, A. Rustioni and R. J. Weinberg (1996). "EM colocalization of AMPA and NMDA receptor subunits at synapses in rat cerebral cortex." Neuroscience Letters **210**: 37-40.

Kharazia, V. N. and R. J. Weinberg (1997). "Tangential synaptic distribution of NMDA and AMPA receptors in rat neocortex." Neurosci Lett **238**(1-2): 41-44.

Kim, E. and M. Sheng (2004). "PDZ domain proteins of synapses." Nat Rev Neurosci **5**(10): 771-781.

Koch, C. and T. Poggio (1983). "A theoretical analysis of electrical properties of spines." Proc R Soc Lond B Biol Sci **218**(1213): 455-477.

Kopach, O., K. Zheng and D. A. Rusakov (2020). "Optical monitoring of glutamate release at multiple synapses in situ detects changes following LTP induction." Mol Brain **13**(1): 39.

Kopec, C. D., E. Real, H. W. Kessels and R. Malinow (2007). "GluR1 links structural and functional plasticity at excitatory synapses." J Neurosci **27**(50): 13706-13718.

Korkmaz, S., D. Goksuluk and G. Zararsiz (2014). "MVN: An R package for assessing multivariate normality." The R Journal **6**(2): 151–162.

Korn, H. and D. S. Faber (1991). "Quantal analysis and synaptic efficacy in the CNS." Trends Neurosci **14**(10): 439-445.

Kruijssen, D. L. H. and C. J. Wierenga (2019). "Single synapse LTP: A matter of context?" Front Cell Neurosci **13**: 496.

Kullmann, D. M. (1994). "Amplitude fluctuations of dual-component EPSCs in hippocampal pyramidal cells: implications for long-term potentiation." Neuron **12**(5): 1111-1120.
Kullmann, D. M. (2012). "The mother of all battles 20 years on: is LTP expressed pre- or postsynaptically?" J Physiol **590**(Pt 10): 2213-2216.
Kullmann, D. M., G. Erdemli and F. Asztely (1996). "LTP of AMPA and NMDA receptor-mediated signals: evidence for presynaptic expression and extrasynaptic glutamate spill-over." Neuron **17**(3): 461-474.
Kwon, H. B. and B. L. Sabatini (2011). "Glutamate induces de novo growth of functional spines in developing cortex." Nature **474**(7349): 100-104.
Kwon, T., M. Sakamoto, D. S. Peterka and R. Yuste (2017). "Attenuation of synaptic potentials in dendritic spines." Cell Rep **20**(5): 1100-1110.
Lancaster, H. O. (1963). "Correlationand complete dependence of random variables." The Annals of Mathematical Statistics **34**(4): 1315-1321.
Lang, C., A. Barco, L. Zablow, E. R. Kandel, S. A. Siegelbaum and S. S. Zakharenko (2004). "Transient expansion of synaptically connected dendritic spines upon induction of hippocampal long-term potentiation." Proc Natl Acad Sci U S A **101**(47): 16665-16670.
Larkman, A., K. Stratford and J. Jack (1991). "Quantal analysis of excitatory synaptic action and depression in hippocampal slices." Nature **350**(6316): 344-347.
Laroche, S., M. L. Errington, M. A. Lynch and T. V. P. Bliss (1987). "Increase in [H-3] glutamate release from slices of dentate gyrus and hippocampus following classical-conditioning in the rat." Behavioural Brain Research **25**(1): 23-29.
Lee, K. S., F. Schottler, M. Oliver and G. Lynch (1980). "Brief bursts of high-frequency stimulation produce two types of structural change in rat hippocampus." J Neurophysiol **44**(2): 247-258.
Lee, S. J., Y. Escobedo-Lozoya, E. M. Szatmari and R. Yasuda (2009). "Activation of CaMKII in single dendritic spines during long-term potentiation." Nature **458**(7236): 299-304.

Lee, V. M. (2001). "Biomedicine. Tauists and βaptists united--well almost!" Science **293**(5534): 1446-1447.
Lester, R. A. and C. E. Jahr (1992). "NMDA channel behavior depends on agonist affinity." J Neurosci **12**(2): 635-643.
Liao, D., N. A. Hessler and R. Malinow (1995). "Activation of postsynaptically silent synapses during pairing-induced LTP in CA1 region of hippocampal slices." Nature **375**: 400-404.
Lisman, J. (2017). "Glutamatergic synapses are structurally and biochemically complex because of multiple plasticity processes: long-term potentiation, long-term depression, short-term potentiation and scaling." Philos Trans R Soc Lond B Biol Sci **372**(1715).
Lisman, J. and S. Raghavachari (2006). "A unified model of the presynaptic and postsynaptic changes during LTP at CA1 synapses." Sci STKE **2006**(356): re11.
Luscher, C., R. C. Malenka and R. A. Nicoll (1998). "Monitoring glutamate release during LTP with glial transporter currents." Neuron **21**(2): 435-441.
Lynch, G. and M. Baudry (1984). "The biochemistry of memory: a new and specific hypothesis." Science **224**(4653): 1057-1063.
MacDougall, M. J. and A. Fine (2014). "The expression of long-term potentiation: reconciling the preists and the postivists." Philos Trans R Soc Lond B Biol Sci **369**(1633): 20130135.
MacDougall, M. J. and A. Fine (2019). "Optical quantal analysis." Front Synaptic Neurosci **11**: 8.
Mainen, Z. F., Z. Jia, J. Roder and R. Malinow (1998). "Use-dependent AMPA receptor block in mice lacking GluR2 suggests postsynaptic site for LTP expression." Nat Neurosci **1**(7): 579-586.
Mainen, Z. F., R. Malinow and K. Svoboda (1999). "Synaptic calcium transients in single spines indicate that NMDA receptors are not saturated." Nature **399**(6732): 151-155.
Makino, H. and R. Malinow (2009). "AMPA receptor incorporation into synapses during LTP: the role of lateral movement and exocytosis." Neuron **64**(3): 381-390.

Maletic-Savatic, M. (1999). "Rapid dendritic morphogenesis in CA1 hippocampal dendrites induced by synaptic activity." Science **283**(5409): 1923-1927.
Malinow, R. (1991). "Transmission between pairs of hippocampal slice neurons: Quantal levels, oscillations, and LTP." Science **252**(5006): 722-724.
Malinow, R. and R. C. Malenka (2002). "AMPA receptor trafficking and synaptic plasticity." Annu Rev Neurosci **25**: 103-126.
Malinow, R., N. Otmakhov, K. I. Blum and J. Lisman (1994). "Visualizing hippocampal synaptic function by optical detection of Ca2+ entry through the N-methyl-D-aspartate channel." Proc Natl Acad Sci U S A **91**(17): 8170-8174.
Malinow, R. and R. W. Tsien (1990). "Presynaptic enhancement shown by whole-cell recordings of long-term potentiation in hippocampal slices." Nature **346**(6280): 177-180.
Manabe, T. and R. A. Nicoll (1994). "Long-term potentiation: Evidence against an increase in transmitter release probability in the CA1 region of the hippocampus." Science **265**(5180): 1888-1892.
Markram, H., J. Lubke, M. Frotscher and B. Sakmann (1997). "Regulation of synaptic efficacy by coincidence of postsynaptic APs and EPSPs." Science **275**(5297): 213-215.
Marvin, J. S., B. G. Borghuis, L. Tian, J. Cichon, M. T. Harnett, J. Akerboom, A. Gordus, S. L. Renninger, T. W. Chen, C. I. Bargmann, M. B. Orger, E. R. Schreiter, J. B. Demb, W. B. Gan, S. A. Hires and L. L. Looger (2013). "An optimized fluorescent probe for visualizing glutamate neurotransmission." Nat Methods **10**(2): 162-170.
Masugi-Tokita, M. and R. Shigemoto (2007). "High-resolution quantitative visualization of glutamate and GABA receptors at central synapses." Curr Opin Neurobiol **17**(3): 387-393.
Masugi-Tokita, M., E. Tarusawa, M. Watanabe, E. Molnar, K. Fujimoto and R. Shigemoto (2007). "Number and density of AMPA receptors in individual synapses in the rat cerebellum as revealed by SDS-digested freeze-fracture replica labeling." J Neurosci **27**(8): 2135-2144.

Matsubara, A., J. H. Laake, S. Davanger, S. Usami and O. P. Ottersen (1996). "Organization of AMPA receptor subunits at a glutamate synapse: A quantitative immunogold analysis of hair cell synapses in the rat organ of Corti." Journal of Neuroscience **16**(14): 4457-4467.

Matsuo, N., L. Reijmers and M. Mayford (2008). "Spine-type-specific recruitment of newly synthesized AMPA receptors with learning." Science **319**(5866): 1104-1107.

Matsuzaki, M., G. C. Ellis-Davies, T. Nemoto, Y. Miyashita, M. Iino and H. Kasai (2001). "Dendritic spine geometry is critical for AMPA receptor expression in hippocampal CA1 pyramidal neurons." Nat Neurosci **4**(11): 1086-1092.

Matsuzaki, M., N. Honkura, G. C. Ellis-Davies and H. Kasai (2004). "Structural basis of long-term potentiation in dendritic spines." Nature **429**(6993): 761-776.

Meyer, D., T. Bonhoeffer and V. Scheuss (2014). "Balance and Stability of Synaptic Structures during Synaptic Plasticity." Neuron **82**(2): 430-443.

Montgomery, J. M. and D. V. Madison (2004). "Discrete synaptic states define a major mechanism of synapse plasticity." Trends Neurosci **27**(12): 744-750.

Morris, R. G., P. Garrud, J. N. Rawlins and J. O'Keefe (1982). "Place navigation impaired in rats with hippocampal lesions." Nature **297**(5868): 681-683.

Moser, M. B., M. Trommald and P. Andersen (1994). "An increase in dendritic spine density on hippocampal CA1 pyramidal cells following spatial learning in adult rats suggests the formation of new synapses." Proc Natl Acad Sci U S A **91**(26): 12673-12675.

Muller, D. and G. Lynch (1988). "Long-term potentiation differentially affects two components of synaptic responses in hippocampus." Proc Natl Acad Sci U S A **85**(23): 9346-9350.

Murthy, V. N., T. Schikorski, C. F. Stevens and Y. Zhu (2001). "Inactivity produces increases in neurotransmitter release and synapse size." Neuron **32**(4): 673-682.

Nagerl, U. V., N. Eberhorn, S. B. Cambridge and T. Bonhoeffer (2004). "Bidirectional activity-dependent morphological plasticity in hippocampal neurons." Neuron **44**(5): 759-767.

Nevian, T. and B. Sakmann (2006). "Spine Ca2+ signaling in spike-timing-dependent plasticity." J Neurosci **26**(43): 11001-11013.
Nicholson, C. and J. M. Phillips (1981). "Ion diffusion modified by tortuosity and volume fraction in the extracellular microenvironment of the rat cerebellum." J Physiol **321**: 225-257.
Nicoll, R. A. (2003). "Expression mechanisms underlying long-term potentiation: a postsynaptic view." Philos Trans R Soc Lond B Biol Sci **358**(1432): 721-726.
Nicoll, R. A. (2017). "A brief history of long-term potentiation." Neuron **93**(2): 281-290.
Nicoll, R. A. and K. W. Roche (2013). "Long-term potentiation: Peeling the onion." Neuropharmacology.
Nicoll, R. A. and D. Schmitz (2005). "Synaptic plasticity at hippocampal mossy fibre synapses." Nat Rev Neurosci **6**(11): 863-876.
Nielsen, T. A., D. A. DiGregorio and R. A. Silver (2004). "Modulation of glutamate mobility reveals the mechanism underlying slow-rising AMPAR EPSCs and the diffusion coefficient in the synaptic cleft." Neuron **42**(5): 757-771.
Noguchi, J., M. Matsuzaki, G. C. Ellis-Davies and H. Kasai (2005). "Spine-neck geometry determines NMDA receptor-dependent Ca2+ signaling in dendrites." Neuron **46**(4): 609-622.
Nusser, Z., R. Lujan, G. Laube, J. D. Roberts, E. Molnar and P. Somogyi (1998). "Cell type and pathway dependence of synaptic AMPA receptor number and variability in the hippocampus." Neuron **21**(3): 545-559.
Nusser, Z., E. Mulvihill, P. Streit and P. Somogyi (1994). "Subsynaptic segregation of metabotropic and ionotropic glutamate receptors as revealed by immunogold localization." Neuroscience **61**(3): 421-427.
O'Keefe, J. (1976). "Place units in the hippocampus of the freely moving rat." Exp Neurol **51**(1): 78-109.
Padamsey, Z., R. Tong and N. Emptage (2019). "Optical quantal analysis using Ca(2+) indicators: A robust method for assessing transmitter release probability at excitatory synapses by imaging single glutamate release events." Front Synaptic Neurosci **11**: 5.

Petralia, R. S., J. A. Esteban, Y. X. Wang, J. G. Partridge, H. M. Zhao, R. J. Wenthold and R. Malinow (1999). "Selective acquisition of AMPA receptors over postnatal development suggests a molecular basis for silent synapses." Nature Neuroscience **2**(1): 31-36.

Pierce, D. A. and R. L. Dykstra (1969). "Independence and the normal distribution." The American Statistician **23**(4): 39.

Plant, K., K. A. Pelkey, Z. A. Bortolotto, D. Morita, A. Terashima, C. J. McBain, G. L. Collingridge and J. T. Isaac (2006). "Transient incorporation of native GluR2-lacking AMPA receptors during hippocampal long-term potentiation." Nat Neurosci **9**(5): 602-604.

Popov, V. I., H. A. Davies, V. V. Rogachevsky, I. V. Patrushev, M. L. Errington, P. L. Gabbott, T. V. Bliss and M. G. Stewart (2004). "Remodelling of synaptic morphology but unchanged synaptic density during late phase long-term potentiation (LTP): a serial section electron micrograph study in the dentate gyrus in the anaesthetised rat." Neuroscience **128**(2): 251-262.

Racca, C., F. A. Stephenson, P. Streit, J. D. Roberts and P. Somogyi (2000). "NMDA receptor content of synapses in stratum radiatum of the hippocampal CA1 area." J Neurosci **20**(7): 2512-2522.

Raghavachari, S. and J. E. Lisman (2004). "Properties of quantal transmission at CA1 synapses." J Neurophysiol **92**(4): 2456-2467.

Rall, W. (1960). "Membrane potential transients and membrane time constant of motoneurons." Exp Neurol **2**: 503-532.

Rall, W. (1967). "Distinguishing theoretical synaptic potentials computed for different soma-dendritic distributions of synaptic input." J Neurophysiol **30**(5): 1138-1168.

Ramón y Cajal, S. (1893). "Neue darstellung vom histologischen bau des centralnervensystem." Arch. Anat. Entwick(319-428).

Regehr, W. G., M. R. Carey and A. R. Best (2009). "Activity-dependent regulation of synapses by retrograde messengers." Neuron **63**(2): 154-170.

Reid, C. A., D. B. Dixon, M. Takahashi, T. V. Bliss and A. Fine (2004). "Optical quantal analysis indicates that long-term potentiation at single hippocampal

mossy fiber synapses is expressed through increased release probability, recruitment of new release sites, and activation of silent synapses." J Neurosci **24**(14): 3618-3626.
Reid, C. A., R. Fabian-Fine and A. Fine (2001). "Postsynaptic calcium transients evoked by activation of individual hippocampal mossy fiber synapses." Journal of Neuroscience **21**(7): 2206-2214.
Robert, A. and J. R. Howe (2003). "How AMPA receptor desensitization depends on receptor occupancy." Journal of Neuroscience **23**(3): 847-858.
Rose, C. R. and A. Konnerth (2001). "NMDA receptor-mediated Na+ signals in spines and dendrites." J Neurosci **21**(12): 4207-4214.
Rosenmund, C., Y. Stern-Bach and C. F. Stevens (1998). "The tetrameric structure of a glutamate receptor channel." Science **280**(5369): 1596-1599.
Rungta, R. L., H. B. Choi, J. R. Tyson, A. Malik, L. Dissing-Olesen, P. J. C. Lin, S. M. Cain, P. R. Cullis, T. P. Snutch and B. A. MacVicar (2015). "The cellular mechanisms of neuronal swelling underlying cytotoxic edema." Cell **161**(3): 610-621.
Rusakov, D. A. and D. M. Kullmann (1998). "Extrasynaptic glutamate diffusion in the hippocampus: ultrastructural constraints, uptake, and receptor activation." J Neurosci **18**(9): 3158-3170.
Sanderson, T. M., J. Georgiou and G. L. Collingridge (2020). "Illuminating Relationships Between the Pre- and Post-synapse." Front Neural Circuits **14**: 9.
Sanhueza, M. and J. Lisman (2013). "The CaMKII/NMDAR complex as a molecular memory." Molecular Brain **6**(10): 1-8.
Savtchenko, L. P. and D. A. Rusakov (2007). "The optimal height of the synaptic cleft." Proc Natl Acad Sci U S A **104**(6): 1823-1828.
Savtchenko, L. P., S. Sylantyev and D. A. Rusakov (2013). "Central synapses release a resource-efficient amount of glutamate." Nat Neurosci **16**(1): 10-12.
Sayer, R. J., M. J. Friedlander and S. J. Redman (1990). "The time course and amplitude of EPSPs evoked at synapses between pairs of CA3/CA1 neurons in the hippocampal slice." J Neurosci **10**(3): 826-836.

Sayer, R. J., S. J. Redman and P. Andersen (1989). "Amplitude fluctuations in small EPSPs recorded from CA1 pyramidal cells in the guinea pig hippocampal slice." J Neurosci **9**(3): 840-850.
Schikorski, T. and C. F. Stevens (1997). "Quantitative ultrastructural analysis of hippocampal excitatory synapses." Journal of Neuroscience **17**(15): 5858-5867.
Schneider, C. A., W. S. Rasband and K. W. Eliceiri (2012). "NIH Image to ImageJ: 25 years of image analysis." Nat Methods **9**(7): 671-675.
Schnell, E., M. Sizemore, S. Karimzadegan, L. Chen, D. S. Bredt and R. A. Nicoll (2002). "Direct interactions between PSD-95 and stargazin control synaptic AMPA receptor number." Proc Natl Acad Sci U S A **99**(21): 13902-13907.
Scoville, W. B. and B. Milner (1957). "Loss of recent memory after bilateral hippocampal lesions." J Neurol Neurosurg Psychiatry **20**(1): 11-21.
Shepherd, G. M. and K. M. Harris (1998). "Three-dimensional structure and composition of CA3-->CA1 axons in rat hippocampal slices: implications for presynaptic connectivity and compartmentalization." J Neurosci **18**(20): 8300-8310.
Shi, S. H., Y. Hayashi, R. S. Petralia, S. H. Zaman, R. J. Wenthold, K. Svoboda and R. Malinow (1999). "Rapid spine delivery and redistribution of AMPA receptors after synaptic NMDA receptor activation." Science **284**(5421): 1811-1816.
Simons, S. B., Y. Escobedo, R. Yasuda and S. M. Dudek (2009). "Regional differences in hippocampal calcium handling provide a cellular mechanism for limiting plasticity." Proc Natl Acad Sci U S A **106**(33): 14080-14084.
Sinnen, B. L., A. B. Bowen, J. S. Forte, B. G. Hiester, K. C. Crosby, E. S. Gibson, M. L. Dell'Acqua and M. J. Kennedy (2017). "Optogenetic Control of Synaptic Composition and Function." Neuron **93**(3): 646-660 e645.
Skrede, K. K. and D. Malthe-Sørenssen (1981). "Increased resting and evoked release of transmitter following repetitive electrical tetanization in hippocampus: a biochemical correlate to long-lasting synaptic potentiation." Brain Research **208**(2): 436-441.

Skrede, K. K. and R. H. Westgaard (1971). "The transverse hippocampal slice: a well-defined cortical structure maintained in vitro." Brain Res **35**(2): 589-593.
Smith, T. C. and J. R. Howe (2000). "Concentration-dependent substate behavior of native AMPA receptors." Nat Neurosci **3**(10): 992-997.
Smith, T. C., L. Y. Wang and J. R. Howe (2000). "Heterogeneous conductance levels of native AMPA receptors." J Neurosci **20**(6): 2073-2085.
Song, S., K. D. Miller and L. F. Abbott (2000). "Competitive Hebbian learning through spike-timing-dependent synaptic plasticity." Nat Neurosci **3**(9): 919-926.
Sorra, K. E. and K. M. Harris (1993). "Occurrence and three-dimensional structure of multiple synapses between individual radiatum axons and their target pyramidal cells in hippocampal area CA1." J Neurosci **13**(9): 3736-3748.
Sorra, K. E. and K. M. Harris (1998). "Stability in synapse number and size at 2 hr after long-term potentiation in hippocampal area CA1." J Neurosci **18**(2): 658-671.
Spacek, J. and K. M. Harris (1997). "Three-dimensional organization of smooth endoplasmic reticulum in hippocampal CA1 dendrites and dendritic spines of the immature and mature rat." J Neurosci **17**(1): 190-203.
Stein, V., D. R. House, D. S. Bredt and R. A. Nicoll (2003). "Postsynaptic density-95 mimics and occludes hippocampal long-term potentiation and enhances long-term depression." J Neurosci **23**(13): 5503-5506.
Stevens, C. F. and Y. Wang (1995). "Facilitation and depression at single central synapses." Neuron **14**(4): 795-802.
Stevens, C. F. and Y. Y. Wang (1994). "Changes in reliability of synaptic function as a mechanism for plasticity." Nature **371**(6499): 704-707.
Stiles, J. R. and T. M. Bartol (2001). "Monte Carlo methods for simulating realistic synaptic microphysiology using MCell." Computational Neuroscience: 87-127.
Stricker, C., A. C. Field and S. J. Redman (1996). "Changes in quantal parameters of EPSCs in rat CA1 neurones in vitro after the induction of long-term potentiation." J Physiol **490 (Pt 2)**: 443-454.
Stuart, G. and N. Spruston (1998). "Determinants of voltage attenuation in neocortical pyramidal neuron dendrites." J Neurosci **18**(10): 3501-3510.

Sturgill, J. F., P. Steiner, B. L. Czervionke and B. L. Sabatini (2009). "Distinct domains within PSD-95 mediate synaptic incorporation, stabilization, and activity-dependent trafficking." J Neurosci **29**(41): 12845-12854.
Takumi, Y., V. Ramirez-Leon, P. Laake, E. Rinvik and O. P. Ottersen (1999). "Different modes of expression of AMPA and NMDA receptors in hippocampal synapses." Nat Neurosci **2**(7): 618-624.
Tanaka, J., Y. Horiike, M. Matsuzaki, T. Miyazaki, G. C. Ellis-Davies and H. Kasai (2008). "Protein synthesis and neurotrophin-dependent structural plasticity of single dendritic spines." Science **319**(5870): 1683-1687.
Tanzi, G. (1893). "I fatti i le indizioni nell'odierna istologi del sistema nervoso." Riv. Sper. Freniatr **19**: 419-472.
Tomita, S., H. Adesnik, M. Sekiguchi, W. Zhang, K. Wada, J. R. Howe, R. A. Nicoll and D. S. Bredt (2005). "Stargazin modulates AMPA receptor gating and trafficking by distinct domains." Nature **435**(7045): 1052-1058.
Toni, N., P. A. Buchs, I. Nikonenko, C. R. Bron and D. Muller (1999). "LTP promotes formation of multiple spine synapses between a single axon terminal and a dendrite." Nature **402**(6760): 421-425.
Tonnesen, J., G. Katona, B. Rozsa and U. V. Nagerl (2014). "Spine neck plasticity regulates compartmentalization of synapses." Nat Neurosci **17**(5): 678-685.
Trojanowski, J. Q. (2002). "Tauists, Baptists, Syners, Apostates, and new data." Ann Neurol **52**(3): 263-265.
Turner, D. A. (1988). "Waveform and amplitude characteristics of evoked responses to dendritic stimulation of CA1 guinea-pig pyramidal cells." J Physiol **395**: 419-439.
Ucar, H., S. Watanabe, J. Noguchi, Y. Morimoto, Y. Iino, S. Yagishita, N. Takahashi and H. Kasai (2021). "Mechanical actions of dendritic-spine enlargement on presynaptic exocytosis." Nature **600**: 686-689.
Van Harreveld, A. and E. Fifkova (1975). "Swelling of dendritic spines in the fascia dentata after stimulation of the perforant fibers as a mechanism of post-tetanic potentiation." Exp Neurol **49**(3): 736-749.

Voronin, L. L. (2003). ""Presynaptic silence" may be golden." Neuropharmacology **45**: 439-449.
Voronin, L. L., R. S. Altinbaev, I. T. Bayazitov, S. Gasparini, A. V. Kasyanov, C. Saviane, L. Savtchenko and E. Cherubini (2004). "Postsynaptic depolarisation enhances transmitter release and causes the appearance of responses at "silent" synapses in rat hippocampus." Neuroscience **126**(1): 45-59.
Wahl (1996). "Monte Carlo Simulation of Fast Excitatory Synaptic Transmission at a Hippocampal Synapse
."
Ward, B., L. McGuinness, C. J. Akerman, A. Fine, T. V. Bliss and N. J. Emptage (2006). "State-dependent mechanisms of LTP expression revealed by optical quantal analysis." Neuron **52**(4): 649-661.
Whitlock, J. R., A. J. Heynen, M. G. Shuler and M. F. Bear (2006). "Learning induces long-term potentiation in the hippocampus." Science **313**(5790): 1093-1097.
Xu, W., O. M. Schluter, P. Steiner, B. L. Czervionke, B. Sabatini and R. C. Malenka (2008). "Molecular dissociation of the role of PSD-95 in regulating synaptic strength and LTD." Neuron **57**(2): 248-262.
Yang, Y., X. B. Wang, M. Frerking and Q. Zhou (2008). "Spine expansion and stabilization associated with long-term potentiation." J Neurosci **28**(22): 5740-5751.
Yuste, R. and T. Bonhoeffer (2001). "Morphological changes in dendritic spines associated with long-term synaptic plasticity." Annu Rev Neurosci **24**: 1071-1089.
Yuste, R. and W. Denk (1995). "Dendritic spines as basic functional units of neural integration." Nature **375**: 682-684.
Yuste, R., A. Majewska, S. S. Cash and W. Denk (1999). "Mechanisms of calcium influx into hippocampal spines: heterogeneity among spines, coincidence detection by NMDA receptors, and optical quantal analysis." J Neurosci **19**(6): 1976-1987.

Zakharenko, S. S., L. Zablow and S. A. Siegelbaum (2001). "Visualization of changes in presynaptic function during long-term synaptic plasticity." Nat Neurosci **4**(7): 711-717.
Zheng, K., T. P. Jensen, L. P. Savtchenko, J. A. Levitt, K. Suhling and D. A. Rusakov (2017). "Nanoscale diffusion in the synaptic cleft and beyond measured with time-resolved fluorescence anisotropy imaging." Sci Rep **7**: 42022.
Zheng, K. and D. A. Rusakov (2015). "Efficient integration of synaptic events by NMDA receptors in three-dimensional neuropil." Biophys J **108**(10): 2457-2464.